

5-2022

MEMBRANE BIOREACTOR FOR ENHANCED ENZYMATIC HYDROLYSIS OF CELLULOSE

Saleha Abdullah Al-Mardeai

Follow this and additional works at: https://scholarworks.uaeu.ac.ae/all_dissertations



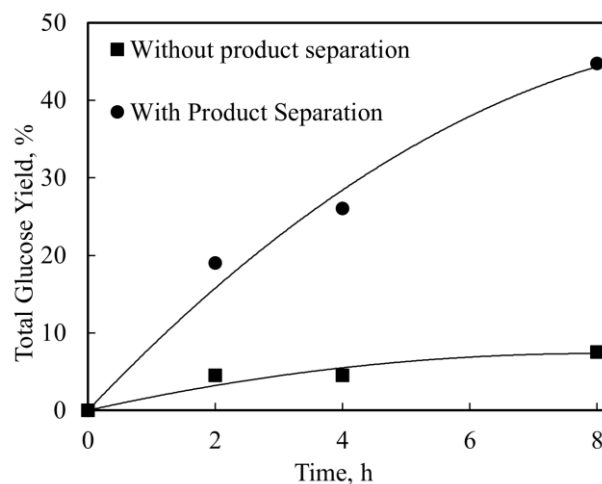
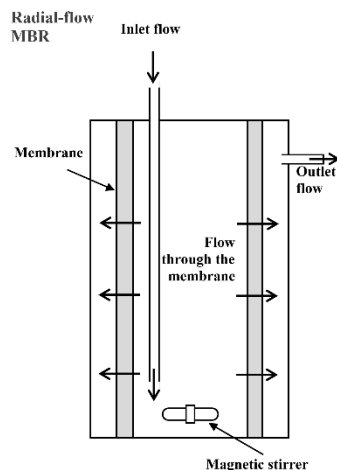
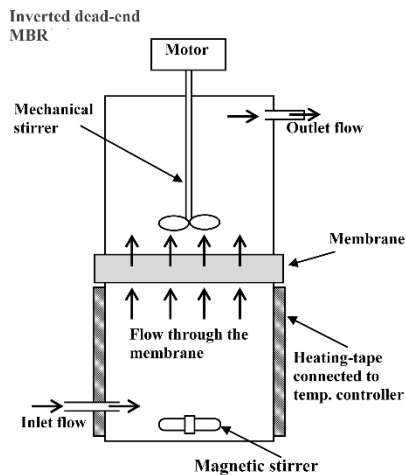
Part of the [Chemical Engineering Commons](#)



DOCTORATE DISSERTATION NO. 2022:3

**MEMBRANE BIOREACTOR FOR ENHANCED
ENZYMATIC HYDROLYSIS OF CELLULOSE**

Saleha Abdullah Al-Mardeai





Membrane Bioreactor for Enhanced Enzymatic Hydrolysis of Cellulose

Saleha Abdullah Al-Mardeai

United Arab Emirates University
College of Engineering
Department of Chemical and Petroleum
Engineering
Al-Ain, UAE

KU Leuven
Arenberg Doctoral School
Faculty of Engineering Science
Department of Chemical Engineering
Leuven, Belgium

This dissertation is submitted in partial fulfilment of the requirements for the degree of Doctor of Philosophy (PhD) in chemical Engineering (UAEU) and Doctor of Engineering Science (PhD): Chemical Engineering (KU Leuven)

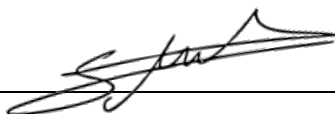
Under the Supervision of:
Professor Sulaiman Al-Zuhair and Professor Bart Van der Bruggen

May 2022

Declaration of Original Work

I, Saleha Abdullah Al-Mardeai, the undersigned, a graduate student at the United Arab Emirates University (UAEU) and KU Leuven, and the author of this dissertation entitled “*Membrane Bioreactor for Enhanced Enzymatic Hydrolysis of Cellulose*”, hereby, solemnly declare that this dissertation is my own original research work that has been done and prepared by me under the supervision of Professor Sulaiman Al-Zuhair, in the College of Engineering at UAEU, and Professor Bart Van der Bruggen in the Department of Chemical Engineering at KU Leuven. This work has not previously formed the basis for the award of any academic degree, diploma or a similar title at this or any other university. Any materials borrowed from other sources (whether published or unpublished) and relied upon or included in my dissertation have been properly cited and acknowledged in accordance with appropriate academic conventions. I further declare that there is no potential conflict of interest with respect to the research, data collection, authorship, presentation and/or publication of this dissertation.

Student's Signature: _____



Date: 23.05.2022

Copyright © 2022 Saleha Abdullah Al-Mardeai
All Rights Reserved

Advisory Committee

1) Advisor: Sulaiman Al-Zuhair

Title: Professor

Department of Chemical and Petroleum Engineering

College of Engineering

United Arab Emirates University

2) Advisor: Bart Van der Bruggen

Title: Professor

Department of Chemical Engineering

KU Leuven, Belgium

3) Co-advisor: Emad Elnajjar

Title: Associate Professor

Department of Mechanical Engineering

College of Engineering

United Arab Emirates University

4) Co-advisor (external): Boguslaw Kruczek

Title: Professor

Ottawa University, Canada

5) Co-advisor (external): Raed Hashaikeh

Title: Professor

New York University, UAE

Approval of the Doctorate Dissertation

This Doctorate Dissertation is approved by the following Examining Committee Members:

1) Sulaiman Al-Zuhair

Title: Professor

Department of Chemical and Petroleum Engineering

United Arab Emirates University

Signature  Date 22.05.2022

2) Bart Van der Bruggen

Title: Professor

Department of Chemical Engineering

KU Leuven, Belgium

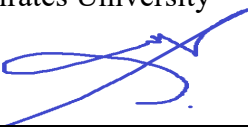
Signature  Date 22.05.2022

3) Basim Abu-Jdayil

Title: Professor

Department of Chemical and Petroleum Engineering

United Arab Emirates University

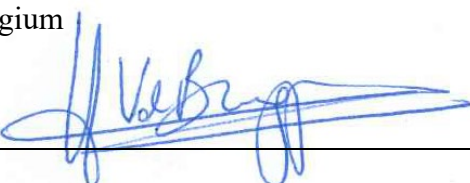
Signature  Date 23/05/2022

4) Lise Appels

Title: Associate Professor

Department of Chemical Engineering

KU Leuven, Belgium

Signature i.o.  Date 23/5/2022

5) Pedro Fardim

Title: Professor

Department of Chemical Engineering

KU Leuven, Belgium

Signature  _____ Date May 23, 2022

6) D. Grant Allen

Title: Professor

Department of Chemical Engineering and Applied Chemistry

University of Toronto, Canada

Signature  _____ Date May 22, 2022

Abstract

With the rising environmental concerns related to fossil fuels utilization and the depletion of these resources, interest in bioethanol from lignocellulosic waste as an alternative, sustainable energy source has been increasing. Date palm waste is considered a good feedstock for bioethanol production, especially in countries of large date palm plantations, such as the United Arab Emirates.

In the lignocellulose to bioethanol process, the enzymatic hydrolysis of celluloses to produce simple sugars that can be converted to bioethanol by fermentation is the most challenging step, and enhancing it is essential for efficient and feasible operation. Enzyme inhibition by the products is one of the several problems that hinders the cellulose bioconversion. To resolve this problem, a novel membrane bioreactor (MBR) was designed with an inverted dead-end filtration concept for simultaneous removal of the product during the reaction. Polyethersulfone membranes (PES) were used, and their selectivity in allowing only product permeation was proven. The effects of water flowrate and initial substrate concentration were investigated, and a mathematical kinetic model that was based on the mechanistic steps was developed to predict the dynamic behavior of the system, and the kinetic parameters were estimated by fitting the experimental data. The experimental results were also used to develop a statistical non-linear interactive model. Using standard cellulose, the glucose production yield increased from 7% without product separation to 45% with product separation. Both kinetic and statistical models showed good agreement (R^2 : 0.96 and 0.97, respectively). The process was optimized, and the optimal conditions were determined to be at substrate concentration of 2.67 g/L and a water flowrate of 0.8 mL/min, at which a maximum yield of 86.7% was achieved.

To increase the efficiency of the process by increasing solids loading and mixing quality, another novel tubular radial-flow MBR was designed. The effectiveness of the inverted dead-end MBR versus radial-flow MBR designs was assessed using real, complex lignocellulose biomass, namely date seeds (DSs). The tubular radial-flow MBR used here had more than a 10-fold higher membrane surface area than the flat-sheet MBR design. With simultaneous product separation using the flat-sheet inverted dead-end filtration MBR, a total reducing sugars yield of 10.8% from pretreated DSs was achieved within 8 h of reaction, which was three times higher than the yield without product separation, which was only 3.5% within the same time and under the same conditions. The superiority of the tubular radial-flow MBR to hydrolyze pretreated DSs was

confirmed with a total reducing sugars yield of 29% within 8 h. A detailed kinetic model was developed to predict the dynamic behavior of the tubular radial-flow MBR, and the kinetic parameters were estimated from the experimental data. The novel reactor was proved to successfully operate at high solids loading, and with a developed statistical non-linear interactive model the total reducing sugars production was optimized with optimal conditions of substrate concentration of 28.9 g/L and water flowrate of 1.2 mL/min resulting in a maximum glucose production of 8.7 g. In addition, the effects of different glucose concentrations, water flowrates, and membrane cut-offs on glucose diffusion were studied. The promising results obtained by this research could pave the way for an economic lignocellulose-to-bioethanol process.

Keywords: Cellulose, Enzymatic hydrolysis, Kinetic model, Membrane bioreactor, Product inhibition, Product separation, Substrate inhibition.

Title and Abstract (in Arabic)

المفاعل الحيوي الغشائي لتعزيز التحلل المائي الأنزيمي للسليولوز

الملخص

مع تزايد المخاوف البيئية المتعلقة باستخدام الوقود الأحفوري واستنفاد هذه الموارد، يتزايد الاهتمام بالإيثانول الحيوي من النفايات السليولوزية كبديل، مصدر طاقة مستدام. تعتبر مخلفات نخيل التمر من المواد الأولية الجيدة لإنتاج البيويثانول، خاصة في البلدان التي تضم مزارع نخيل التمر الكبيرة، مثل الإمارات العربية المتحدة.

في عملية تحويل المواد السليولوزية إلى البيويثانول، فإن التحلل المائي الأنزيمي للسليولوز لإنتاج السكريات البسيطة التي يمكن تحويلها إلى إيثانول حيوي عن طريق التخمر هو الخطوة الأكثر تحديًا، وتعزيزها ضروري للتشغيل الفعال والمجدي. يعد تثبيط الإنزيم بواسطة المنتجات أحد المشكلات العديدة التي تعيق التحويل الحيوي للسليولوز. لحل هذه المشكلة، تم تصميم مفاعل حيوي غشائي جديد (MBR) بمفهوم ترشيح نهاية مسدود مقلوب للإزالة المتزامنة للمنتج أثناء التفاعل. تم استخدام أغشية البولي إيثير سلفون (PES)، وتم إثبات انتقائها في السماح بنفاذ المنتج فقط. تم دراسة تأثير تدفق الماء والتركيز الأولي للركيزة، وتم تطوير نموذج حركي رياضي شامل يعتمد على الخطوات الميكانيكية للتنبؤ بالسلوك الديناميكي للنظام، وتم تقدير المعلمات الحركية من خلال ملاءمة البيانات التجريبية. كما تم استخدام النتائج التجريبية لتطوير نموذج إحصائي تفاعلي غير خطي. باستخدام السليولوز القياسي، زاد إنتاج الجلوكوز من 7% دون فصل المنتج إلى 45% مع فصل المنتج. أظهر كلا النموذجين الحركي والإحصائي توافق جيد ($R^2: 0.96$ و 0.97 على التوالي). تم تحسين العملية وتم تحديد الظروف المثلى لتكون عند تركيز الركيزة 2.67 جم / لتر وتدفق ماء قدره 0.8 مل / دقيقة، حيث تم تحقيق أقصى عائد 86.7%.

لزيادة كفاءة العملية عن طريق زيادة جودة التخمير والخلط الصلبة، تم تصميم مفاعل آخر جديد للتدفق الشعاعي نصف قطري. تم تقييم فعالية المفاعل المسدود المقلوب مقابل تصميمات MBR ذات التدفق الشعاعي باستخدام الكتلة الحيوية الحقيقية والمعقدة من السليولوزية، وهي بذور التمر. بذور التمر يحتوي MBR الأنوبي ذو التدفق الشعاعي المستخدم هنا على مساحة سطح غشاء أعلى بمقدار 10 أضعاف من تصميم MBR ذي الصفيحة المسطحة. مع فصل المنتج المتزامن باستخدام الترشيح المسدود المقلوب ذو الطرف المسدود MBR، تم تحقيق عائد جلوكوز بنسبة 10.8% من DSs المُعالجة مسبقًا خلال 8 ساعات من التفاعل، وهو أعلى بثلاث مرات من الناتج دون فصل المنتج، والذي كان 3.5% فقط في نفس الوقت وبنفس الشروط. تم تأكيد تفوق MBR الأنوبي ذو التدفق الشعاعي على DSs المُعالجة بالماء مع عائد جلوكوز بنسبة 29% خلال 8 ساعات. تم تطوير نموذج حركي مفصل للتنبؤ بالسلوك الديناميكي للتدفق الشعاعي الأنوبي MBR، وتم تقدير المعلمات الحركية من البيانات التجريبية. ثبت أن المفاعل الجديد يعمل بنجاح عند تحميل صلب عالٍ، وباستخدام نموذج إحصائي تفاعلي غير خطي مطور، تم تحسين إنتاج الجلوكوز الكلي بالظروف المثلى لترابط الركيزة البالغ 28.9 جم / لتر ومعدل تدفق الماء 1.2 مل / دقيقة مما أدى إلى يبلغ الحد الأقصى لإنتاج الجلوكوز 8.7 جم. بالإضافة إلى ذلك، تمت دراسة تأثير تركيزات الجلوكوز المختلفة، ومعدلات تدفق المياه، وانقطاعات الأغشية على انتشار الجلوكوز. النتائج الواعدة التي تم الحصول عليها من خلال هذا البحث يمكن أن تمهد الطريق لعملية اقتصادية من السليولوزية إلى البيويثانول.

مفاهيم البحث الرئيسية: السليلوز، التحلل الأنزيمي، النموذج الحركي، المفاعل الحيوي الغشائي، تثبيط المنتج، فصل المنتج، تثبيط الركيزة.

Abstract (Dutch)

Met de toenemende bezorgdheid over het milieu over het gebruik van fossiele brandstoffen en de uitputting van deze hulpbronnen, is de belangstelling voor bio-ethanol uit lignocellulose-afval als alternatieve, duurzame energiebron toegenomen. Afval van dadelpalm wordt beschouwd als een goede grondstof voor de productie van bio-ethanol, vooral in landen met grote dadelpalmplantages, zoals de Verenigde Arabische Emiraten.

In het proces van lignocellulose naar bio-ethanol is de enzymatische hydrolyse van celluloses om eenvoudige suikers te produceren die door fermentatie in bio-ethanol kunnen worden omgezet, de meest uitdagende stap, en het verbeteren ervan is essentieel voor een efficiënte en haalbare werking. Enzymremming door de producten is een van de vele problemen die de bioconversie van cellulose belemmeren. Om dit probleem op te lossen, werd een nieuwe membraanbioreactor (MBR) ontworpen met een omgekeerd 'dead-end' filtratieconcept voor gelijktijdige verwijdering van het product tijdens de reactie. Er werden polyethersulfonmembranen (PES) gebruikt en hun selectiviteit bij het toestaan van alleen productpermeatie werd bewezen. De effecten van waterflowrate en initiële substraatconcentratie werden onderzocht, en een grondig wiskundig kinetisch model dat was gebaseerd op de mechanistische stappen werd ontwikkeld om het dynamische gedrag van het systeem te voorspellen, en de kinetische parameters werden geschat door de experimentele gegevens te fitten. De experimentele resultaten werden ook gebruikt om een statistisch niet-lineair interactief model te ontwikkelen. Bij gebruik van standaardcellulose nam de opbrengst aan glucoseproductie toe van 7% zonder productscheiding tot 45% met productscheiding. Zowel kinetische als statistische modellen lieten een goede overeenkomst zien (R^2 : respectievelijk 0.96 en 0.97). Het proces werd geoptimaliseerd en de optimale omstandigheden werden bepaald op een substraatconcentratie van 2,67 g/L en een waterflowrate van 0,8 ml/min, waarbij een maximale opbrengst van 86,7% werd bereikt.

Om de efficiëntie van het proces te verhogen door de kwaliteit van het laden en mengen van vaste stoffen te verhogen, werd een andere nieuwe buisvormige MBR met radiale stroming ontworpen. De effectiviteit van de omgekeerde 'dead-end' MBR versus radiale stroom MBR-ontwerpen werd beoordeeld met behulp van echte, complexe lignocellulose-biomassa, namelijk dadelzaden (DS's). De hier gebruikte buisvormige MBR met radiale stroming had een meer dan 10 keer groter membraanoppervlak dan het MBR-ontwerp met vlakke plaat. Met gelijktijdige

productscheiding met behulp van de platte-vel omgekeerde dead-end filtratie MBR, werd een glucoseopbrengst van 10,8% uit voorbehandelde DS's bereikt binnen 8 uur na de reactie, wat drie keer hoger was dan de opbrengst zonder productscheiding, die slechts 3,5% was binnen dezelfde tijd en onder dezelfde voorwaarden. De superioriteit van de buisvormige MBR met radiale stroming om voorbehandelde DS's te hydrolyseren werd binnen 8 uur bevestigd met een glucoseopbrengst van 29%. Er werd een gedetailleerd kinetisch model ontwikkeld om het dynamische gedrag van de buisvormige MBR met radiale stroming te voorspellen, en de kinetische parameters werden geschat op basis van de experimentele gegevens. De nieuwe reactor bleek succesvol te werken bij een hoge vastestofbelasting, en met een ontwikkeld statistisch niet-lineair interactief model werd de totale glucoseproductie geoptimaliseerd met optimale omstandigheden van substraatovereenstemming van 28,9 g/L en een waterstroomsnelheid van 1,2 ml/min, resulterend in een maximale glucoseproductie van 8,7 g. Daarnaast werden de effecten van verschillende glucoseconcentraties, waterstroomsnelheden en membraanafsnijdingen op glucosediffusie bestudeerd. De veelbelovende resultaten van dit onderzoek kunnen de weg vrijmaken voor een economisch lignocellulose-naar-bio-ethanolproces.

Trefwoorden: Cellulose, Enzymatische hydrolyse, Kinetisch model, Membraanbioreactor, Productremming, Productscheiding, Substraatremming.

Acknowledgements

Who does not thank people, does not thank God. Hence, I would like to express my deepest appreciation to my advisors; Professor Sulaiman Al-Zuhair and Professor Bart Van der Bruggen. Thank you for being supportive, guiding, and a role model for how an advisor should be, I am extremely fortunate to be your student. I am extremely grateful to my co-advisors, Professor Boguslaw Kruczek, Dr. Emad Elnajjar, Professor Raed Hashaikeh for their continuous support and feedback, the completion of my work would not have been possible without them. I would also like to extend my deepest gratitude to my examination committee, Professor Grant Allen, Professor Pedro Fardim, Dr. Lise Appels, and Professor Basim Abu-Jdayil for their efforts and time.

My father who is the greatest person in my life, my mother who believed and supported me when no one else did, my special one that without this journey will not be achieved, my brothers who backed up me when I needed them the most especially in the past three years, I am deeply indebted to all of you.

Dedication

To my beloved precious father, mother, and family

Table of Contents

Title	i
Declaration of Original Work	ii
Advisory Committee	iv
Approval of the Doctorate Dissertation	v
Abstract	vii
Title and Abstract (in Arabic)	ix
Abstract (Dutch).....	xi
Acknowledgements	xiii
Dedication	xiv
Table of Contents	xv
List of Tables.....	xviii
List of Figures	xix
List of Abbreviations.....	xxii
Chapter 1: Introduction	1
1.1 Statement of the Problem	1
1.2 Research Objectives	1
1.3 Hypothesis and Novelty Statement	2
Chapter 2: Lignocellulosic Bioethanol Production	4
2.1 Ethanol Feedstock	4
2.2 Lignocellulose	5
2.2.1 Date Seeds	7
2.3 Lignocellulose to Bioethanol Process	8
2.3.1 Pretreatment	8
2.3.2 Hydrolysis	14
2.4 Enzyme Kinetics and Modeling	16
Chapter 3: Challenges of lignocellulose Enzymatic Hydrolysis and Potential Solutions.....	21
3.1 Heterogeneous Mixture	21
3.2 Enzyme Inhibition	21
3.3 Immobilization: Solution for Heterogeneous Mixture Challenge.....	23
3.4 Membrane Technology: Solution for Product Inhibition Challenge.....	24
3.4.1 MBRs Configurations	25
3.4.2 Membrane Selection.....	30
3.4.3 Key Factors Affecting the Performance of MBRs	31
Chapter 4: Materials and Methods	37

4.1 Chemical and Enzymes	37
4.2 MBR with Inverted Dead-end Filtration Concept.....	38
4.2.1 The MBR Design	38
4.2.2 Standard Cellulose Hydrolysis with Product Separation	41
4.2.3 Kinetic Model.....	42
4.3 Radial-flow Tubular MBR	46
4.3.1 Radial-flow MBR Design.....	46
4.3.2 Enzymatic Hydrolysis with Product Separation.....	50
4.3.3 Kinetic Modeling.....	50
4.4 Glucose Permeation Analysis	55
4.5 Analytical Methods	56
4.5.1 Total Reducing Sugars Analysis	56
4.5.2 Protein Analysis	56
4.5.3 Enzyme Assay	57
4.5.4 Biomass Characterization.....	57
4.5.5 Membrane Characterization	59
Chapter 5: Results and Discussion	61
5.1 Inverted Dead-end MBR.....	61
5.1.1 Selective Glucose Permeation.....	61
5.1.2 Effect of the Process on the Membranes.....	64
5.1.3 Enzymatic Hydrolysis with Product Separation.....	69
5.1.4 Effects of the Substrate Concentration and Water Flowrate on Standard Cellulose Hydrolysis.....	71
5.1.5 Evaluation of the Kinetic Model Parameters	74
5.1.6 Statistical Analysis	77
5.2 Radial-flow Tubular MBR Analysis	79
5.2.1 Biomass Characterization and the Effect of Pretreatment on Substrate.....	79
5.2.2 Enzymatic Hydrolysis with Product Separation.....	84
5.2.3 Effects of the Substrate Concentration and Water Flowrate on DSs Hydrolysis.....	89
5.2.4 Kinetic Model.....	95
5.2.5 Sensitivity Analysis.....	98
5.2.6 Statistical Analysis	99
5.3 Glucose Permeation	102
5.3.1 Parametric Study	102
5.3.2 Statistical Analysis	106
Chapter 6: Conclusion and Future Perspectives.....	110
6.1 Conclusion.....	110
6.2 Future Perspectives	111
References	113
List of Publications	132

Appendix 133

List of Tables

Table 1: Applications of integrated membrane bioreactors (MBRs) in enzymatic hydrolysis of cellulose	27
Table 2: Summary of factors to be considered for enhanced production yield in MBRs	35
Table 3: Summary of advantages and disadvantageous of different MBR designs.....	36
Table 4: Levels of two factors affecting the glucose production in the enzymatic hydrolysis of cellulose	42
Table 5: Levels of two factors affecting total reducing sugars production in the enzymatic hydrolysis of the substrate	50
Table 6: Levels of the factors tested on diffusion of glucose through PES membranes	56
Table 7: Estimations of the kinetic model parameters	75
Table 8: Total glucose yield after 6 h at different substrate concentrations (X_1) and water flowrates (X_2)	77
Table 9: Response surface regression analyses of product yield versus substrate concentration (X_1) and water flowrate (X_2)	78
Table 10: Kinetic model parameters estimation.....	97
Table 11: Response Surface Regression: product produced versus substrate concentration and water flowrate	100
Table 12: Total reducing sugars produced after 8 h at different substrate concentrations (X_1) and water flowrates (X_2).....	102
Table 13: Response surface regression analysis of glucose permeation rate versus glucose concentration (X_1), water flowrates (X_2), and MWCOs (X_3)	107
Table 14: Glucose permeation rate after 3 h at different glucose concentrations (X_1), water flowrates (X_2), and MWCOs (X_3)	108

List of Figures

Figure 1: Schematic diagram of the lignocellulosic structure composed of cellulose, hemicellulose, and lignin.....	6
Figure 2: Biorefinery process of ethanol production from lignocellulosic feedstock.....	8
Figure 3: A schematic diagram of the bioconversion of lignocellulosic biomass to fermentable glucose.....	15
Figure 4: Reaction mechanism of enzymatic hydrolysis of cellulose.....	17
Figure 5: Schematic diagrams of different MBR configurations.....	29
Figure 6: Filter cake formation in dead-end MBR on membrane surface.....	34
Figure 7: Schematic diagram of the inverted dead-end MBR.....	38
Figure 8: Radial-flow MBR design.....	47
Figure 9: Flow diagram of (A) inverted dead-end, and (B) radial flow tubular MBRs.....	49
Figure 10: Yields of permeated glucose and cellulase to the upper cell through PES-30, at pH 4.8, 48°C, water flow of 0.4 mL/min ($\tau = 15.6$ h) and initial glucose and cellulase concentrations of 40 g/L and 3.2 g/L, in the lower cell respectively.....	63
Figure 11: Effect of initial concentration, C_0 , on the permeated glucose through PES-30 membrane by pure natural diffusion.....	64
Figure 12: Cross-sectional SEM images of PES membrane (A) PES-10 before the process, (B) PES-10 after the process, (C) PES-30 before the process, and (D) PES-30 after the process.....	65
Figure 13: FTIR spectra of the investigated PES membranes.....	68
Figure 14: XRD of the investigated PES membrane, PES-10 and PES-30, before and after the process.....	69
Figure 15: Comparison in glucose production yield in MBR with and without glucose separation under the same conditions using substrate and cellulase concentrations of 6.67 g/L and 0.48 g/L, at pH 4.8 and 48°C and water flow of 0.4 mL/min ($\tau = 31.3$ h).....	70
Figure 16: Total glucose yields, and glucose produced in reaction cell operated using PES membranes of different molecular weight cutoffs with initial substrate and cellulase concentrations of 6.67 g/L and 0.48 g/L, respectively, and a water flowrate of 0.4 mL/min ($\tau = 31.3$ h), at 48°C and a pH of 4.8. Acc, accumulated glucose in the reaction cell; FR, water flow flowrate; Tot, total glucose yield; C_0 , substrate concentration.....	71
Figure 17: Total glucose yield and glucose produced in reaction cell operated using a PES-10 membrane with constant substrate and cellulase concentrations of 13.33 g/L and 0.48 g/L, respectively, and different water flowrates, at 48°C and a pH of 4.8 Acc, accumulated glucose in the reaction cell; FR, water flowrate (mL/min); τ , residence time (h); Tot, total glucose yield; C_0 , substrate concentration.....	72

Figure 18: Total glucose yields and glucose produced in reaction cell operated using a PES-10 membrane with different substrate concentrations, a cellulase concentration of 0.48 g/L, and a water flowrate of 0.8 mL/min ($\tau = 15.6$ h). At 48°C and a pH of 4.8 Acc, accumulated glucose in the reaction cell; FR, water flow flowrate; Tot, total glucose yield; Co, substrate concentration.....	74
Figure 19: Three-dimensional plot of total glucose yields as a function of the substrate concentration and water flowrate after 6 h of enzymatic hydrolysis at 48°C and a pH of 4.8 using the polyethersulfone PES-10 membrane for product separation.	79
Figure 20: X-ray diffraction spectra of fresh, HCl+NaOH pretreated, and NaOH pretreated DSs	81
Figure 21: Fourier-transform infrared spectra of fresh, HCl+NaOH pretreated, and NaOH pretreated DSs	83
Figure 22: Scanning electron microscopy images of (A) fresh, (B) HCl+NaOH pretreated, and (C) NaOH pretreated DSs.....	84
Figure 23: Production yield from NaOH pretreated DSs with and without permeation, and standard cellulose with permeation in the inverted dead-end MBR using substrate and enzyme concentrations of 13.3 g/L and 0.48 g/L, respectively, at pH 4.8, 48°C, and water flowrate of 0.8 mL/min ($\tau = 15.6$ h)	87
Figure 24: Reducing sugars production yield from NaOH pretreated DSs using inverted dead-end MBR and radial flow MBR, using substrate and enzyme concentrations of 13.3 g/L and 0.48 g/L, respectively at pH 4.8, 48°C, and water flowrate of 0.8 mL/min ($\tau = 15.6$ h).....	89
Figure 25: Total reducing sugars produced using different water flowrates of 0.4, 0.8, and 1.2 mL/min ($\tau = 31.3, 15.6,$ and 10.4 h, respectively), and substrate concentrations of (A) 14.3 g/L, (B) 21.4 g/L, and (C) 39.6 g/L, operated at pH 4.8, 48°C, enzymes concentration of 0.48 g/L and PES-10	91
Figure 26: Total reducing sugars production after 8 h using different water flowrates of 0.4, 0.8, and 1.2 mL/min ($\tau = 31.3, 15.6,$ and 10.4 h, respectively), and substrate concentrations of 14.3 g/L, 21.4 g/L, and 39.6 g/L, (A) total reducing sugars produced, g, and (B) total reducing sugars yield, %. At pH 4.8, 48°C, enzymes concentration of 0.48 g/L and PES-10	95
Figure 27: Comparison between the experimentally determined total reducing sugars produced and the kinetics model predictions at pH 4.8, 48°C, enzymes concentration of 0.48 g/L, PES-10, and the center water flowrate of 0.8 mL/min ($\tau = 15.6$ h) (<i>i.e.</i> , X_2 factor level of zero) different initial substrate concentrations.....	97
Figure 28: Sensitivity analysis of estimated parameters on the total reducing sugars produced.....	99
Figure 29: 3-D plot of total reducing sugars produced using PES-10 after 8 h. Operated at pH 4.8 and 48°C as a function of substrate concentration and water flowrate....	101

Figure 30: Effects of initial glucose concentrations, C_0 (g/L), and water flowrates, FR (mL/min), corresponding to residence time, τ (h), on permeated glucose through PES-10 membrane.	103
Figure 31: Glucose permeation rate using PES-30 at (A) 0.4 mL/min ($\tau = 31.3$ h) water flowrate and different initial glucose concentrations, (B) glucose concentration of 40 g/L and different water flowrates and (C) glucose concentration of 40 g/L, 0.4 mL/min ($\tau = 31.3$ h) water flowrate and different MWCOs.....	105
Figure 32: Combined effects of initial glucose concentration and water flowrate on glucose permeation rate through PES-10 membrane	109

List of Abbreviations

k_{-s}	Backward Rate Constant for Reversible ES Intermediate Formation
k_{c2}	Backward Rate Constant for the Reversible ES_c Intermediate Formation
k_{x2}	Backward Rate Constant for the Reversible Non-Productive ES_x Intermediate Formation
k_{EP2}	Backward Rate Constants for the Competitive Inhibition
$[P]$	Concentration of the Glucose
P	% Change in the Total Glucose Produced
CBR	Continuous Bioreactor
CA	Cellulose Acetate
DSs	Date Seeds
DNS	Dinitrosalicylic Acid
E	Enzyme
EP	Enzyme-Product Complex
ES	Enzyme-Substrate Complex
k_s	Forward Rate Constant Reversible ES Intermediate Formation
k_{EP}	Forward Rate Constant for the Competitive Inhibition
k_{c1}	Forward Rate Constant for the Reversible ES_c Intermediate Formation
k_{x1}	Forward Rate Constants for the Reversible Non-Productive ES_x Intermediate Formation
k_{EP1}	Forward Rate Constants for the Competitive Inhibition Of The Product

FTIR	Fourier-Transform Infrared
S_c	Hydrolyzable Substrate
h	Height
HCl	Hydrochloric Acid
$[S_0]$	Initial Substrate Concentration
ID	Internal Diameter
MBR	Membrane Bioreactor
MWCO	Molecular Weight Cut-Off
K_c	Mass Transfer Coefficient
NF	Nanofiltration
NY	Nylon
ϕ	Non-Hydrolyzable Fraction Coefficient
S_x	Non-Hydrolyzable Substrate
P	Product
C_A	Product Concentrations in the Solid
$C_{A\infty}$	Product Concentrations in the Solution
n_g	Permeation Rate
PES	Polyethersulfone
PS	Polysulfone
PVP	Poly Vinyl Pyrrolidone
k_p	Rate Constant for the Surface Reaction
A_s	Surface Area of the Solid
$[S]$	Substrate Concentration
v	Superficial Velocity

SEM	Scanning Electron Microscopy
NaOH	Sodium Hydroxide
STR	Stirred Tank Reactor
σ	Substrate Accessibility Coefficient
t	Time
Y	Total Glucose Yield
UF	Ultrafiltration
V_c	Volume of the Solid
V_t	Volume of the Total Solution
V	Volume of the Reaction Cell
XRD	X-Ray Diffraction

Chapter 1: Introduction

1.1 Statement of the Problem

The bioconversion process of lignocellulose to ethanol is considered a promising method to satisfy the need for alternative, sustainable, and environmentally friendly energy sources instead of the depleting fossil fuels. Date palm trees are predominating on the farmland of the Middle East, with their cellulose rich parts, the accumulation of the waste is an issue that is annually increasing, especially in the United Arab Emirates (UAE) [1]. Deploying enzymes for the conversion of lignocellulose to mono-sugars, which is the feed for ethanol production, has attracted attention for decades. However, the kinetics of enzymatic hydrolysis are slow in nature and the lignocellulose is of a complex structure. Combining these two facts results in a complicated process that needs to be deeply understood to overcome its drawbacks and enhance its economic feasibility. The two main problems of the enzymatic hydrolysis are enzymes inhibition with the product and the heterogeneous nature of the substrate. As the hydrolysis reaction progresses, glucose is produced and accumulated in the system, which reduces the activity of the enzyme. This is referred to as product inhibition. It would be very costly to continuously replace the deactivated enzymes. In addition, in a continuous process, the enzyme needs to be retained inside the reactor for repeated uses and elimination of loss from the system with the effluents and products. The conventional way to confine enzyme within the reactor is to use it in immobilized form. However, this is not possible with cellulose hydrolysis, as the substrate itself is heterogeneous. Hence, there is a need for a system that tackles the product accumulation and enzyme confinement to improve the kinetics of the reaction and the reusability of the enzyme.

1.2 Research Objectives

To enhance the enzymatic hydrolysis of cellulose and reduce the total biorefinery cost two major challenges must be overcome: product inhibition and low solid loading. To solve these

issues, a continuous reactor and an ultrafiltration membrane are integrated in a system to allow enhancing the enzymatic hydrolysis of cellulose through continuous removal of the product. The membrane should have the capability to filter only the desired product and reject enzymes to allow its repeated use. This is hypothesized to enhance the kinetics of the reaction and lower the cost of the process. Experimental analysis is used to prove this concept and determine the dynamic model of the system in the integrated membrane MBR system.

The main objective of this work is to design and test novel MBRs for enhanced hydrolysis of lignocellulose from date palm waste to be used as a real biomass for bioethanol production. Accordingly, the objectives of this work are as follows:

- Experimental analysis of simultaneous reaction and product separation through a membrane reactor will be used to develop a reliable kinetic model to describe the process;
- Enzymatically convert cellulose from date palm waste to fermentable glucose for bioethanol production;
- Design and operate a novel MBR adapting an inverted dead-end filtration concept to eliminate the membrane fouling and enhance the hydrolysis yield;
- Develop a model for the inverted dead-end MBR considered both the reaction kinetics and the convective diffusion;
- Design and operate a radial flow tubular MBR of enhanced hydrolysis yield through high solids loading and enhanced product diffusion;
- Develop a model for the radial flow tubular MBR considering the reaction kinetics, the dynamic changes in the substrate structure, and with simultaneous product separation.

1.3 Hypothesis and Novelty Statement

The use of ultrafiltration membranes to simultaneously remove glucose from the reaction is proposed to improve glucose production and retain the enzymes. The novelty of this research

is in the designed MBRs, including both the inverted dead-end and the radial flow tubular MBR, and the detailed analysis of the product diffusion out of the reaction system and its effect on the reaction. The hypothesis will be tested in both MBRs and the effect of the main key factors will be determined. A model that combines reaction kinetics with product separation will be developed, which helps in better understanding of the system. The use of the system for the hydrolysis of waste biomass abundantly available in the UAE will be another novel aspect of this work presenting realistic results.

Chapter 2: Lignocellulosic Bioethanol Production

The concurrent increase in population and industrialization resulted in an escalation in energy demand, with fossil fuels being the main source [2]. However, fossil fuels are nonrenewable resources of energy and their use has an adverse impact on the environment [3]. Therefore, finding a more sustainable and greener source of energy is a necessity [4]. Biofuels, which are renewable energy sources produced from biomass, have been receiving an increasing attention as potential substitutes for fossil fuel, particularly in the transport sector, due to their sustainability and low environmental impact [4]. Bioethanol is a biofuel that is used as an additive to petrol derived gasoline in conventional engines to reduce the harmful impacts of combustion emissions and can also be used pure in slightly modified engines. Brazil for example depends heavily on bioethanol, produced from sugarcane, as an energy source, accounting for 18% of the total energy consumption in the nation [5]. However, sugarcane and other conventional feedstock that are considered food stock are not preferred to be used for energy production. Lignocellulosic biomass on the other hand is considered more appropriate, as it is generally not used as a direct feed source and most of it is considered biomass waste, making it a sustainable feedstock for biofuels production [6–8]. However, this type of biomass is considered recalcitrant, due to the presence of lignin, which is strongly linked to the cellulose forming a protection shield. In addition, the cellulose structure in most lignocelluloses is highly crystalline, rendering incomplete enzymatic hydrolysis inevitable [9, 10]. Different approaches have been used to separate the cellulose from other components in the lignocellulosic structure before converting it to sugars that can be easily converted to bioethanol by fermentation [11].

2.1 Ethanol Feedstock

Biomass feedstock is a material of biological origin that can be converted to different bio-based products such as ethanol in a biorefinery. There are three types of biomass feedstocks based

on the composition and the origin of the biomass: first-generation, second- and third-generation feedstock [12].

First-generation biomass is edible biomass that is easy to process. The most common types of the first-generation feedstock for ethanol production are starch-rich and sugar crops. Sugar crops, such as sugar cane, sugar beet, and sugar sorghum are biomass composed mainly of mono or disaccharides. Starch-rich crops, such as corn and wheat, are composed primarily of starch. Due to their composition, the conversion of those feedstocks to bioethanol is easy and inexpensive [13].

Lignocellulose and algae are examples of second- and third-generation feedstock, which comprises non-food part residues. Unlike the first-generation biomass, lignocellulosic biomass is the inedible part of the plant, which is composed mainly of cellulose, hemicellulose, and lignin. Agricultural waste, such as straw, corn stover, corn cob and bagasse, forestry wastes, like wood chips, and municipal and industrial wastes are all examples of lignocellulosic biomasses that can be used for ethanol production. Algae biomass, on the other hand, are composed of triglycerides, which can be utilized for the production of other energy products besides the carbohydrates that can be used for ethanol production [13].

2.2 Lignocellulose

Lignocellulose is composed of three main components, cellulose, hemicellulose, and lignin. Other components are also found in smaller amounts in the structure, such as extractives and ash. Lignocellulose is predominated by cellulose consisting of 40-50% of the total structure, followed by hemicellulose, which is estimated to be 25-30%, and lastly 15-20% lignin [14]. A schematic diagram of the lignocellulosic structure is shown in Figure 1.

Cellulose is composed of repeated units of cellobiose, which constitutes two glucose molecules linked together by β -1,4 glycosidic linkage. Repeated units of glucose give rise to a

glucan unit, which is estimated to be between 2000 to 2700 units [15]. The degree of polymerization is determined by the glucan units contained in the cellulose structure [16]. The polymer chains constituting cellulose are linked through covalent and non-covalent bonds forming microfibrils [17]. The structure of cellulose is dominated by a crystalline structure in which the microfibrils are arranged in parallel, while the rest of the structure is amorphous [18].

Hemicellulose is made of repeated units of different sugar monomers, including xylose, arabinose, mannose, galactose, and glucose. The sugar monomer composing the chain is determining the type of hemicellulose, which can be either linear or branched, surrounding the cellulose [19]. Lignin, on the other hand, is composed of phenylpropane units, which each is composed of coumaryl alcohol, coniferyl alcohol, and sinapyl alcohol. Lignin is known to have a three-dimensional structure linked to the remaining components, hemicellulose and cellulose, thus providing rigidity to the cell wall and protection from the activity of the microorganisms and other environmental factors [20].

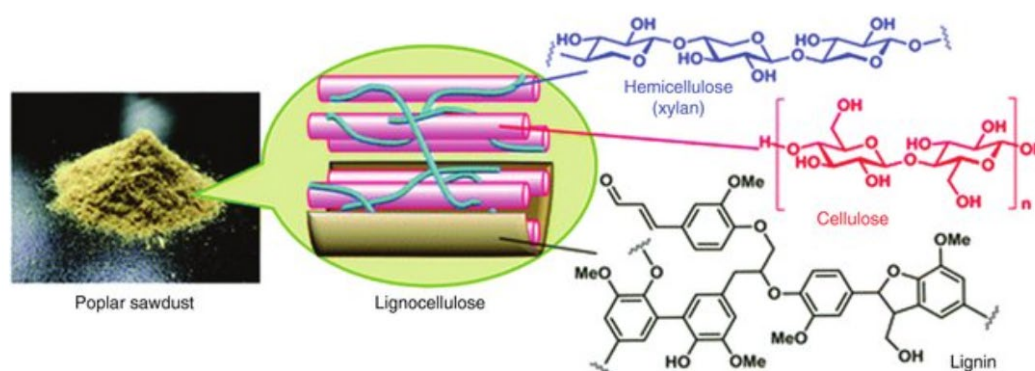


Figure 1: Schematic diagram of the lignocellulosic structure composed of cellulose, hemicellulose, and lignin [21]

2.2.1 Date Seeds

Date palms, *Phoenix dactylifera*, is an abundant bio-source in the Middle East [22]. Statistics show that 83.7% of the total global production of dates comes from the Middle East, with the United Arab Emirates being one of the world top 10 producers [23]. The different wastes produced from the date palms, such as date fruit, dry dates, petiole, leaf axis, and date seeds, are potential feedstock for energy production [24]. Between the years 2010 and 2013, the annual world production of dates increased from 7 million tons to 7.63 million tons, with an average yield of 6.86 tons per hectare [25]. As date seeds (DSs) account for around one-third the date fruit weight [25], its production rate exceeds one million ton per year [26].

The composition of DSs differs for different cultivars, growth conditions, fertilizers used, and fruit maturity [26]. However, their general composition has been reported to be 5.1–6.5% protein, 9–12.7% oil, 1.1–1.2% ash, and 73.1–83.1% total carbohydrate on a dry weight basis [25]. The high carbohydrates content makes DSs a potential feedstock for producing fermentable sugars for bioethanol production [25]. Similar to other lignocellulosic biomass, DSs are mainly composed of cellulose, hemicellulose, and lignin [27]. The mass percentages of the three components in the lignocellulosic biomasses are reported to be 40-50 wt% cellulose, 15-30 wt% hemicellulose, and 20-30 wt% lignin [28]. Besides cellulose, which is mainly composed of glucose [29], hemicellulose is also a sugar polymer. Analysis of hemicellulose from date seeds show that the largest component is xylose, accounting for 21.9 wt%, followed by uronic acid at 4.3 wt%, arabinose 1.2 wt%, and traces of mannose, galactose, and glucose [30]. The analysis of lignin, on the other hand, comprised of oxygenated phenyl propane units of three alcohols, namely coniferyl, sinapyl, and *p*-coumaryl [31].

2.3 Lignocellulose to Bioethanol Process

A representative diagram of ethanol production from lignocellulosic feedstock is shown in Figure 2. The process includes size reduction through mechanical methods, followed by pretreatment in which the biomass structure is further disrupted and separated. Hydrolysis comes then, which is the scope of this work, where the polysaccharides are broken down into monomers such as glucose, xylose, and arabinose. Fermentation is where the simple sugars are converted to ethanol.

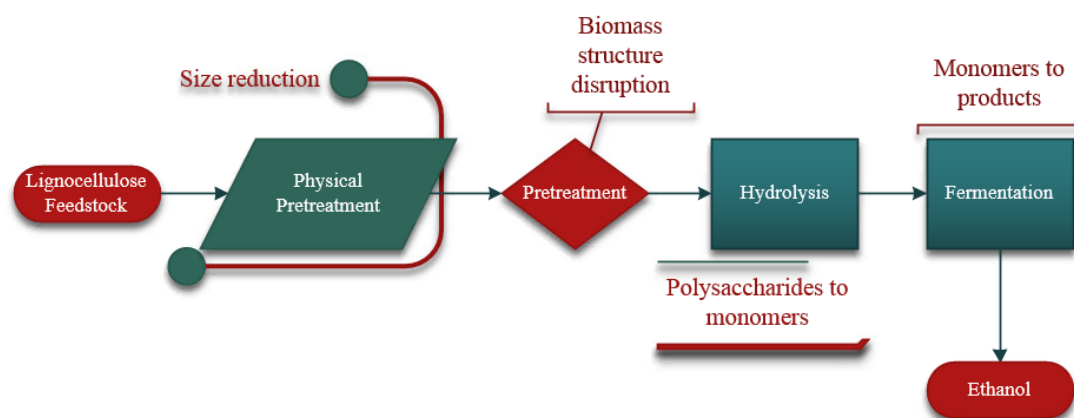


Figure 2: Biorefinery process of ethanol production from lignocellulosic feedstock

2.3.1 Pretreatment

Pretreatment is the step in which the lignocellulose biomass is converted from being recalcitrant to a form ready for the enzymatic hydrolysis [32]. An efficient pretreatment must be able to recover the full lignocellulosic components with fewer degradation byproducts. In addition, it must be feasible and effective on different biomass quantities and types [32]. There are different types of pretreatment methods used for lignocellulosic biomass that can be classified into physical, chemical, and biological pretreatments.

2.3.1.1 Physical Pretreatment

Most of the biochemical conversion processes involve physical pretreatment as a first step to reduce the particle size, which increases the surface area to volume ratio, and reduces the degree of polymerization and crystallinity of the biomass, thus, enhancing the conversion rate [33]. The enzymatic hydrolysis of cotton cellulose was enhanced with a glucose yield up to 99.8% in 50 h when the particle size was reduced from 25 to 0.78 μm [34]. There are different types of physical treatments such as chipping, shredding, milling, and grinding; these differ in the end particle size. In general, decreasing the particle size below 0.3 mm was proved to increase the conversion yield of glucose [35].

2.3.1.2 Chemical Pretreatment

Acidic pretreatment

Hemicellulose and cellulose are partially solubilized by both diluted and concentrated acids. However, the concentrated acids are not favored due to their severe effects on the biomass and the process, such as cellulose degradation and inhibitors production [36]. Dilute acids are used with a concentration a range of 0.5-2.5%, at a temperature range of 100 to 200°C [36]. Different studies have investigated the effect of dilute sulfuric acid pretreatment on enhancing the enzymatic hydrolysis step [37, 38]. Pretreating rice straw with 1% (w/w) sulfuric acid enhanced the efficiency of the enzymatic hydrolysis to reach 70% due to the increase in the pore volume of the biomass, which resulted in a glucose and xylose combined yield of 83% after 72 h [39]. Although the enzymatic hydrolysis is enhanced by this type of pretreatment, the partial hydrolysis of cellulose results in more crystalline cellulose, thus, lower the conversion yield compared to other pretreatment methods [40].

Alkaline pretreatment

Unlike the acid pretreatment, in the alkaline pretreatment, alkaline reagent interacts, breaks down, and isolate lignin only from the biomass, which can enhance the enzymatic hydrolysis with lower cost, and a simple process scheme [41]. The use of alkaline compounds such as sodium hydroxide, sodium carbonate and ammonia allows this pretreatment method to be superior over other methods due to the fact that these compounds are non-corrosive chemicals, requiring mild conditions [41]. In addition, this method is highly selective for lignin removal while retaining cellulose and hemicellulose intact, and the absence of inhibitors production enhances the fermentation step. It was found that pretreating rice straw with ultrasound-assisted alkaline (NaOH) improved the digestible cellulose yield by a factor of 3.5 compared to untreated biomass [42]. The suggested pretreatment method was found to increase the surface area accessible for cellulases, and increases the porosity compared to the same biomass treated with heat only. However, the crystallinity index in this pretreatment generally increases, which is primarily due to the lignin removal and not cellulose structural changes [41]. However, the degree of polymerization was found to decrease when the pretreatment with NaOH below 8 wt% concentration was carried out, which caused separation in the cellulose lattice [43]. In addition, pretreating sugarcane bagasse with 20% aqueous ammonia for 48 h at 50°C was found to result in 57.3% total sugar release in the subsequent enzymatic hydrolysis [44].

Oxidative pretreatment

Oxidizing agents like oxygen, ozone, and hydrogen peroxide are used remove lignin, however, a partial break of some of the hemicellulose is observed. In addition, those agents are not selective for only lignin, but they can attack cellulose and lead to the production of by-products such as aliphatic aldehydes and aliphatic organic acids, which inhibit the subsequent enzymatic hydrolysis [45]. This pretreatment method can be combined with other methods to improve the

degradation of lignocellulose and enhance the enzymatic hydrolysis. For example, corn stover was pretreated in a two-stage process, the first stage was the pretreatment with dilute hydrochloric acid (1 wt%) for 40 min at 120°C, followed by the second stage of alkaline wet oxidative pretreatment with 12.6 wt% ammonium hydroxide with pressurized oxygen (3 MPa) at 130°C for the same timing. This two-stages process was found to give around 86% lignin removal, 82.8% and 71.5% xylan, and glucan yields, respectively [46].

2.3.1.3 Physicochemical Pretreatment

This class of pretreatment changes the structure of the biomass both physically and chemically. There are different types used, such as solvent fractionation, steam explosion, liquid hot water, and carbon dioxide explosion.

Solvent fractionation

Solvent fractionation is the partial solubilization of lignocellulosic components through breaking down hydrogen bonds between the fibrils, which is due the fact that different lignocellulosic components have different solubilities in different solvents [33]. This type of pretreatment involves the use of organic solvents, ionic liquids, or phosphoric acid.

Organic solvents, such as ethanol in the presence of an acid catalyst, are used to extract lignin from the biomass and, thus, reduce the crystallinity [47]. However, some properties of those solvents have restricted the application of organosolv, organic solvents, as a pretreatment method. For example, the use of low boiling point organosolv, such as ethanol, acetone, methanol, and ethyl acetate [47], requires operating at high pressure. In addition, if those solvents are flammable, safety issues should be considered [48]. However, the fractionation of corn stover biomass using ethanol resulted in a 91% glucan content after lignin removal, while fractionation of giant miscanthus and wheat straw with ethanol was not efficient [49]. In addition, the use of organic amine, such as polyamine, as a catalyst to ethanol fractionation, showed to help in boosting the

delignification of corn stover biomass that removed 82% lignin and resulted in a sugar yield of 83% [50]. Furthermore, the combination of sulfuric acid and ethanol for wheat straw pretreatment was found to enhance the extraction of fermentable sugars to 89% in comparison with other organosolv tested, such as methanol, butanol, acetone, and diethylene glycol [51]. Although different solvents have been reported to fractionate lignocellulose, residence time, biomass loading, byproduct production, and structural disruption are all factors to be taken into consideration in selecting the most convenient pretreatment method. For example, using cellulose solvents, such as concentrated phosphoric acid, showed better structural disruption and 97% glucan yield in 24 h compared to the use of dilute sulfuric acid that attained 84% in 72 h, however, the effect of using such concentrated acids in inhibitor production was not reported [52, 53].

Ionic liquids (ILs) such as 1-allyl-3-methylimidazolium chloride [AMIMCl], -allyl-3-methylimidazolium acetate [EMIM][AC] and 1-butyl-3-methylimidazolium chloride [BMIMCl] showed to effectively solubilize cellulose from the biomass [54]. Due to the presence of anions such as chloride, cellulose can bind via hydrogen with the ionic liquid. Cellulose can be then recovered using an antisolvent such as water, which will break down these bonds, after which the recovery of the used IL is possible and can be reused [54]. Thus, pretreatment with ILs is an area of interest in research [55]. A sugar yield of 89% and 87% from sugarcane bagasse and wheat straw, respectively, were achieved with both biomasses pretreated with [EMIM][AC] [56]. Pretreating wheat straw with 1-ethyl-3-methyl-imidazolium acetate showed competitive results when followed by xylanases before cellulose hydrolysis, these two pre-steps helped in improving the accessibility of cellulose by the enzymes, which allowed for up to 99% cellulosic degradation, and 97.6% xylose yield [57].

Steam explosion

This commonly used pretreatment method involves the application of high pressure and temperature followed by a sudden decrement in the pressure leading to a break down in the lignocellulosic structure [58]. A better biomass disruption was found when steam explosion was combined with other pretreatment methods. For example, elephant grass was treated with different concentrations of sulfuric acid to yield around 52% digestible cellulose, while barley straw biomass pretreated with steam explosion and extrusion reached up to 84% glucan [59–63]. However, this pretreatment results in by-products production, similar to the dilute acid pretreatment, that inhibit the enzymatic hydrolysis, which requires a subsequent detoxification step before the enzymatic hydrolysis [64]. The formation of acetic acid, furfural, 5-HMF and vanillin showed insignificant inhibition on the cellulases, however, formic acid inactivated the enzymes, this effect increased with increasing the solids loading [65].

2.3.1.4 Biological Pretreatment

Biological pretreatment involves the use of bacterial and fungal strains, like *Bacillus sp*, *Trichoderma reesei*, *Thermomonospora sp*, and *Phanerochaete chrysosporium*, to degrade the lignocellulose structure [66, 67]. Due to the ability of these organisms to release enzymes such as lignin peroxidase and laccases, lignin is removed from the lignocellulosic structure [68]. The most applied fungus known for its ability to degrade lignocellulose is the white-rot fungus. Using *Ceriporiopsis subvermispora* to pretreat sugarcane bagasse at 27°C for 60 days resulted in 47% sugar yield [69]. The biological pretreatment advances on other pretreatment technology in that it is a non-energy requiring method, environmentally friendly, and cost-efficient. However, it is a time consuming pretreatment method, which results in low yield, rendering it feasibility in biorefinery processes [70].

2.3.2 Hydrolysis

There are different ways in which cellulose can be hydrolyzed to fermentable sugars. Chemical, biological, and other methods as well, such as gamma-ray, electron-beam, and microwave irradiation, which all have been reported. However, chemical and biological hydrolysis are the most commonly used due to their feasibility and effectiveness [71–73].

2.3.2.1 Chemical Hydrolysis

Chemical hydrolysis involves the use of chemicals, such as diluted and concentrated acids. The use of concentrated acid helps in enhancing the sugar yield and can be carried out under low temperatures compared to dilute acid hydrolysis. However, the acid consumption, in this case, is high, and further downstream processing, such as detoxification, is required. In addition, this process requires a long residence time, and it is costly to recover the acid for reuse. On the other hand, dilute acid hydrolysis has a lower yield, requires high temperatures, and non-useful byproducts are produced [74, 75].

2.3.2.2 Enzymatic Hydrolysis

The massive applications of different cellulases in various fields have attracted attention for their use in bioenergy production. The main sources of commercial cellulases are *Trichoderma reesei* and *Aspergillus niger* [76]. Cellulase plays a key role in the enzymatic hydrolysis. It is a multi-component system that breaks polymer chains into fermentable sugars, as shown in Figure 3 [77]. It is composed of three types of enzymes, endoglucanase, cellobiohydrolases (exoglucanase), and β -glucosidases. Endoglucanases work synergistically with exoglucanase, and the hydrolysis initiates with endoglucanase, which attacks the polymer chain at random sites creating reducing and non-reducing ends. Exoglucanase then acts on those ends to convert them to shorter polysaccharides chains consisting of two glucose units, called cellobiose. The last component, β -glucosidase, will break down cellobiose from the mid-point producing two glucose

units. The latter is considered the rate-limiting step for the hydrolysis due to its sensitivity of the enzymes towards the end product, glucose, leading to product inhibition [78]. Studies have shown that each cellulase-producing microorganism exhibits the lack of one or more types of cellulases leading to inefficient hydrolysis. *A. niger* and *Trichoderma atroviride* were found to be mostly β -glucosidases producers, and lack the other two [78]. Thus, different cellulase recipes from different sources are key to enhance the conversion rate. It was reported that the catalytic activity of commercial cellulases derived from *T. reesei* and *A. niger* can be improved by the addition of crude cellulases from five different fungal strains, namely *Chaetomium thermophilum*, *Thielavia terrestris*, *Thermoascus aurantiacus*, *Corynascus thermophilus*, and *Myceliophthora thermophile*, when pretreated barley straw was hydrolyzed [79].

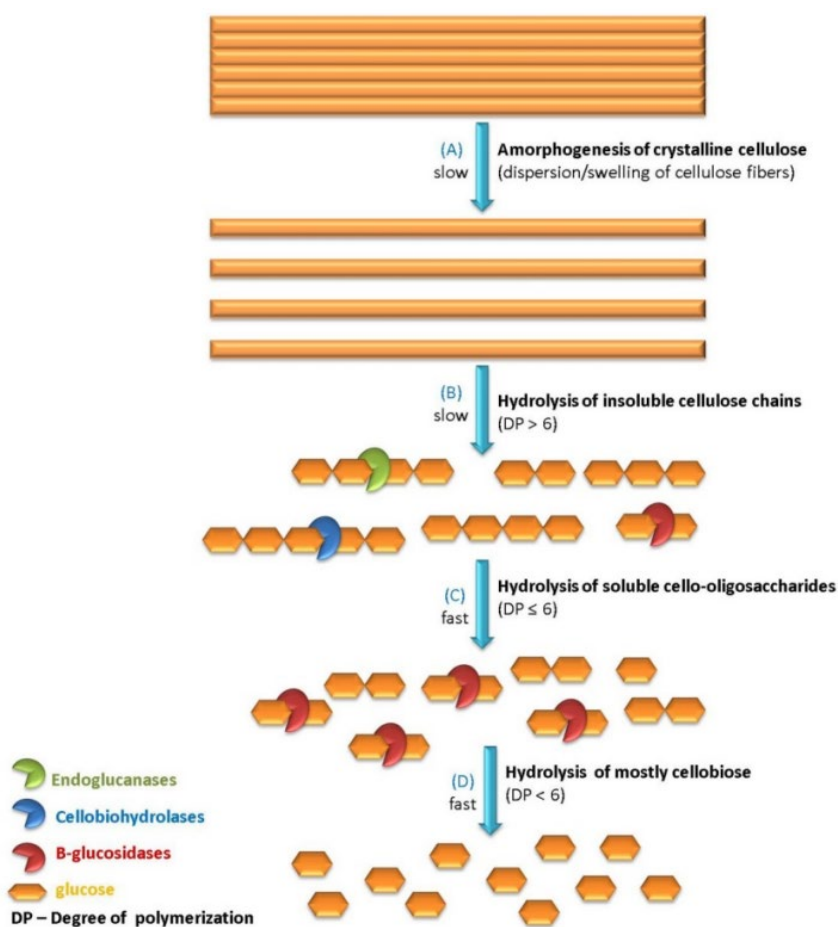


Figure 3: A schematic diagram of the bioconversion of lignocellulosic biomass to fermentable glucose [80]

2.4 Enzyme Kinetics and Modeling

The mechanism of the enzymatic hydrolysis of cellulose is similar to other enzymatic reactions. Figure 4 illustrates the mechanism and kinetics of each step. In the first step, the enzyme is adsorbed onto the surface of the substrate. After which, two pathways are possible; enzyme either binds to an active site, denoted as productive binding, or to a non-active site, denoted as non-productive binding. In the former pathway, the enzyme-substrate complex is formed and can proceed to the catalytic reaction step during which the glycosidic bond is broken. The enzyme-product complex is formed and then separated to release the product from the enzyme, and the enzyme active site is free again for another binding. Therefore, the rate of the catalytic reaction is directly proportional to the rate of substrate productive binding to the active sites [81]. However, if the substrate is adsorbed through a non-productive pathway, the substrate acts as an inhibitor and the catalytic process is inhibited. Thus, no product is formed in this pathway and the enzyme is inactive [81]. This proves the fact that as the enzymatic hydrolysis progresses, the substrate surface dynamically changes [82]. Cellulose is composed of hydrolyzable and non-hydrolyzable (inert) parts. At the enzyme-substrate surface, the enzyme breaks down cellulose leaving the inert at that layer, proceeding to the next layer, which contains also cellulose and inert too [82]. As the reaction continues, the enzyme is adsorbed deeper into the substrate, shrinking the available substrate surface area.

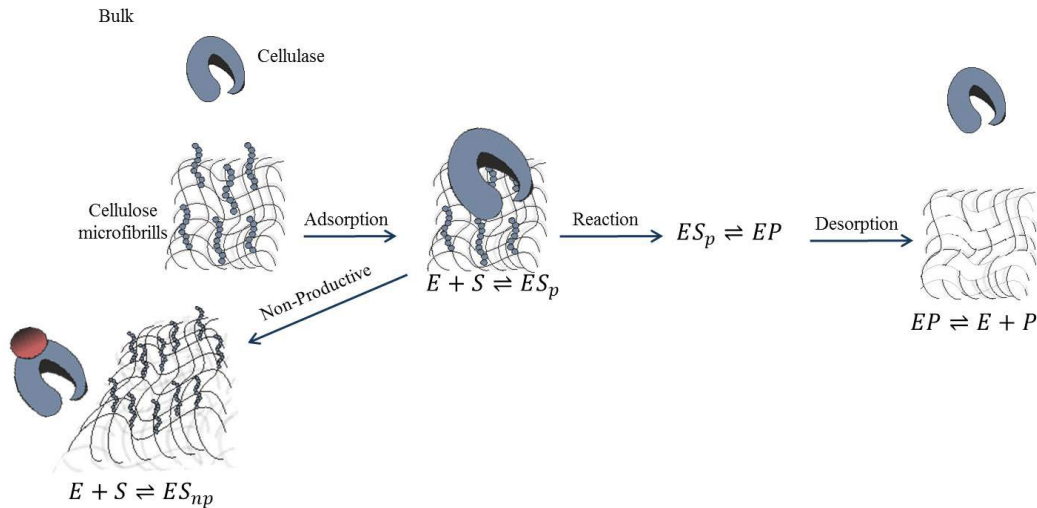


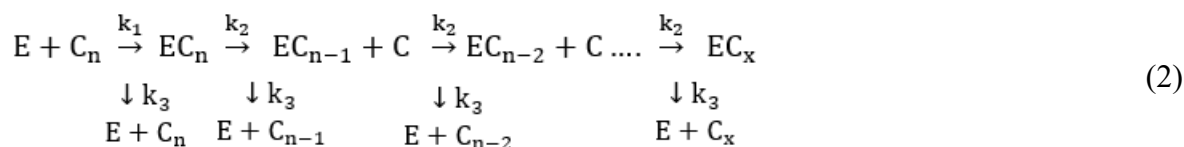
Figure 4: Reaction mechanism of enzymatic hydrolysis of cellulose

Different mechanisms for cellulase kinetics were proposed by different researchers, trying to fully understand the process. The mechanism shown in Equation (1) was proposed to explain the burst phase for a soluble substrate and non-processive enzyme, that cleaves cellulose randomly and not processivity. The processive action of an enzyme means that enzymes bind to the cellulose and cleaves it for multiple cycles continuously before it dissociates [83].



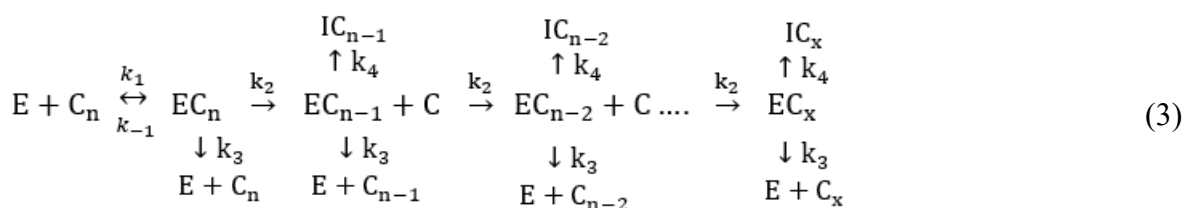
The model suggests that an enzymatic reaction produces two products; one of them, P_1 , is produced rapidly at the beginning of the reaction, with k_1 and k_2 being larger than k_3 . The enzyme then accumulates as EP_2 complex, which dissociates slowly with time to produce P_2 . This can be proven by monitoring the concentrations of P_1 and P_2 as a function of time, in which P_1 increases during the first stage of the reaction before it goes to steady-state [83–85]. However, key factors affecting the mechanism of the enzymes, such as product inhibition, is not considered.

To account for the processive action of the enzyme, Equation (1) was modified to include multiple cycles of the catalytic action of cellobiohydrolase, as shown in Equation (2)



In this model, the cellulose cleavage is occurred enzyme's cleaving of the cellulose strand is occurred consecutively, in a processive manner, and goes through many cycles of consecutive reactions before it dissociates. The hydrolysis initiates by the binding of cellobiohydrolase, E, to cellulose strand containing n cellobiose units, C_n , to form an enzyme-substrate complex, EC_n . After this, it can either produce one cellobiose unit, C, with a rate constant k_2 or dissociate back to enzyme and cellulose with dissociation rate constant k_3 . The reaction continues with the same steps, but with shorter cellulose strands in each cycle and with the possibility of the dissociation of the enzyme. After multiple cycles of cleaving cellobiose units, the desorption rate is slowed down because of the inhibition by cellobiose leading to the accumulation of enzyme-substrate complex (EC_x), since k_2 is larger than k_3 , and a further decline in the kinetics is observed [83–85].

The drawback of this model is that it is assuming a constant substrate concentration, which is valid only at the beginning of the reaction when it is higher than the concentration of the enzymes. Hence, the accessibility and affinity of the enzyme to bind to the rest of the cellulose strand is not considered [86]. In addition, the inhibition effect is considered only by cellobiose, while mono-sugars are not considered. This model was further modified to include the consideration of enzyme deactivation by an irreversible binding to the substrate, Equation (3).



The inhibition of the enzyme during the processive hydrolysis, Equation (3), was proposed in the assessment of the hydrolysis of the microcrystalline cellulose, which is composed of amorphous and totally hydrolyzable cellulose, which reported that the decline in the kinetics was due to the enzyme-substrate irreversible binding [87]. However, the model does not consider enzyme inhibition by the end product, and ignores the mass transfer limitations, which are significant in heterogeneous reactions.

Product inhibition effect was included in a model developed by Huang [88] and Peitersen et al. [89], in which cellulose as a substrate binds reversibly to the enzyme to form either productive or non-productive enzyme-substrate complex. Productive complex may then proceed to the forward direction to produce the product, P. Once product is released, product inhibition might occur upon binding to the enzyme, which is irreversible in this model. The mechanistic steps of this model are presented by Equations (4)-(7).





In this mechanism, the substrate is presented in two fractions, hydrolyzable substrate that can produce a product upon binding with the enzyme (S_c), and non-hydrolyzable substrate (S_x) that results in non-productive binding and deactivates enzymes. The reversible binding of the enzyme to the hydrolysable and non-hydrolyzable substrates and to the product are accounted for in this model. In addition, unlike previous models, the active surface concentration, which is represented by S_c , is considered rather than the total mass concentration, which gives an insight into the quality of the substrate and represents better the mechanism of the reaction [82, 90, 91]. Moreover, this presentation incorporates the dynamic changes that occur in the substrate surface during the enzymatic hydrolysis, which helps in predicting the conversion decline as the reaction proceeds. However, the different types of cellulases are not distinguished but rather assumed to be one type with the same function for simplicity, unlike models proposed by Zyl et al. [92] and Zhang [93] that distinguished the action of endoglucanase and exoglucanase in separate steps. In the model described in Equations (4)-(7), product inhibition is represented by the reversible formation of an enzyme-product complex. In more recent models, different additions were accounted for, like the heterogeneous substrate, the degree of polymerization, inhibition effect, the rapid decline in the initial rates, and the pretreatment effect on hydrolysis yield. However, this model will be used as the base for modeling in this research with modifications to estimate the kinetic parameters involved in the enzymatic hydrolysis of selected lignocellulosic biomass.

Chapter 3: Challenges of lignocellulose Enzymatic Hydrolysis and Potential Solutions

The use of lignocellulose for ethanol production increases the income of farmers, provides more jobs, and reduces gas emissions by increasing the green lands [94]. However, due to the difficulty of the hydrolysis of lignocelluloses, the cost of production, estimated at 0.60 €/L, is higher than the market prices of ethanol, which is 0.23 €/L, making the overall process economically unfeasible [95–97]. Overcoming the barriers that slow down the hydrolysis process and enhance the yield would change the situation and make the large-scale production more feasible.

3.1 Heterogeneous Mixture

Lignocellulose is a recalcitrant substrate, since it is composed of different components, with some of them being resistant to enzyme degradation. In addition, the crystalline cellulose substrate forms a heterogeneous mixture, wherein the enzyme, which has to be used in its free form, binds to the heterogeneous substrate for the reaction to proceed. The slow kinetics of enzymatic hydrolysis of cellulose are correlated with the heterogeneous nature of the substrate that affects the diffusion of enzymes to the substrate. In addition, the necessity of using the enzyme in a soluble form brings another difficulty in continuous reactor systems, as the enzymes, in this case, are continuously lost with the effluent, which makes the process unfeasible. Due to its low conversion and high cost, the contribution of the enzymatic hydrolysis could exceed 50% of the total bioethanol production cost [98–108].

3.2 Enzyme Inhibition

There are three pathways by which the enzyme can be inhibited, namely, competitive, non-competitive, and uncompetitive inhibition. In competitive inhibition, the inhibitor competes with the substrate for the active site and binds to only free enzymes. In non-competitive inhibition, the

inhibitor binds only to the enzyme-substrate complex. In contrast, in uncompetitive inhibition, the inhibitor binds to either the free enzyme or enzyme-substrate complex [109]. In competitive inhibition, the inhibition effect can be reduced by increasing the substrate concentration. This decreases the chance of inhibitor binding to the enzyme, while the K_i value remains unchanged. However, the K_m value also increases with the substrate loading. On the other hand, the non-competitive inhibitor acts on the enzyme-substrate complex. Hence, the addition of more substrate does not help in the case of inhibition [110].

Surface accessibility is one of the factors affecting the conversion rate, which results in declining the adsorption of enzymes to the substrate with time [111]. At first glance, increasing the solids loading in the reaction could be considered a strategy to overcome this problem. With different solids loadings, however, a similar trend of an instant increase in the conversion was found to be followed by a decline. Nevertheless, with higher solids loading, the increment in the initial phase of the reaction was higher. The instant increase can be attributed to the instant occupation of most of the active sites on the enzyme, and productive binding occurs with more substrate available [108]. However, as the enzymatic hydrolysis progresses, the substrate surface dynamically changes and the non-hydrolyzable parts are more and exposed for enzyme to bind with, thus, with time the non-productive enzyme-substrate complex is increasing. In addition, there are three interconnecting causes of the decrement that is observed during the hydrolysis, which are mass transfer, mixing speed, and product concentration. The main inhibitors of cellulase are the hydrolysis products. Out of all the hydrolysis products, xylose showed a non-competitive inhibition with cellulase, whereas glucose and cellobiose both showed competitive inhibition [90, 112]. Much less inhibition was reported for galactose and mannose [108].

3.3 Immobilization: Solution for Heterogeneous Mixture Challenge

Enzymatic hydrolysis of lignocellulose has been suggested as a potentially sustainable approach for ethanol production. However, challenges including the high cost and recyclability of the enzyme render the large-scale production unfeasible. During the reaction, cellulase is lost with the product, and a purification unit is thus required to purify the product and recycle the enzyme. To simplify the separation and reusability of the enzyme, immobilization by entrapment within a matrix using different methods, such as covalent binding and crosslinking, has been intensively investigated [113–116]. Several reports have emphasized the positive effect of immobilization on the stability of cellulase. For example, immobilizing cellulase into polyacrylic acid nanogel showed enhanced thermal stability, and 75% of enzyme activity was maintained at 80°C [117]. Using magnetic nanoparticles in enzyme immobilization also attracted interest due to the large surface area and high enzyme loading capacity [118]. The capacity of the immobilized enzymes on the magnetic nanospheres can increase with surface charge, which can stabilize the catalytic activity of the enzymes, and enhance thermal and pH stability [119–121]. Although immobilizing cellulase on polyvinyl alcohol/Fe₂O₃ magnetic nanoparticles enhanced the conversion yield more than the use of free enzymes, enzyme activity was reduced to 40% within four cycles [122].

Despite the advantages of immobilization in enhancing cellulase stability and simplifying the separation, the use of immobilized cellulase with the highly crystallized lignocellulose biomass that remains insoluble in an aqueous solution is not practical. Immobilization results in fixing enzymes on or within solid support, which limits its accessibility to the heterogeneous substrate. This adds resistance, which further reduces the hydrolysis rate. Above that, as cellulose contains hydrolyzable and non-hydrolyzable parts, using the enzyme in immobilized form would prevent it from reaching deep within the cellulose matrix to reach the hydrolyzable cellulose as the reaction proceeds, and the surface hydrolyzable parts are consumed [123–125]. Therefore,

using the enzyme in soluble form is inevitable for achieving an appreciable reaction rate. This necessitates finding another way to separate the enzyme from the product and facilitating its repeated use.

3.4 Membrane Technology: Solution for Product Inhibition Challenge

Conventional bioreactors, of different designs, have been used in industry for bioethanol production from cellulosic materials. However, they all face one or more of the problems explained above. For example, stirred tank bioreactors (STRs) have been commonly used in industry due to their high solid loading advantage. However, in these types of reactors, enzyme deactivation is inevitable as a result of product inhibition and the shear stress generated by vigorous agitation [126]. In addition, as the enzyme must be used in a soluble form, due to the heterogeneous nature of the reactant, it is used for a single pass only in the STRs and then lost with the effluents. To overcome the shear deactivation problem in the reactor, a horizontal rotating tubular bioreactor has been suggested and different rotation agitation impellers in STRs were adopted. However, a reduction in shear stress imposed on the enzymes was only observed when the enzyme loss and deactivation due to product inhibition were not eliminated. Therefore a large-scale production using the current reactor designs would remain unfeasible [127].

MBRs have been proposed as promising solutions for the product inhibition effect, by selectively separating the produced inhibitors. In addition, by using membranes of proper cut-offs, the large enzyme molecules could be retained, which prevents their loss with the effluent and allows for their repeated use for a longer reaction time. At the same time, the smaller product molecules are separated from the reaction, without the need for additional purification [128], which eliminates product inhibition and maintains enzyme activity. Shear stress imposed on the enzymes could also be reduced in MBRs, which further maintains the activity of the enzymes.

The superiority of MBR over STR can be seen in the comparison between the yields of enzymatic hydrolysis achieved using both reaction systems. For example, hydrolysis of parchment coffee, composed mainly of xylan, in an MBR and an STR under the same conditions, showed that at a low solid loading of 1 mg/mL both reactors reached 97% conversion within 3 h. However, with increasing the solid reactants loading to 10 mg/mL, the superiority of the MBR became more evident achieving a conversion of 78%, whereas the conversion using the STR was only 53% [129]. This decrease in conversion in both reactor systems was due to the increase in the produced sugars concentration, which resulted in product inhibition. In addition, under the same agitation, the increase in solid substrate concentration reduced the mixing efficiency. Although the effect of solid loading is expected to be the same in both reactor systems, the reduced product inhibition effect in the MBR system was the reason for its better performance.

3.4.1 MBRs Configurations

Generally, filtration can be integrated with a bioreactor system in two configurations, wherein the membrane is either in a separate unit or submerged or in contact with the reaction vessel [130]. Figure 5 shows schematic diagrams of different MBR configurations adopted in different studies. In a hybrid membrane reactor, Figures. 5A and 5B, the reaction is carried out in one vessel, and then the reaction slurry is passed to a different unit, where the filtration membrane is placed, which makes this configuration easier to scale up. In comparison to the reaction in a batch system, enzymatic hydrolysis of olive mill solid residues in a continuous MBR coupled with separate ultrafiltration (Carbosep M5) in a crossflow filtration mode, 10 kDa, similar to the configuration in Figure 5A, showed enhanced conversion. Under the same conditions, a glucose yield of 45% was achieved in the MBR within 14 h, whereas in the batch system, 24 h was required to achieve the same yield [131]. However, this enhanced performance was not observed when an MBR coupled with ultrafiltration polyethersulfone membrane of 50 kDa molecular weight cut-off (MWCO) was used for saccharification of washed corn stover using 20 FPU/g cellulases

(*Trichoderma longibrachiatum*). This was attributed strongly to the loss of enzymes in the system [132]. In addition, a techno-economical assessment of an MBR coupled, in a crossflow filtration mode, with an ultrafiltration unit of 10 kDa MWCO used for the hydrolysis of α -cellulose pretreated with ionic liquid showed that the process is economically unfeasible. In this study, the end products, glucose, and cellobiose, that permeate from the ultrafiltration unit were further purified in a nanofiltration unit to separate the intermediate cellobiose. In the last stage, an electro dialysis unit was used to remove the ionic liquid used in the pretreatment step. The overall cost of glucose was estimated to be 2.75 €/kg, which is relatively expensive [133]. Despite their advantage in retaining the enzyme and allowing its repeated use, in a separate MBR-filtration configuration, the reaction slurry must be pumped to the filtration unit and recycled back to the reaction vessel, which adds to the production cost on the one hand, and might cause enzyme deactivation and loss on the other hand. In addition, the advantages of simultaneous separation of product are not provided in such configurations. Furthermore, fouling is more pronounced as recycling the reaction slurry between the reaction vessel and the ultrafiltration unit requires applying pressurized filtration to maintain a constant permeate flux. The problem is more severe in a crossflow filtration, wherein filter cake layer formation is high. Pumping the reaction slurry to the ultrafiltration unit at a high speed may reduce the accumulation. However, this requires much energy and even when an agitation at 500 rpm was used to eliminate cake layer formation at a filtration pressure of 1 bar, a decrease in membrane permeation was still observed [133].

To avoid using multiple systems with pumping systems, integrated MBRs, in which the products are simultaneously separated, have attracted attention [134]. Besides using fewer units with no inter-pumping, which reduced the overall cost, the simultaneous separation of the products pushes the reaction forward and reduces enzyme inhibition. Examples of different integrated MBRs reported in the literature are shown in Table 1.

Table 1: Applications of integrated membrane bioreactors (MBRs) in enzymatic hydrolysis of cellulose

MBRs Configurations	Membrane			Substrate		Enzyme	Operational conditions								Conversion	Ref.
	Type	Composite	MWCO	Type	Pretreatment		Flux	Substrate (g/L)	Enzyme (g/L)	T (°C)	pH	Press (bar)	t (h)	Mixing (rpm)		
Dead-end filtration	UF	Polysulfone	10 kDa	Alpha-cellulose fiber	-	C8546 <i>T. reesei</i>	7-9 L/m ² h	25	0.1	40	4.7	0.7	48	- ^a	53%	[112]
		Cellulose acetate	10 kDa	Xylan extracted from coffee parchment	-	Xylanase, <i>A. niger</i>	nd	1	0.11	40	4.6	nd	3	200	97%	[129]
		PES	10 kDa	Microcrystalline Cellulose	NaOH	Cellic CTec2- with high level of β -glucosidase	10 mL/ min	100	2.4	50	5	nd	8	200	7.6%	[135]
		Polysulfone	10 kDa	Corn Stover	Aquas ammonia (SAA) Dilute sulfuric acid-sodium hydroxide	(A) Spezyme CP, <i>T. reesei</i> (B) Novozyme 188	-	5 10	(A) 60 (B)30 CBU/g	45	4.8	0.6	20	120	82% 94%	[136]
Submerged filtration	Dialysis	Spectra/Pro 6	1 kDa	Wheat straw	Heat	(A) Celluclast 1.5L <i>T. reesei</i> (B) Novozyme 188 <i>A. niger</i>	-	1	(A) 4.1, and (B) 1.08	50	5	-	72	350	28%	[137]
Tubular filtration	UF	Fitevig 500N-Non-woven textile-polyethylene (PE)	nd	Solka Floc powder	-	Celluclast <i>T. reesei</i>	80 mL/ min	25	3	50	4.8	-	25	-	50%	[138]
				Mavicell cellulose pellets	Heat								10	-	70%	

^a 300 V electric pulse was subjected on membrane for 20 s

In most investigated integrated MBRs, in which reaction and separation are carried out in one unit, the dead-end filtration concept was adapted, where the flow direction is perpendicular to the membrane [130]. In these MBRs, the membrane is placed at the bottom of a stirred tank reactor (STR), as shown in Figure 5C. The reactants are placed above the membrane and the low molecular weight products, glucose and cellobiose, permeate to the bottom stream. Similar to other MBRs, dead-end filtration showed enhanced cellulose conversion compared to a conventional STR. For example, α -cellulose hydrolysis conversion of 53% was achieved in a dead-end filtration MBR with a flat sheet polysulfone membrane of 10 kDa MWCO, whereas the conversion was only 35% in a STR under the same reaction conditions [112]. The superior performance of dead-end filtration MBR was also shown in the enzymatic hydrolysis of corn stover, pre-treated with combined acid and alkaline. The hydrolysis conversion in the MBR was 94% compared to only 77% in a continuous bioreactor (CBR) under the same reaction conditions [136]. Despite their favorable characteristics in reducing product inhibition and retaining the enzyme, there are several limitations in dead-end filtration MBRs that restricted their large-scale application for enzymatic hydrolysis of cellulose. For example, they have limited solid substrate loading, which negatively impacts yields. That is mainly because high substrate concentrations result in insufficient mixing and increased surface deposition and filter cake formation. These problems reduce the membrane permeability and result in damaging the membrane by molecules deposition [139]. Vigorous mixing near the membrane surface could be used to minimize these effects, but it results in increased shear stress, which has a damaging effect on enzyme activity. To overcome the cake formation of the substrate on the ultrafiltration surface, a modified configuration with multiple membranes system was proposed. A nylon sealed bag containing the pretreated cellulose is submerged in a reaction vessel containing buffer and enzyme. The bag has relatively large openings that allow the enzyme to diffuse in, but prevents the cellulose from diffusing out, and thus trap substrate and eliminate its deposition on the ultrafiltration membrane.

The glucose molecules, produced inside the sealed bag, diffuse to the outer vessel and are separated using a separate ultrafiltration unit [135]. Although the concept of this modified configuration is promising on a small bench scale, its applicability in large-scale production might be difficult. In addition, when the concept was tested, the accumulation of substrate on the ultrafiltration membrane surface was indeed eliminated, but the proteins molecules accumulated on the membrane forming a gel layer that reduced membrane permeability [140].

Another MBR configuration that was also tested, to enhance the solid loadings, is the tubular reactor, shown in Figure 5D. The tubular membrane found in the center of the MBR provides a large surface area for the separation process. This results in more efficient product separation, which results in a faster rate and reduction of the reactor volume. In addition, the diffusion resistance of enzyme-substrate is expected to be low in such a configuration. However, this configuration was also theoretically simulated [141].

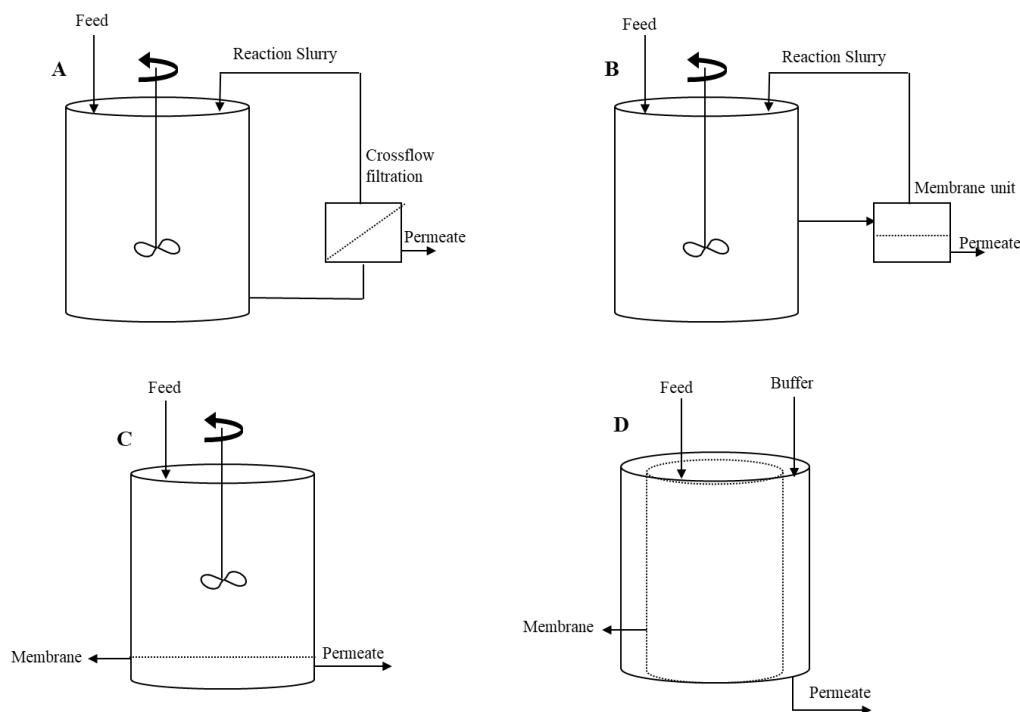


Figure 5: Schematic diagrams of different MBR configurations. (A) external filtration unit coupled with STR in crossflow module, (B) external filtration in the dead-end module, (C) dead-end filtration MBR, and (D) Tubular MBR

3.4.2 Membrane Selection

The success of an MBR to effectively retain the enzymes while easily permeating the product depends on the type and properties of the membrane used in the reactor [130]. Ultrafiltration (UF) and nanofiltration (NF) membranes are the two types that have been commonly reported in enzymatic hydrolysis applications [130]. However, UF membranes, which have an average pore size in the range of 0.5 to 100 kDa, are the ones used to selectively retain the large enzyme molecules in the main hydrolysis reactor, which is the focus of this thesis. NF membranes, on the other hand, which have an average pores size of in the 150 to 1000 Da, are used to concentrate product [130, 142], which is essential for enhancing the downstream processes and reducing the production cost [143].

UF membranes can be fabricated from different materials, which include polysulfone (PS), polyethersulfone (PES), cellulose acetate (CA), nylon (NY), and ceramics [144]. The membranes most commonly used in MBRs for enhancing the enzymatic cellulose hydrolysis are PES membranes, with MWCO of 10 to 50 kDa. This is mainly due their hydrophobicity, which gives them the ability to effectively reject cellulase enzymes without interfering with the reaction [130]. The PES hydrophobicity, however, was found to increase the membrane fouling. Therefore, hydrophilic polymers, such as poly vinyl pyrrolidone (PVP), have been suggested to be added to the membrane as an antifouling agent [145, 146]. Having said that, the high-water solubility of the added hydrophilic polymers resulted in their leaching out during the process, and thus, the antifouling properties did not last for long and was lost after multiple usages of the membrane [145]. Ceramic membranes appear to be more interesting for industrial applications, due to their high physical and mechanical strengths, which PES membranes lack, allowing them to withstand high permeation fluxes suitable for large-scale production [147]. The performance of a ceramic membrane was examined in a hybrid MBR with a crossflow filtration mode, in which reaction was carried out in a stirred tank reactor, and compared to that of a PES membrane [148]. An MBR

with a tubular ceramic membrane, 5 kDa MWCO, containing three channels was operated in continuous mode with a permeation flowrate of 215 mL/min and 0.5 bar of back pressure. The MBR with PES membrane, 5 and 10 kDa MWCO, was operated in a semi continuous operation mode with 120 mL/min flowrate and at 1.2 bar of back pressure. Although both membranes showed high enzyme retention reaching over 98%, their ability to maintain the activity of the enzyme and the permeation flux for multiple cycles was different. The 5 kDa PES membrane maintained active enzymes for 6 cycles, which was indicated by the consistent hydrolysis yield of 94%. However, a decline in permeation flux was observed, which was attributed to the pore blockage by the non-hydrolyzed glucose oligomers. The performance was improved when PES membrane of a larger MWCO of 10 kDa was used, in which the activity and permeation flux were maintained for 9 cycles. The performance of the 5 kDa ceramic membrane was found to be similar to that of the 10 kDa PES membrane, which suggests that it could be a better alternative to PES membranes because of its higher mechanical strength [148].

3.4.3 Key Factors Affecting the Performance of MBRs

The performance of MBRs is influenced by different parameters that are related to the enzymatic hydrolysis reaction, the reactor configuration, and the membrane properties. Table 2 shows a summary of the main factors affecting the enzymatic hydrolysis, and advantages and disadvantages of the different MBRs discussed in this thesis are presented in Table 3. The temperature and pH of the reaction system are important factors to be optimized to operate at the highest activity and stability of the enzyme for enhanced hydrolysis rate and yield [149]. The activity and stability of cellulase also depends on the microbial strain used for its production of the recipe of prepared enzymatic cocktail [128]. Other factors that also affect the enzymatic activity, but received much less attention, are salts and ionic strength of the reaction medium [150]. For example, the presence of sodium ions from sodium acetate buffer used in many studies to adjust the pH of the reaction was found to enhance the endoglucanase action but suppressing

exoglycanase [150]. The two effects could be balanced at a concentration of sodium ions that depends on the source of the cellulase used.

The performance of an MBR for enzymatic hydrolysis cellulose is affected by substrate related factors, which are directly correlated with the pretreatment step [149]. The lignocellulosic biomass pretreatment is considered a crucial step that does not only determines the success of the hydrolysis step, but also the subsequent steps. The efficiency of the pretreatment method, which depends on the type of lignocellulosic material [151], is measured by the digestibility of the resultant cellulose. More than 90% sugar yield should be achieved in less than three days using an enzyme loading lower than 10 FPU/g cellulose [152]. The crystallinity index of the pretreated lignocellulose, which measures the recalcitrance of cellulose, has been linked to the efficiency of the hydrolysis. Efficient pretreatment results in a lower crystallinity index, which allows for a better accessibility of enzymes through the amorphous cellulose matrix [151]. For example, pretreating rice straw with ultrasound-assisted alkaline (NaOH) improved the digestible cellulose yield by a factor of 3.5, compared to untreated biomass [42]. This pretreatment method was found to increase the porosity and reduced the crystallinity index of the biomass, which enhanced the accessibility of cellulase, compared to the same biomass treated with heat only. The pretreatment with NaOH below 8 wt% was also shown to cause separation in cellulose lattice and decreased its polymerization [43]. On the other hand, despite its strong effect on removing lignin and hemicellulose, acid-alkali pretreatment, 0.1 M hydrochloric acid and 0.1 M sodium hydroxide, of lignocelluloses showed an increase in the crystallinity, which was mainly attributed to the action of acid in removing the amorphous cellulose leaving behind the recalcitrant cellulose only. Therefore, delignification by alkaline pretreatment has been suggested to be adequate for enhancing enzyme accessibility of the treated substrate [144]. Comparing sodium hydroxide pretreatment with mechanical pretreatment, using ball milling, on wheat straw cellulose, showed that alkaline pretreatment enhanced better the hydrolysis rate. Complete hydrolysis of biomass

pretreated with NaOH was attained in 10 h, whereas that pretreated with ball milling required 24 h. This shows that the significance of lignin removal, attained by the alkaline treatment, is more significant on enhancing the hydrolysis than particle size reduction, attained by the ball milling. However, a better hydrolysis was attained when both pretreatments were combined [153].

Enzyme and substrate loading are other important parameters that affect the technical and economic feasibility of cellulose hydrolysis process. Although increasing the substrate concentration is expected to increase the hydrolysis yield, studies showed that this is only correct up to a certain concentration, above which substrate inhibition occurs and poor mixing due to the viscous slurry, resulting in a reduction in the hydrolysis rate [154]. In addition, a high substrate concentration in some MBRs configuration enhances membrane fouling, which has a strong effect on the feasibility of the process [155]. The increase in enzyme concentration also contributes to membrane fouling wherein the former contributes to the external fouling, whereas the latter contributes more to internal fouling. Figure 6 shows the filter cake formation, which increases the hydraulic resistance manifested as a decline in permeate flux. Physical or chemical cleaning is usually applied to remove the accumulated molecules on the membrane surface. Physical cleaning can be achieved either by backflushing in which water flux is reversed for short period of time to disrupt the cake layer, or by relaxation in which membrane cleaning is scoured with air bubbles [156]. Chemical cleaning on the other hand is used when the fouling is irreversible, by using a dissolving reagent. However, with both methods, the permeability cannot be completely retained, and the membranes would require replacement. Fouling is more severe in crossflow filtration systems, which should be operated below a critical flux, above which fouling starts to build up. Nevertheless, fouling would still be inevitable, and was observed even at low fluxes. Pumping the reaction slurry was also suggested to slow down substrate accumulation, by redistribution of the molecules on the membrane surface, and thus, controlling the rate of accumulation. Nevertheless, such an approach adds to the energy requirements and increases the operating expenses [157].

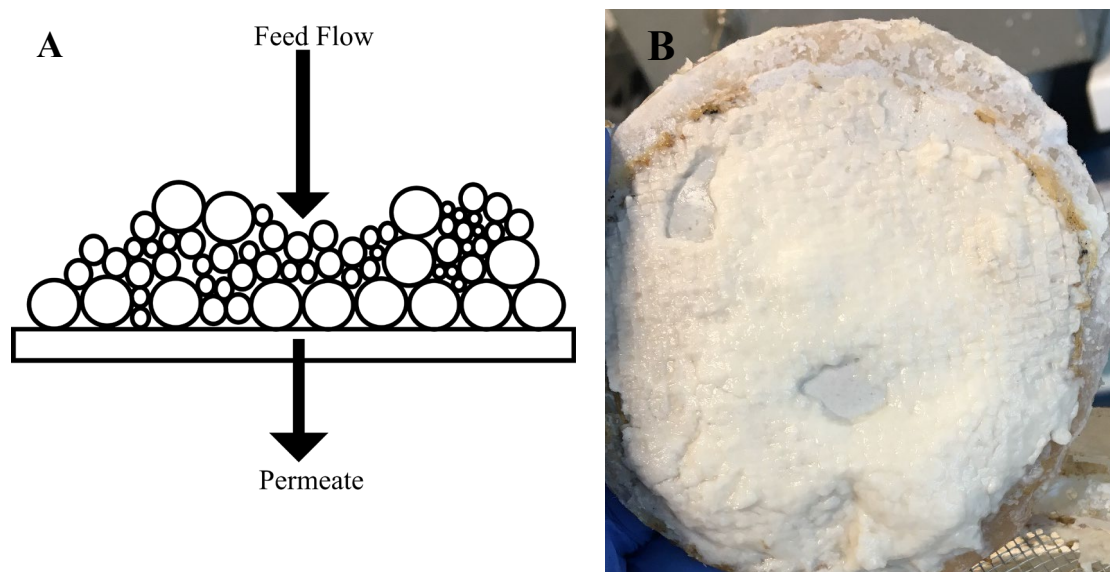


Figure 6: Filter cake formation in dead-end MBR on membrane surface. A) schematic diagram of the deposition of solutes on the membrane surface, and B) real accumulation of standard cellulose molecules on a PES membrane

In an attempt to minimize membrane fouling, Gan et al. applied an electrical pulse directed on the membrane by installing a cathode in the form a stainless-steel mesh physically supporting the membrane from the bottom and an anode placed above the membrane with 1 mm distance. After fouling, the membrane surface was subjected to an electric pulse of 300 V for 20 s, which positively increased the permeation by a factor six. However, this improvement sustained for only 120 s before declining again. In addition, it resulted in conformational changes in the enzyme, which affected its activity [112]. Thus, a need for another design, or method, to minimize membrane fouling still exists.

Agitation is another parameter that can be adjusted to increase the cellulose conversion, and MBR performance. The effect of the agitation speed on carboxymethyl cellulose conversion was investigated in a stirred tank reactor facilitated with a hanging bar impeller and a 10 kDa PES membrane installed at the bottom of the reactor, in dead-end filtration mode. An enhancement in the conversion, reaching about 90% within 1 hour and 55°C was achieved when the highest agitation speed of 1200 rpm was used, whereas the lowest tested speed of 300 rpm resulted in

almost 80% under the same conditions [150]. This enhancement is attributed to the sufficient mixing in the reaction cell that allowed for better mass transfer, as well as enhanced disruption of local accumulation of products surrounding enzymes that facilitates substrate- enzyme adsorption [158].

Table 2: Summary of factors to be considered for enhanced production yield in MBRs

Enzymatic hydrolysis	Enzyme-related factors	<ul style="list-style-type: none"> - pH - Temperature - Product inhibition - Enzyme loading - Enzyme source - Salt and ionic strength
	Substrate-related factors	<ul style="list-style-type: none"> - Substrate inhibition - Mixing efficiency - Solid loading - Pretreatment type
Membrane performance	Membrane-related factors	<ul style="list-style-type: none"> - Reactor design - Membrane material - MWCO - Membrane maintenance - Membrane fouling

Table 3: Summary of advantages and disadvantages of different MBR designs

MBR design		Advantages	Disadvantages
Hybrid MBRs	Reaction and filtration are separated	<ul style="list-style-type: none"> - Membrane advantages - Easy to scale up 	<ul style="list-style-type: none"> - Multiple units in the system - Enzymes lose and deactivation - Pressurized pumping - Energy consumption - Membrane fouling - Economically unfeasible
	Dead-end filtration MBR	<ul style="list-style-type: none"> - Simple set-up 	<ul style="list-style-type: none"> - Solid loading limitation - Enzyme deactivation due to shear stress - Severe membrane fouling
Reaction and filtration combined	Inverted dead-end filtration MBR	<ul style="list-style-type: none"> - Membrane fouling elimination - Enhanced conversion yield 	<ul style="list-style-type: none"> - Solid loading limitation
	Tubular MBR	<ul style="list-style-type: none"> - Enhanced membrane surface area - Low enzyme-substrate resistance - Small reactor volume 	<ul style="list-style-type: none"> - Limited research investigated

Chapter 4: Materials and Methods

4.1 Chemical and Enzymes

All chemicals and enzymes were purchased from Sigma-Aldrich, USA. Commercial cellulases *Trichoderma reesei* was used for hydrolysis. 3,5-Dinitrosalicylic acid (DNS) and glucose oxidase were used for sugar measurements. Bradford reagent was used for protein detection. Glucose powder (99.5%) was used in the diffusion process and for calibration. Pure cellulose filter papers, with grade 1 and 150 mm diameter, were used as standard substrate in the screening experiment. Hydrochloric acid (HCl) 99.8%, Sodium hydroxide (NaOH) 98%, and ethanol 99.8% are used to pretreat the lignocellulosic biomass, date Seeds (DSs). Microdyn Nadir polyethersulfone (PES) ultrafiltration membranes (297 x 210 mm) were obtained from Sterlitch with three cut-off values, 10, 30 and 50 kDa. All the work has been done using PES-10 membrane, however, in some cases different MWCOs were used to confirm the absence of membrane fouling, determine the permeability, and analyzing permeation rate. For pH control, 0.1 M acetate buffer at pH 4.8 was prepared by the addition of 5.524 g of sodium acetate (99%) to 800 mL deionized water, followed by the addition of 1.961 g of acetic acid (99%). The solution pH was measured by a pH indicator, HCl and NaOH was both used to adjust the pH to 4.8. After which, deionized water was added to reach 1 L volume.

4.2 MBR with Inverted Dead-end Filtration Concept

4.2.1 The MBR Design

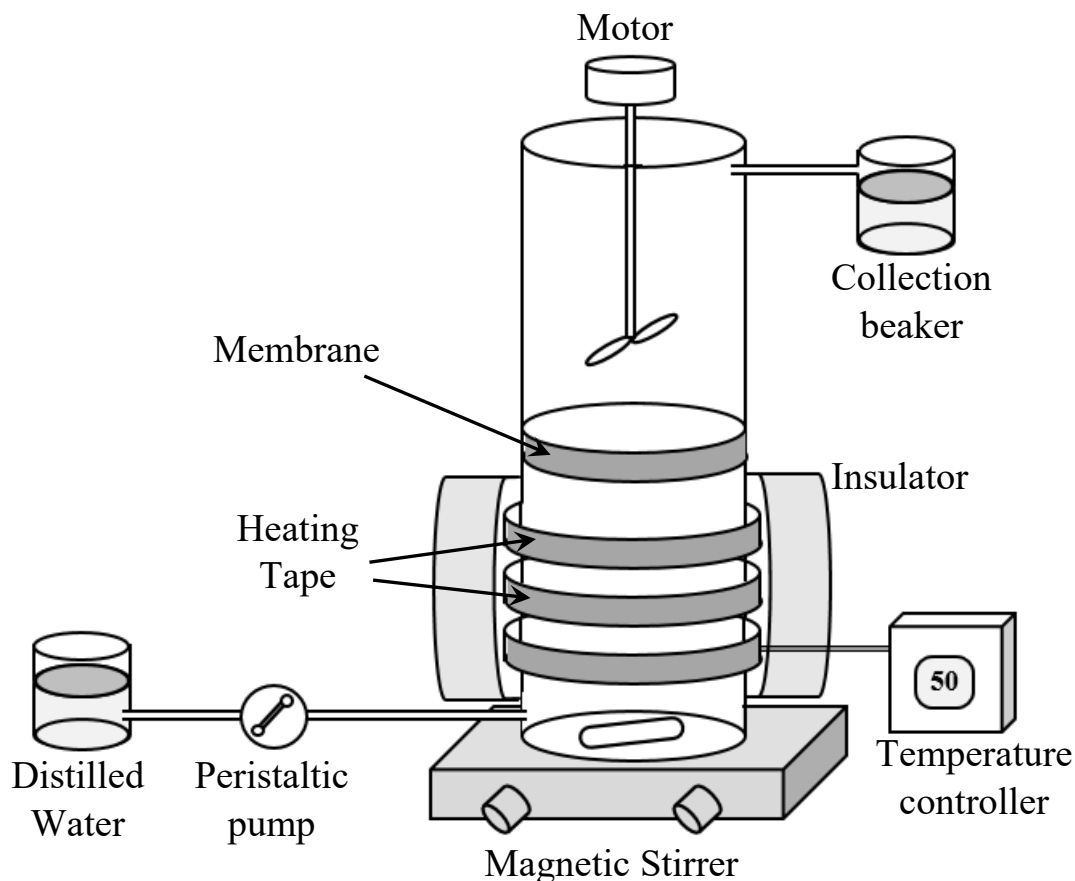


Figure 7: Schematic diagram of the inverted dead-end MBR

The MBR was designed and built to comprise two zones, each with an internal diameter, ID, of 7.5 cm and height, h , of 15 cm, which corresponds to a height to diameter ratio of 2. These two zones are separated by a PES membrane, as shown in Figure 7. The volumes of the bottom and the upper chambers were 750 and 650 mL, respectively. The reaction was carried out in the bottom chamber, in which the substrate and enzymes were charged. The upper chamber contained only distilled water. This design, which is opposite to the dead-end filtration concept, which was not reported in the literature before, was proposed to decrease substrate accumulation on the membrane surface and the internal fouling. In previous studies on enzymatic cellulose hydrolysis

with simultaneous product separation, a dead-end MBR, in which the membrane was placed at the bottom of the reaction cell, or in a separate unit adapting dead-end filtration concept, was used. With such a design, the substrate deposition on the membrane due to gravity was inevitable, resulting in the formation of a filter cake on the membrane [112, 159]. To minimize this effect, the membrane in this study was placed on top of the reaction cell, which contrasts with the dead-end filtration concept. This approach rendered the gravity effect favorable and decreased substrate accumulation on the membrane surface, and together with the height of the reaction cell of the MBR, settling of the substrate particles before reaching the membrane surface was possible. The PES membrane was secured on the top of the reaction cell by tightly gluing its perimeter to a woven stainless steel wire mesh that provided physical support during the diffusion process. To avoid leakage, the attached membrane on the mesh was sealed with epoxy adhesive glue. The system was exposed to several leakage tests before being used in the experiment.

Buffered distilled water, at the pH and temperature of the reaction was continuously passed through the system during the reaction using a peristaltic pump (Shenchen, China) to create the water flux through the membrane. The water entered from the lowermost part of the bottom chamber and exited from the top of the upper chamber and was then collected in a beaker. To avoid any possible physical damage to the membrane, the water flux through the system was maintained within the lower range of the pump that has a total range of 0.004 – 4.4 mL/min. The weight of the water in the upper chamber provided an additional support to the membrane against the water flux entering from the bottom chamber.

The produced sugar molecules, in the bottom chamber, would permeate the membrane and move to the upper chamber that contained only distilled water. Both chambers were agitated with a speed enough to create turbulence for good mixing, while avoiding excessive shear stress that can denature the enzyme. Agitation of the lower part of the reaction cell, which was another

modification not used in previous designs, created turbulence for mixing and at the same time contributed to the reduction of the internal fouling and filter cake formation on the membrane. This positive effect of tangential forces, caused by mixing, on reducing fouling on membrane surfaces has been confirmed in a previous study [160]. Therefore, in the present study, it was reasonable to assume that filter cake deposition would not be encountered. While the agitation speed in the reaction cell was enough to create turbulence, it was kept low to avoid harsh shear stresses that might denature the enzymes. The latter was not a concern in the upper cell. Therefore, the reaction cell was agitated with a magnetic stirrer bar, whereas the upper zone was agitated using a mechanical stirrer (IKA-WERK, Germany) with a higher speed to provide efficient distribution of the diffused glucose. Membrane damage was not encountered since agitation was parallel to the membrane. The temperature of the reaction was maintained by covering the bottom zone of the reaction cell with insulated heating tape (Thermolyne, Sigma) fitted with a thermocouple that was connected to a temperature controller (TC4S-14R). The bottom zone was further covered with wool insulation and wrapped with aluminum foil to minimize any heat loss and temperature fluctuation.

To start the process in the inverted dead-end MBR, acetate buffer solution in distilled water at pH 4.8 and 48°C was pumped through the system until the liquid fills both, the lower and upper, chambers and the liquid starts to overflow from the top chamber. The used pH and temperature are selected because they are the optimum for cellulase [161]. After that, a substrate solution in a pH 4.8 buffer at 48°C, of known amount of substrate, was slowly added to the bottom chamber through the inlet port. The enzyme was then added to bottom chamber to start the reaction. The bottom chamber was agitated by magnetic stirrer at a speed of 450 rpm which corresponds to Reynold's number of 1313, whereas the upper chamber was agitated with a mechanical stirrer at a higher speed of 1000 rpm, which corresponds to Reynolds number of 4572. In both chambers, the flow is turbulent since the Reynolds number is above 60 [162]. Throughout the experiment, a

buffer solution at the same reaction pH and temperature was pumped through the inlet port of the bottom chamber at the desired flow rate. The water flowed through the membrane, selectively carrying the product as it is produced, to the upper chamber. To ensure enzyme throughout the process, the temperature, pH, and shear stress in the lower chamber were carefully controlled and monitored. The pH value was found to insignificantly change from the beginning of the experiment, at which it was measured to be 4.8, to 4.81 at the end.

4.2.2 Standard Cellulose Hydrolysis with Product Separation

In the inverted dead-end MBR, filter paper was used as a model substrate as it contains pure alpha cellulose and a minimal ash content of approximately 0.007%. To prove the concept of this study, the yield of the enzymatic cellulose hydrolysis with product separation, in the developed MBR, was compared with that of the reaction system without product separation. The effects of the main operational parameters, *i.e.*, substrate concentration and water flowrate, on the process output variable, the glucose production yield, were investigated. A total of 9 experimental runs was suggested by the general factorial design. The ranges and levels of the input variables for the enzymatic cellulose hydrolysis used in the Minitab software are presented in Table 4. The tested flowrates, 0.2, 0.4, and 0.8, correspond to residence times of 62.5, 31.3, and 15.6 h, respectively.

The total amount of produced product consists of the amount of product in the bottom chamber (referred to in this manuscript as “accumulated”), in the upper chamber, and in the collected overflow. Hence, the amount of product was determined by summing the multiplication of the measured product concentrations in the bottom and upper chamber by their respected volumes and the measured product concentration in the overflow by the collected amount at the specific sample time. The sum of the three calculated amounts was then divided by the amount of the substrate initially added to the bottom chamber. The resulting number is referred to,

throughout the work, as total product yield or total reducing sugars yield. A sample calculation of the total product yield is presented in the Appendix. In this work, all samples were collected in triplicates, and the results presented in all figures are the average values with the standard deviations shown as error bars.

Table 4: Levels of two factors affecting the glucose production in the enzymatic hydrolysis of cellulose

Factors level	-1	0	1
Glucose concentration, X_1 (g/L)	2.67	6.67	13.33
Flowrate, X_2 (mL/min)	0.2	0.4	0.8

4.2.3 Kinetic Model

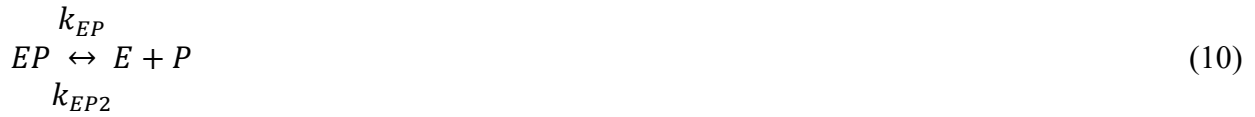
The dynamic model of the system included the following seven steps: (1) enzyme diffusion from the bulk of the bottom zone to the substrate surface, (2) enzyme binding to the substrate, both productive and nonproductive, (3) the reaction from productive binding produces the product, (4) desorption of the product from the enzyme surface to the bulk, which represents the product-inhibition effect, (5) diffusion of the product from the bulk to the membrane surface, (6) diffusion of the product through the membrane, and (7) diffusion of the product from the other side of the membrane to the bulk in the upper zone.

Due to the mixing in the lower and upper zones, any convection–diffusion event (steps 1, 5, and 7) was assumed to be instantaneous. Additionally, competitive inhibition of cellulase was assumed to have been conducted by only glucose [159, 163]. Inhibition by the non-hydrolyzable part of the substrate was not considered in this model because the substrate used was fully composed of amorphous cellulose [164]. Cellulases, a mixture of three distinct enzymes, endoglucanase, exoglucanase, and β -glucosidase, working in synergy, were treated as a single

enzyme that accomplishes complete cellulose hydrolysis. The cellulase used in this work was from *T. reesei*, which is a well-known and active cellulases [165]. It is identified for its high yield and production rate [166] and therefore have been reported to be the most commonly used in industrial applications [167]. Conventionally, extracellular cellulases from native *T. reesei* have been described with low β -glucosidase activity. However, this is because β -glucosidase gets trapped in the walls of the organisms once produced, and does not secrete into the culture medium where other types of cellulases are extracted and purified. Due to the development of several techniques that showed enhanced extraction of β -glucosidase, cellulases from *T. reesei* have recently been reported to have good β -glucosidases activity [168, 169]. The enzymes used in this work contained β -glucosidase, as described by the supplier, and the same cellulase was reported to have a good level of β -glucosidase activity [170]. Therefore, the *T. reesei* cellulase is capable of hydrolyzing β -D-glucans as well as (1,4)- β -D-glucosidic linkages. However, to achieve a higher glucose yield, which results in a better performance of the system, a cellulase cocktail with a higher β -glucosidase activity can be used. Thus, the dissociation of cellobiose was assumed to be instantaneous, and its concentration and its inhibitory effect were considered negligible. This assumption was further confirmed with the glucose oxidase method, which is specific for glucose detection. In comparison with the DNS method, less than 2% difference in the two readings has confirmed that cellobiose is negligible.

The reversible binding was considered for both the adsorption and desorption steps to better represent the inhibition effect. Enzyme (*E*) binding to the substrate (*S*) is described by Equation (8), whereas product (*P*) formation and desorption are described by Equations (9) and (10), respectively.





where k_s ($\text{m}^3 \text{g}^{-1} \text{h}^{-1}$) and k_{-s} ($1/\text{h}$) are the forward and backward rate constants for reversible ES intermediate formation, respectively; k_p ($1/\text{h}$) is the rate constant for the surface reaction step; and k_{EP} ($1/\text{h}$) and k_{EP2} ($\text{m}^3 \text{g}^{-1} \text{h}^{-1}$) are the forward and backward rate constants for the competitive inhibition effect of the product on the enzyme, respectively.

Consequently, a set of first-order differential equations, Equations (11)–(13), could be established to describe the rate at each step of the hydrolysis.

$$\frac{d[ES]}{dt} = k_s[E][S] - (k_{-s} - k_p)[ES] \quad (11)$$

$$\frac{d[EP]}{dt} = k_p[ES] + k_{EP2}[E][P] - k_{EP}[EP] \quad (12)$$

$$\frac{d[P]}{dt} = k_{EP}[EP] - k_{EP2}[E][P] \quad (13)$$

Equations (11)–(13) are similar to the ones used in a previous study [164], except that in the presently proposed mechanistic steps, instead of assuming EP complex formation was only due to the inhibition effect, it is assumed to be formed after the cleavage of cellulose and then dissociated to E and P . Only then does the inhibition effect occur as a result of reverse binding. This modification better represents the actual inhibition effect.

Assuming a quasi-steady-state model, the differential Equations (11)–(13) were solved simultaneously in combination with enzyme conservation given by Equation (14), with the initial conditions of $t = 0$, $[S] = [S_0]$, and $[ES] = [EP] = [P] = 0$, and the five rate constants, k_s , k_{-s} , k_p , k_{EP} , and k_{EP2} were estimated. The rate of product formation was then expressed by Equations (15)–(20).

$$1 = E - ES - EP \quad (14)$$

$$\frac{dP}{dt} = \left(\frac{S + K_1 P}{K_2 + K_3 S + K_4 P} - k_{EP2} P \right) - P \frac{v}{V} \quad (15)$$

$$S = 1 - P \quad (16)$$

$$K_1 = \frac{(k_{-s} + k_p) k_{EP2}}{k_p k_s} \quad (17)$$

$$K_2 = \frac{\frac{k_{-s} - 1}{k_p}}{k_s} \quad (18)$$

$$K_3 = \frac{1}{k_p} + \frac{1}{k_{EP}} \quad (19)$$

$$K_4 = \frac{(k_{-s} + k_p) k_{EP2}}{k_{EP} k_s k_p} \quad (20)$$

where E , ES , and EP are the dimensionless mass concentrations of the total cellulase, enzyme–substrate complex, and enzyme–product complex, respectively, defined as the respective concentrations in the reaction cell, $[E]$, $[ES]$, and $[EP]$, divided by the initial enzyme concentration, $[E_0]$; P and S are the dimensionless concentrations of the product and substrate, defined as the concentrations of the glucose, $[P]$, and the substrate, $[S]$, in the reaction cell divided by the initial substrate concentration, $[S_0]$, respectively; V is the volume of the reaction cell; v is the superficial velocity of flowing water in the system; and t is the time.

Assuming the permeation of product out of the reaction cell (lower chamber) to be by pure convection, the total production yield (Y) can then be described using Equation (21), which is the sum of the mass of product accumulated in the reaction cell and of that diffused to the upper cell divided by the initial mass of the substrate.

$$Y = \frac{G}{[S_0]V} = P + \frac{v}{V} \int_0^t P dt \quad (21)$$

4.3 Radial-flow Tubular MBR

4.3.1 Radial-flow MBR Design

The radial flow MBR was designed with an inner zone jacketed with an outer cylinder, as shown in Figure 8. The wall of the inner zone, of an internal diameter, ID, of 8 cm and height, h, of 18.6 cm which corresponds to a height to internal diameter ratio of 2.3, surrounded by an outer cylinder of OD of 15 cm and h of 24 cm, with height to internal diameter ratio of 3, and outer diameter to internal diameter ratio of 1.9. The reaction was carried out in the inner zone where enzymes and substrate were charged, while the outer cylinder contained only distilled water with pH similar to that at the reaction zone. The walls of the inner reaction zone composed of the PES membrane, with a membrane thickness to internal diameter ratio of 0.003, trapped between two woven stainless-steel wire mesh to provide a physical support and secured to the upper and lower disks by tight epoxy adhesive glue and further sealed with silicone to eliminate any possibility of leakage. This was confirmed by subjecting the system to a leakage test before being used in the experiment. The reaction zone was agitated using a magnetic stirrer at 450 rpm, which corresponds to a Reynolds number of 1313, with bar diameter to reactor internal diameter ratio of 0.1, as shown in Section 4.2.1, to create enough turbulence for good mixing while avoiding shear stress that could deactivate the enzymes. The temperature of the reaction was maintained at 48°C by placing the reactor on a hot plate, set at 48°C and covering the outer cylinder with a heating tape (Thermolyne, Sigma) fitted with a thermocouple that was connected to a temperature controller (TC4S-14R). The reactor was further covered with wool insulation and wrapped with aluminum foil to minimize any heat loss and temperature fluctuation. Distilled water at the reaction temperature and adjusted pH 4.8, was introduced to the inner reaction zone using a peristaltic pump (Shenchen, China) and diffused through the membrane, with the produced product, to the outer zone. The water passed from the inner cylinder to the outer cylinder through the membrane in a radial direction and was collected in a beaker. The system was tested at the

same conditions used for the inverted dead-end MBR. Samples to be measured were collected in triplicates, and the results presented in all figures are the average values with the standard deviations shown as error bars.

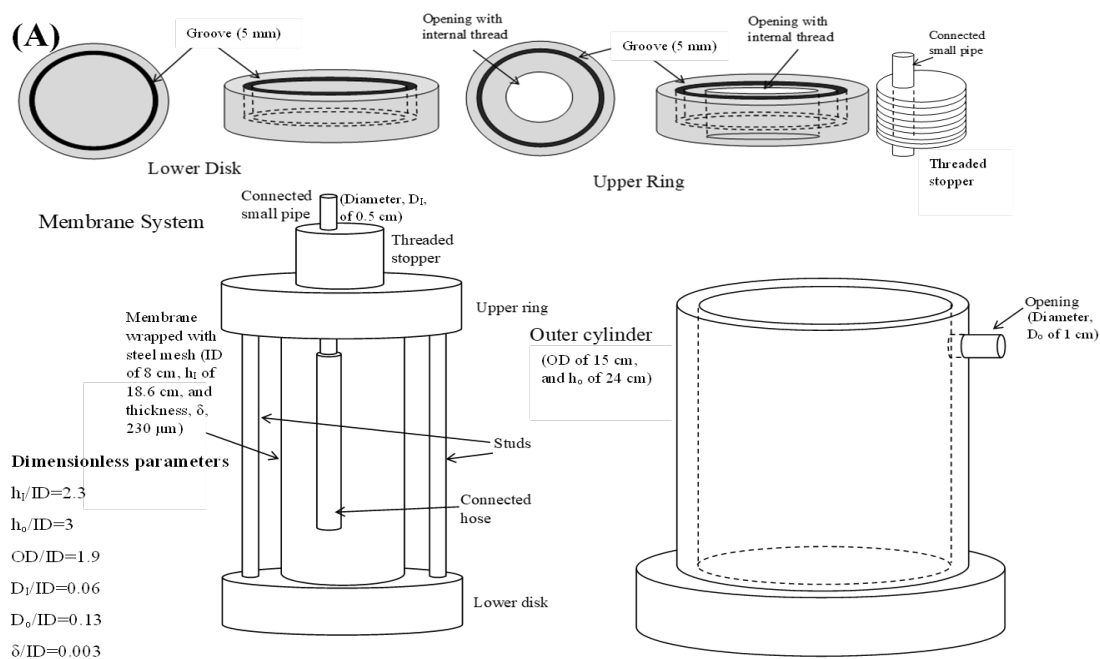


Figure 8: Radial-flow MBR design. (A) Schematic diagram of the radial flow tubular MBR, and (B) photo of the assembled tubular MBR

To start up the process in the radial flow tubular MBR, the outer cylinder was first filled with pH 4.8 buffer solution in distilled water at the desired temperature to reach a volume that was previously determined to cover the entire membrane area. A substrate solution in a pH 4.8 buffer at the same desired temperature was slowly added to the inner cylinder through the unglued threaded stopper while inserting the cylinder in the outer one. This step was carefully carried out to keep an equal volume level in both cylinders to avoid creating a pressure difference across the membrane. A buffer solution at the desired temperature then added through the inlet line to fill the inner cylinder completely, and then the stopper was threaded back and sealed with silicone to avoid leakage. Once steady state was reached, where temperature, pH, and mixing speed were constant, enzymes were added through the inlet line to start the reaction.

Flow diagrams of the inverted dead-end and radial flow MBRs are shown in Figure 9. In the inverted dead-end MBR, glucose and water flow from bottom to top across the membrane against gravity, as shown in Figure 9A. The active membrane surface area and specific area per volume of reaction in the inverted dead-end MBR were 44 cm^2 and $0.06 \text{ cm}^2/\text{cm}^3$, respectively. In the radial flow tubular MBR the flow takes place throughout the entire membrane surface area surrounding the reactor, as showing in Figure 9B. The active membrane surface area and specific area per volume of reaction in the radial flow tubular MBR were 578 cm^2 and $0.62 \text{ cm}^2/\text{cm}^3$. It was clear that the radial flow allowed for more product separation, which shifts the reaction more towards the forward direction.

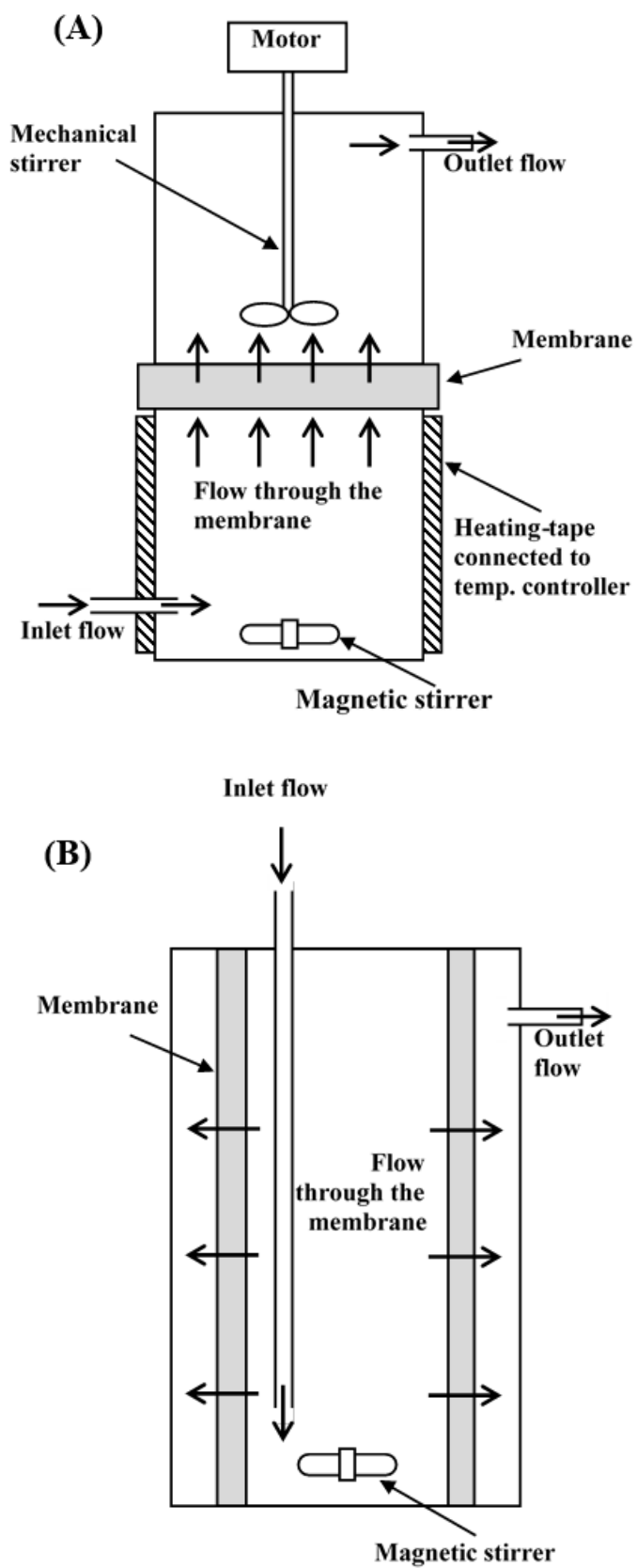


Figure 9: Flow diagram of (A) inverted dead-end, and (B) radial flow tubular MBRs

4.3.2 Enzymatic Hydrolysis with Product Separation

In the radial-flow MBR, enzymatic hydrolysis of DSs at a concentration of 13.3 g/L and water flow of 0.8 mL/min ($\tau = 15.6$ h) was investigated using 0.48 g/L enzyme concentration at 48°C and agitation speed of 450 rpm ($Re = 1313.4$). These conditions were the highest conditions used in the inverted dead-end MBR using standard cellulose. Samples to be measured were collected in triplicates, and the results presented in all figures are the average values with the standard deviations shown as error bars.

4.3.3 Kinetic Modeling

4.3.3.1 The Effect of Substrate Concentration and Water Flowrate

The enzymatic hydrolysis of DSs was investigated using an enzyme concentration of 0.48 g/L at 48°C and pH 4.8, with agitation speed of 450 rpm ($Re = 1313$). The effects of the main operational parameters, *i.e.*, substrate concentration and water flowrate, on total reducing sugars produced, which is the process output variable, were investigated. A total of 9 experimental runs was suggested by the general factorial design. The ranges and levels of the input variables for enzymatic cellulose hydrolysis used in the Minitab software are presented in Table 5. The tested flowrates, 0.4, 0.8, and 1.2, corresponds to residence times of 31.3, 15.6, and 10.4 h, respectively. Samples to be measured were collected in triplicates, and the results presented in all figures are the average values with the standard deviations shown as error bars.

Table 5: Levels of two factors affecting total reducing sugars production in the enzymatic hydrolysis of the substrate

Factors level	-1	0	1
Substrate concentration, X_1 (g/L)	14.3	21.4	39.6
Water flowrate, X_2 (mL/min)	0.4	0.8	1.2

4.3.3.2 Kinetic Model

The dynamic model developed is a modified version of the one proposed in Section 4.2.3 used to describe the simultaneous enzymatic hydrolysis and product separation using standard, completely amorphous, cellulose in an inverted dead-end MBR. The model was modified to take into consideration the complex structure of the real lignocellulosic biomass, namely DSs, used as a substrate in this work. The presence of a non-hydrolyzable portion of the cellulose, which resulted in changes in the structure as the reaction proceeds has been taken into consideration, which was not considered in the previous model.

In the heterogeneous system of lignocellulose hydrolysis, the reaction goes through multiple steps: (1) enzymes diffuse from the bulk to the substrate surface, (2) enzyme-substrate complexes are formed, during which the enzyme molecules can either bind to hydrolyzable or non-hydrolyzable parts of the cellulose, resulting in productive or nonproductive bindings, respectively, (3) productive bindings result in products formation, whereas the non-productive bindings result in activity loss of the attached enzyme molecules, until they detach, representing a substrate inhibition effect, (4) products are produced from the productive enzyme-substrate complex, in which delay in products desorption from the enzyme active sites represent product inhibition effect, (5) diffusion of the desorbed products from the bulk to the membrane surface, (6) diffusion of the products through the membrane, and (8) diffusion of the product from the other side of the membrane to the outer cylinder.

Due to the mixing in the inner cylinder, convection from the bulk to a surface, being of the substrate or the membrane, was assumed to be instantaneous. Additionally, competitive inhibition of cellulase was assumed to be caused by the final products such as glucose. Because β -glucosidase has a higher activity than glucanase, the dissociation of cellobiose was assumed to be instantaneous, and its concentration and its inhibitory effect was considered negligible. In

addition, due to the synergetic action of endoglucanase, exoglucanase, and β -glucosidase, cellulase enzymes were considered as a single enzyme. The latter two assumptions were adapted by most previous kinetic studies [159, 163, 171]. The model proposed in this work took into consideration the changes in the structure and composition of substrate with time and the inhibition by the non-hydrolyzable part of the substrate, as described in a previous study [164]. In addition, enzyme binding to a non-hydrolyzable substrate was considered to be reversible.

Enzyme (E) binding to the hydrolyzable substrate (S_c) is described by Equation (22), whereas the enzyme (E) binding to the non-hydrolyzable substrate (S_x) is presented by Equation (23). Finally, product (P) formation and desorption are described by Equations (24) and (25), respectively.



where S_c and S_x are the hydrolyzable and non-hydrolyzable parts of the substrate, respectively, k_{c1} and k_{c2} are the forward and the backward rate constants for the reversible ES_c intermediate formation, respectively; k_{x1} and k_{x2} are the forward and the backward rate constants for the reversible non-productive ES_x intermediate formation, respectively; k_p is the rate constant for the surface reaction step where the hydrolysable cellulose is broken down to form the product; and k_{EP1} and k_{EP2} are the forward and backward rate constants for the competitive inhibition of the product, respectively.

During the hydrolysis process, the enzymes hydrolyze the hydrolyzable part on the first layer of substrate, leaving the next inside layer exposed to another enzymatic attack. As the reaction continues, the hydrolysis action proceeds from the outer layers of the substrate to inner ones. With each newly exposed layer, another hydrolyzable and non-hydrolyzable parts are exposed. The ratio of the hydrolyzable and non-hydrolyzable parts, represented by non-hydrolyzable fraction coefficient, φ , described by Equations (26) and (27), was assumed constant for a specific type of lignocellulose and pretreatment method [164]. The non-hydrolyzable fraction coefficient at each newly exposed layer was assumed to be constant. To account the drop in substrate accessibility of the exposed layers as the reaction proceeds, substrate accessibility coefficient, σ , was introduced in a previous study [164]. This coefficient changes with time, starting from a value of one at which the substrate is completely accessible to the enzymes and decreases with time, as the reaction proceeds, as described by Equation (28).

$$\varphi = \frac{[S_x]_o}{[S_t]} \quad (26)$$

$$(1 - \varphi) = \frac{[S_c]_o}{[S_t]} \quad (27)$$

$$\sigma = e^{-\alpha t} \quad (28)$$

where $[S_c]_o$, $[S_x]_o$ and $[S_t]$ are the initial hydrolyzable, non-hydrolyzable, and total substrate concentrations, respectively, and α is a constant.

Consequently, a set of first-order differential equations, Equations (29)–(34), could be established to describe the rate at each step of the hydrolysis.

$$\frac{d[ES_c]}{dt} = k_{c_1}[E][S_c] - (k_{c_2} + k_p)[ES_c] \quad (29)$$

$$\frac{d[ES_x]}{dt} = k_{x_1}[E][S_x] - k_{x_2}[ES_x] \quad (30)$$

$$\frac{d[EP]}{dt} = k_p[ES_c] + k_{EP2}[E][P] - k_{EP1}[EP] \quad (31)$$

$$\frac{d[P]}{dt} = k_{EP1}[EP] - k_{EP2}[E][P] - \frac{v}{V}[P] \quad (32)$$

$$\frac{d[S_c]}{dt} = (k_{c_2} + \sigma(1 - \varphi)k_p)[ES_c] - k_{c_1}[E][S_c] \quad (33)$$

$$\frac{d[S_x]}{dt} = k_{x_2}[ES_x] - k_{x_1}[E][S_x] + \sigma\varphi k_p[ES_c] \quad (34)$$

where V is the volume of the reaction cell; v is the superficial velocity of flowing water in the system; and t is the time.

Equations (29)–(34) are similar to the ones proposed in a previous study [164], except that in the presently proposed mechanistic steps, instead of assuming EP complex formation was only due to the inhibition effect, it is assumed to be formed after the cleavage of cellulose and then dissociated to E and P . Only then does the inhibition effect occur as a result of reverse binding. This modification better represents the actual inhibition effect.

The differential Equations (29)–(34) were solved simultaneously with the enzyme conservation equation, given by Equation (35), and initial conditions of $t = 0$, $[S_c] = [S_c]_o$, $[S_x] = [S_x]_o$ and $[ES_c] = [ES_x] = [EP] = [P] = 0$. In addition, as the molecular weight of cellulose monomer is very close to that of the glucose molecule, mass concentration was used instead of mole concentration. Assuming the permeation of product out of the reaction cell (inner tube) to be by pure convection, the total amount of reducing sugars produced can be presented by Equation (36), which is the sum of the mass of total reducing sugars accumulated in the reaction cell and of that diffused to the outer cylinder.

$$[E] = [E_o] - [ES_c] - [ES_x] - [EP] \quad (35)$$

$$G = V[P] + v \int_0^t [P] dt \quad (36)$$

4.3.3.3 Sensitivity analysis

The significance of the estimated kinetic parameters on the total reducing sugars produced was examined using sensitivity analysis. Each parameter was changed ± 5 , ± 10 , ± 15 , and $\pm 20\%$ from the original estimated value [172], while the remaining parameters were remained unchanged. The amount of the total reducing sugars produced was recalculated using Equation (36), and the impact of each parameter was evaluated using Equation (37) [173].

$$P = \frac{P_2 - P_1}{P_1} \times 100 \quad (37)$$

where, P_1 represent the total amount of total reducing sugars produced with the original estimated parameter (0% change), and P_2 is the newly estimated amount with the changed parameter.

4.4 Glucose Permeation Analysis

The permeation rate of glucose through membranes with different MWCOs in the presence of convective flow with water flowrates of 0.1, 0.2, 0.4, 0.8, and 1.6 mL/min, was tested; this correspond residence times of 125, 62.5, 31.3, 15.6, and 10.4 h, respectively, were tested. Central Composite Design (CCD) was used to statistically analyze the permeation and optimize the process. The selected main variables were glucose concentration, water flow, and membrane MWCO. The ranges and levels of the input variables are presented in Table 6. A total of 20 experimental runs, each for 3 h, were suggested by the CCD, 23 equals 8 cube points, 6 replications at the center point and 6 axial points. Samples to be measured were collected in triplicates, and the results presented in all figures are the average values with the standard deviations shown as error bars.

Table 6: Levels of the factors tested on diffusion of glucose through PES membranes

Factors level	$-\alpha$	-1	0	1	$+\alpha$
Glucose concentration, X_1 (g/L)	13.33	26.66	40	53.33	66.67
Water flowrates, X_2 (mL/min)	0.1	0.2	0.4	0.8	1.6
Membrane MWCOs, X_3 (kDa)		10	30	50	

4.5 Analytical Methods

4.5.1 Total Reducing Sugars Analysis

The total reducing sugars concentrations in a sample were measured using the DNS method [170]. The method measures all produced reducing sugars, including, in addition to glucose produced from the hydrolysis of cellulose, xylose produced from hemicellulose. In brief, 45 μ L of sample containing the sugars was mixed with 40 μ L of DNS reagent and diluted with 315 μ L of distilled water to reach a total volume of 400 μ L, and left to incubate for maximum of 5 min at 100°C. After that, the reaction was stopped by incubation in ice for 10 min. The resulting color transformation from yellow to brown was then measured at 540 nm with a UV spectrophotometer (BMG SPECTROstar, Germany).

4.5.2 Protein Analysis

For protein measurement, Bradford reagent, which is an acidic Coomassie blue dye that stably binds to protein, was used. The dye is originally cationic and red in color; if an enzyme is present in the sample then it binds to it and form an anionic form, resulting in a color change from reddish brown to blue, which can be quantified at 595 nm absorbance using a spectrophotometer [174]. Quantifying protein in the sample was done by mixing 20 μ L of the sample with 180 μ L of Bradford reagent and placed in a 96-well plate reader [175]. A spectrophotometer was used to detect proteins at 595 nm, which was calibrated with serial dilutions of cellulase enzymes. The analysis was carried out in triplicate.

4.5.3 Enzyme Assay

The assay for enzyme activity was based on glucose productivity, with one unit of cellulase being defined as the amount of glucose liberated at 37°C and a pH of 5 in 1 h. The concentration of the liberated glucose was measured, as described in Section 4.5.1, and used to determine the activity of the enzyme. The activity of cellulase was determined as 1800 units/g.

4.5.4 Biomass Characterization

4.5.4.1 Biomass Preparation and Analysis

Date seeds (DSs) from Allig dates were obtained from Liwa Company in the UAE. The DSs were washed with distilled water and then sun-dried and grinded. The dried, grinded DSs were screened, and those in the size of 180 µm were used in this work. Extractives are components that naturally exist in, or are attached to, the biomass [176]. To avoid interference of the extractives in the pretreatment and enzymatic hydrolysis processes and to have an unbiased evaluation of the developed MBR, extractives were removed in a Soxhlet extraction unit using ethanol for 8 h. To characterize the substrate, acid-base isolation method, described by [177], was used to quantify the three main constituents, namely cellulose, hemicellulose, and lignin. Briefly, 10 g of substrate was mixed with 200 mL of 0.1 M HCl while being heated at 100°C for 2 h with stirring at 150 rpm. The mixture was vacuum filtered to separate residues containing cellulose and lignin from the liquid containing hemicellulose. The residues were then washed with 20 mL distilled water to remove any remaining hemicellulose left, followed by air drying overnight. The dried residues were then treated with 200 mL of 0.1 M NaOH for 2 h at 100°C under stirring at 150 rpm. Subsequently, the mixture was vacuum filtered to separate residues containing cellulose from the lignin that was solubilized in NaOH. The residues were further washed with 20 mL of 0.1 M of NaOH and air dried.

DSs were treated with both HCl and NaOH, which is referred to in this manuscript as “HCl+NaOH pretreatment”, to partially remove hemicellulose and lignin, respectively. The hydrolysis of HCl+NaOH treated samples, in which both hemicellulose and lignin were partially removed, were compared to samples treated with only NaOH, which is referred to in this manuscript as “NaOH pretreatment”, in which only lignin was partially removed while keeping the hemicellulose. For the latter case, 10 g of substrate sample was treated only with 200 mL of 0.1 M NaOH for 2 h. The partial removal of hemicellulose did not result in any enhancement in the hydrolysis, in fact a slight lower yield was obtained compared to that obtained using NaOH pretreated DSs biomass. Therefore, all the substrate used in all subsequent experiments were on NaOH pretreated (lignin partially removed) DSs.

4.5.4.2 Lignin Analysis

The lignin content of fresh and alkaline treated DSs samples was determined in accordance with NREL LAP-003 protocol [178]. In this protocol, both acid-insoluble lignin, known as Klason lignin, and acid-soluble lignin were quantified. 0.3 g of extractives free sample was treated with 72% sulfuric acid (H_2SO_4) at 30°C for 2 h with mixing every 15 min. The solution was then diluted with 84 mL distilled water to reach 4% acid concentration, after which it was autoclaved for 1 h at 121°C. The sample was then allowed to cool down before being vacuum filtered to separate liquid from the residues. The residual part, which contains the Klason lignin was placed in a muffle furnace at 575°C for 3 h to determine ash content. Whereas, the acid soluble-lignin was determined by measuring the absorbance of the liquid filtrate at 205 nm.

4.5.4.3 Substrate Characterization

The changes in the structural morphology due to pretreatment methods were detected using scanning electron microscopy (SEM) (JCM-5000; NeoScope). Fresh DSs, HCl+NaOH pretreated and NaOH pretreated DSs biomasses were coated with gold using a JFC-1600Auto

Fine Coater (JEOL) to increase the conductivity of the non-conductive catalyst and to prevent the build-up of electrostatic charge at the specimen surface. The samples were inserted into the SEM for observation.

To analyze the functional groups in fresh DSs, HCl+NaOH pretreated and NaOH pretreated DSs biomasses, Fourier transform infrared (FTIR) spectroscopy (IRTracer-100 FTIR spectrophotometer) (Shimadzu, Kyoto, Japan) was used. The FTIR spectra were recorded on an attenuated total reflection Fourier transform infrared (ATR-FTIR) spectrograph using a range of 600–4000 cm^{-1} with an average of 34 scans and a spectral resolution of 4 cm^{-1} .

X-ray diffraction (XRD) analysis was also used to measure changes in the crystallography of the fresh DSs, HCl+NaOH pretreated and NaOH pretreated DSs biomass. XRD scans were performed with a 2θ range of 4° – 90° , step size of $0.02^\circ/\text{s}$, voltage of 40 kV, intensity of 20A, and Cu $K\alpha$ radiation of 1.5406 Å.

4.5.5 Membrane Characterization

The PES membrane was investigated before and after subjection to the process conditions to detect any changes that might happen to it. Both PES-10 and PES-30 membranes were tested before, *i.e.*, as received, and after their use in more than 20 runs (*i.e.*, about 160 h of operation) at different substrate concentrations and water flowrates.

To detect internal fouling or any changes in the internal structure of the membrane, images of cross-sectional cuts of PES-30 were observed using SEM (JCM-5000; NeoScope). Internal fouling may occur when molecules of sizes close to those of the membrane pores are pushed through, as the water is forced across the membrane, resulting in pores blocking. Neither glucose nor the substrate are expected to contribute to the internal fouling, as the former is much smaller, and the latter is much larger than the membranes MWCO. If internal fouling may occur, it would be mainly due to the cellulase molecules, which have molecular weights higher than the

membranes cut-offs, but still in the same order of magnitude. Therefore, internal fouling is expected to be more significant as the MWCO increases and becomes closer to the size of the cellulase. Therefore, the membrane with the higher MWCO, PES-30, was used in this analysis, as if no changes occur in PES-30, then the same can be fairly assumed in PES-10. However, to further confirm, cross-sectional cuts of PES-10 were examined. Samples of PES membranes before and after use were coated with gold using a JFC-1600Auto Fine Coater (JEOL) to increase the conductivity of the non-conductive catalyst and to prevent the build-up of electrostatic charge at the specimen surface. Then, the samples were cleaned to remove silt, dust, and detritus. The samples were mounted on a holder and inserted into the SEM for observation.

To assess surface fouling, FTIR (IRTracer-100 FTIR spectrophotometer) (Shimadzu, Kyoto, Japan) was carried out on the membrane surface. As the probability of the occurrence of this type of fouling is similar to membranes of both MWCOs, both PES-10 and PES-30 were subjected to this analysis. The FTIR spectra were recorded on an attenuated total reflection Fourier transform infrared (ATR-FTIR) spectrograph using a range of 600–4000 cm^{-1} with an average of 34 scans and a spectral resolution of 4 cm^{-1} .

XRD analysis was also used to measure changes in the crystalline structure of the membranes. Similar to FTIR, this test is done on both membranes, PES-10 and PES-30. XRD scans were performed with a 2θ range of 4° – 90° , step size of $0.02^\circ/\text{s}$, voltage of 40 kV, intensity of 20A, and Cu $K\alpha$ radiation of 1.5406 Å.

Chapter 5: Results and Discussion

5.1 Inverted Dead-end MBR

5.1.1 Selective Glucose Permeation

The designed MBR with the PES membrane was subjected to glucose permeation and cellulase rejection analyses. Theoretically, PES membranes should selectively allow permeation of the relatively small glucose molecules (180 Da) and reject the larger molecules of cellulase comprising endoglucanase (~52,000 Da), exoglucanase (~61,000 Da), and β -glucosidase (76,000 Da) [170]. Indeed, the PES membrane with 10 kDa MWCO (PES-10) has previously shown to allow the complete permeation of glucose and the total rejection of cellulase [139, 179–183]. To further confirm this, the permeation of glucose and cellulase to the upper chamber through a PES membrane with larger MWCO membrane of 30 kDa MWCO (PES-30) was investigated. Figure 10 shows the yields of glucose and cellulase in the upper chamber of the MBR over time permeated through the PES-30 membrane with initial glucose and cellulase concentrations of 40 g/L and 3.2 g/L, respectively, and a pure water flowrate of 0.4 mL/min, equivalent to residence time of 31.3 h. The lines shown on the figure are connections between the points, added to highlight the trend. Within 16 h, approximately 50% of the added glucose had permeated to the upper chamber, whereas no cellulase was detected therein. The high selectivity was proven using larger MWCO and higher glucose and cellulase concentrations than those used in subsequent hydrolysis runs. This guaranteed that the high selectivity is sustained at all the lower tested conditions. For example, if no cellulase permeation or internal fouling are detected using the larger MWCO, PES-30, then it would be safe to assume that they would not take place using the lower MWCO, PES-10 membrane. Therefore, the total rejection of cellulase by the PES membranes while permeating glucose molecules was confirmed.

To eliminate the possibility of cellulase being pushed into the pores of the membrane, resulting in internal fouling and a drop in the enzyme bulk concentration, the cellulase concentration in the reaction cell was measured while using the PES-10 membrane. This experiment was conducted using initial glucose and cellulase concentrations of 67 g/L and 0.48 g/L, respectively, and a water flowrate of 0.8 mL/min ($\tau = 15.6$ h). The enzyme concentration was used in the same order of that used in the hydrolysis experiment. As the diffusion of molecules into the membrane pores occurs more easily when the pore size is close to the size of the enzyme molecules, the experiment was repeated using a membrane with a 50 kDa MWCO (PES-50). With both membranes, no drop in cellulase concentrations was detected after 3 h of diffusion, which confirmed that the diffusion effect on enzyme permeation was negligible and the PES membranes had completely rejected cellulases. Another important conclusion that can be made here was the insignificance of the membrane MWCO effect on the process within the investigated MWCO range, especially in the case where the convection–diffusion of glucose was greater than its molecular diffusion. Thus, PES-10 was used in basis all subsequent experiments. However, PES-30 and PES-50 were still used in some cases to confirm the absence of membrane fouling, determining the permeability, and in the permeation rate analysis.

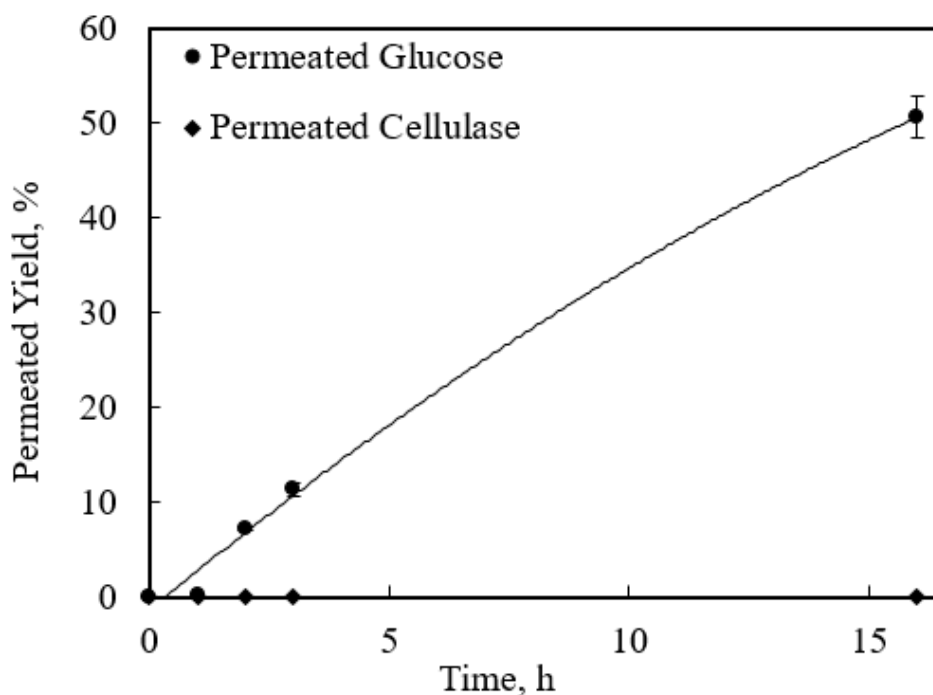


Figure 10: Yields of permeated glucose and cellulase to the upper cell through PES-30, at pH 4.8, 48°C, water flow of 0.4 mL/min ($\tau = 15.6$ h) and initial glucose and cellulase concentrations of 40 g/L and 3.2 g/L, in the lower cell respectively

Permeation of glucose and cellulase by means of a concentration gradient only to the upper chamber through PES-30 was monitored for over 12 h to determine the membrane permeability. Four initial glucose concentrations, 100, 133, 200, and 267 g/L, and cellulase concentration of 4 g/L in the bottom cell were tested. Figure 11 shows the amount of glucose permeated through PES-30 membrane with time. The lines shown on the figure are the connection between the points, added to highlight the trend. It should be noted that the error bars were too small to be observable at the various data points of the curve, which indicates good reproducibility of the data. The amount of cellulase in the upper cell was undetectable, suggesting complete rejection by the membrane. At all tested concentrations, glucose permeated through the membrane was by natural diffusion. As shown in Figure 11, natural diffusion increased with the increase in glucose concentration. This was mainly due to the increase in the driving force, which is concentration gradient. Membrane permeability is defined as the permeation rate normalized by the membrane

surface area, driving force, and membrane thickness active layer. In natural diffusion, the driving force is the concentration gradient. For simplicity the permeability was estimated based on the membrane actual thickness and not the thickness of the active layer of the membrane. Thus, the PES-30 permeability was estimated to be 1.97 h^{-1} .

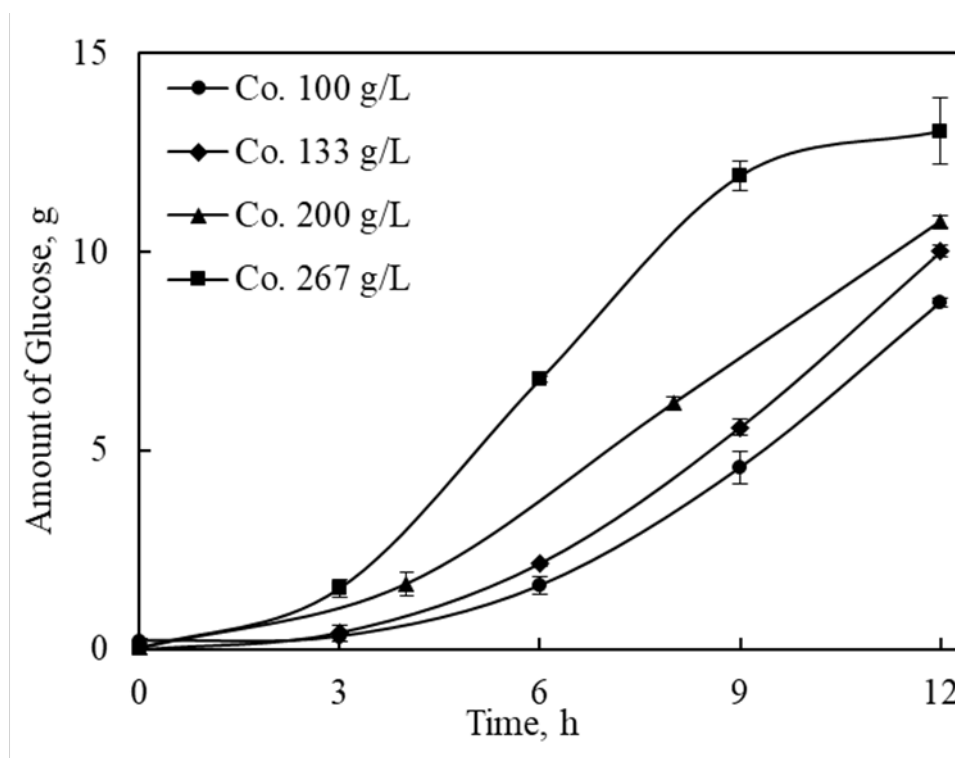


Figure 11: Effect of initial concentration, C_o , on the permeated glucose through PES-30 membrane by pure natural diffusion

5.1.2 Effect of the Process on the Membranes

To confirm that the internal fouling effect was not significant and that subjecting the membrane to the reaction system did not affect the morphology of the membrane, damage it or changed the internal structure, SEM images of PES membranes were taken before, *i.e.*, as commercially received, and after its use in multiple experiments with different substrate concentrations and water flowrates. The SEM images were taken for PES-10 membrane, which was used in most experiments. However, if the internal fouling occurred during the process, it would be expected to be prominent on the larger MWCO membrane, which has pore sizes closer

to the size of the enzymes. Therefore, SEM images of the larger MWCO membrane, PES-30, were also acquired. Figure 12 shows the SEM images of before and after usage of both membranes, PES-10 and PES-30. The PES membranes are composed of a thin skin layer and a thicker supporting layer that more looks like fibers. By looking at the figure, the intact skin layer, the undisrupted structured fibers, the absence of impeded molecules, and the unchanged pore's structure, clearly suggest that no significant changes in the morphology of both of the membranes after submission to the reaction system. Therefore, it can be assumed that internal fouling effect was insignificant.

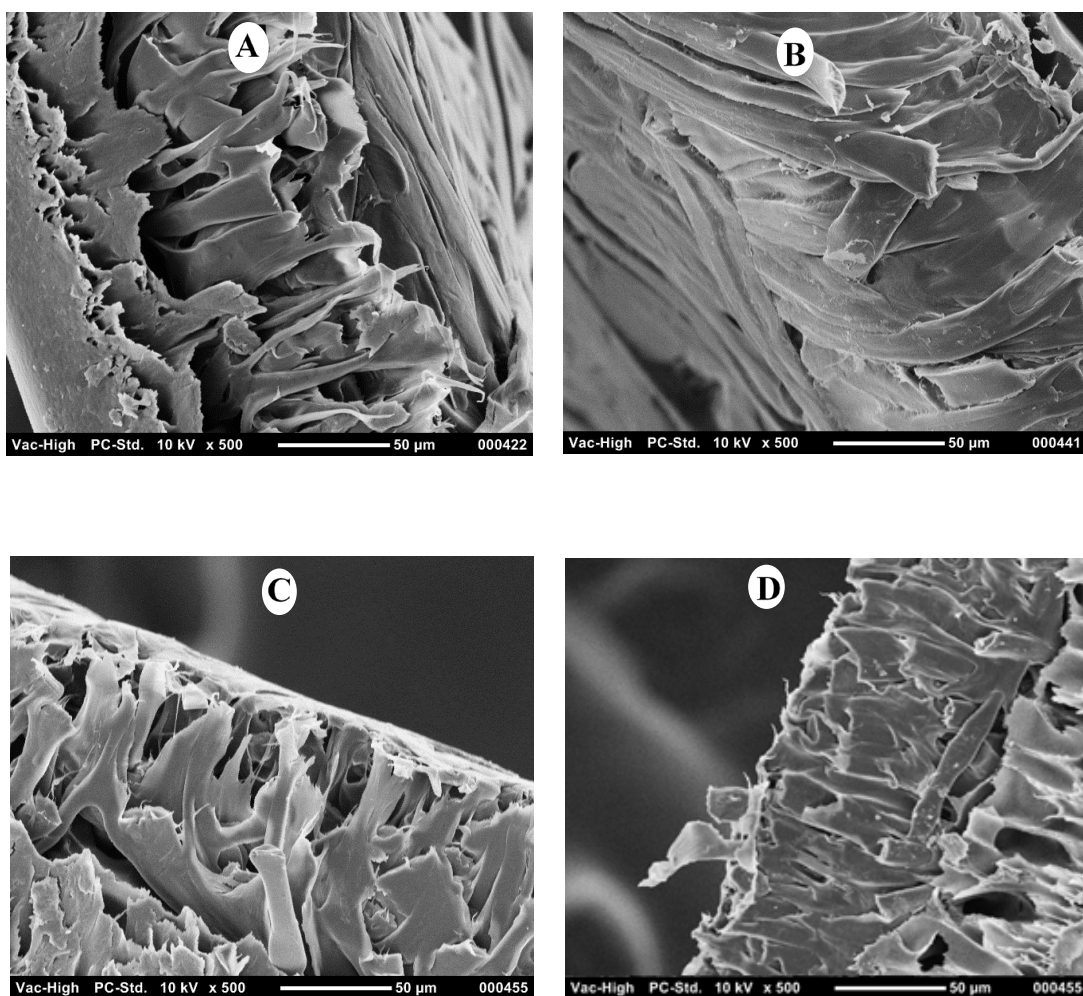


Figure 12: Cross-sectional SEM images of PES membrane. (A) PES-10 before the process, (B) PES-10 after the process, (C) PES-30 before the process, and (D) PES-30 after the process

The absence of surface fouling was also confirmed by analyzing the chemical changes that may have occurred on the membrane during the processes of enzymatic hydrolysis and diffusion using FTIR, as well as to detect enzyme immobilization as FTIR is a common technique used to detect enzyme immobilization on membranes [184–186]. Figure 13 shows the FTIR spectra (range: 600–4000 cm^{-1}) of the PES-10 and PES-30 membranes before and after the enzymatic hydrolysis. The spectra of both the PES membranes were in agreement with those reported in other studies, in which the sustainment of the peaks, similar to those found in this work for the membranes before and after subjection to reaction conditions, were taken as evidence for absence of surface fouling [185, 187, 188]. The peaks at 2913 and 2845 cm^{-1} represent the phenoxy groups that form the backbone of the PES membrane. The peak at 1374 cm^{-1} is a characteristic of $-\text{CH}_3$ bending; the peak at 1152 cm^{-1} can be assigned to the asymmetrical stretching vibration of sulfonic acid groups found in the PES membrane; and the peak at 719 cm^{-1} belongs to aromatic carbons. The spectra of the membranes before and after the reaction generally showed similar peaks. The only changes observed after the process were the appearance of a peak at 1242 cm^{-1} in PES-10 due to the asymmetrical stretching of aromatic Ar–O–Ar ethers and the disappearance of the peak at 1651 cm^{-1} in PES-30 due to the vibration of the amide group. The latter has been reported to be a characteristic of polyvinylpyrrolidone, a material added to the PES membrane [189]. However, these changes were minor and do not suggest any significant change in the PES membrane characteristics following its use in the reaction process. The absence of internal fouling was further confirmed by measuring the enzyme concentration in the lower cell at the beginning and at the end of the reaction. As no drop in the concentration was detected, which was quantified to be 0.48 g/L before and after, it was fairly assumed that enzyme adsorption on the membrane is negligible. This further confirmed the results of the FTIR, which also suggested no presence of adsorbed enzyme.

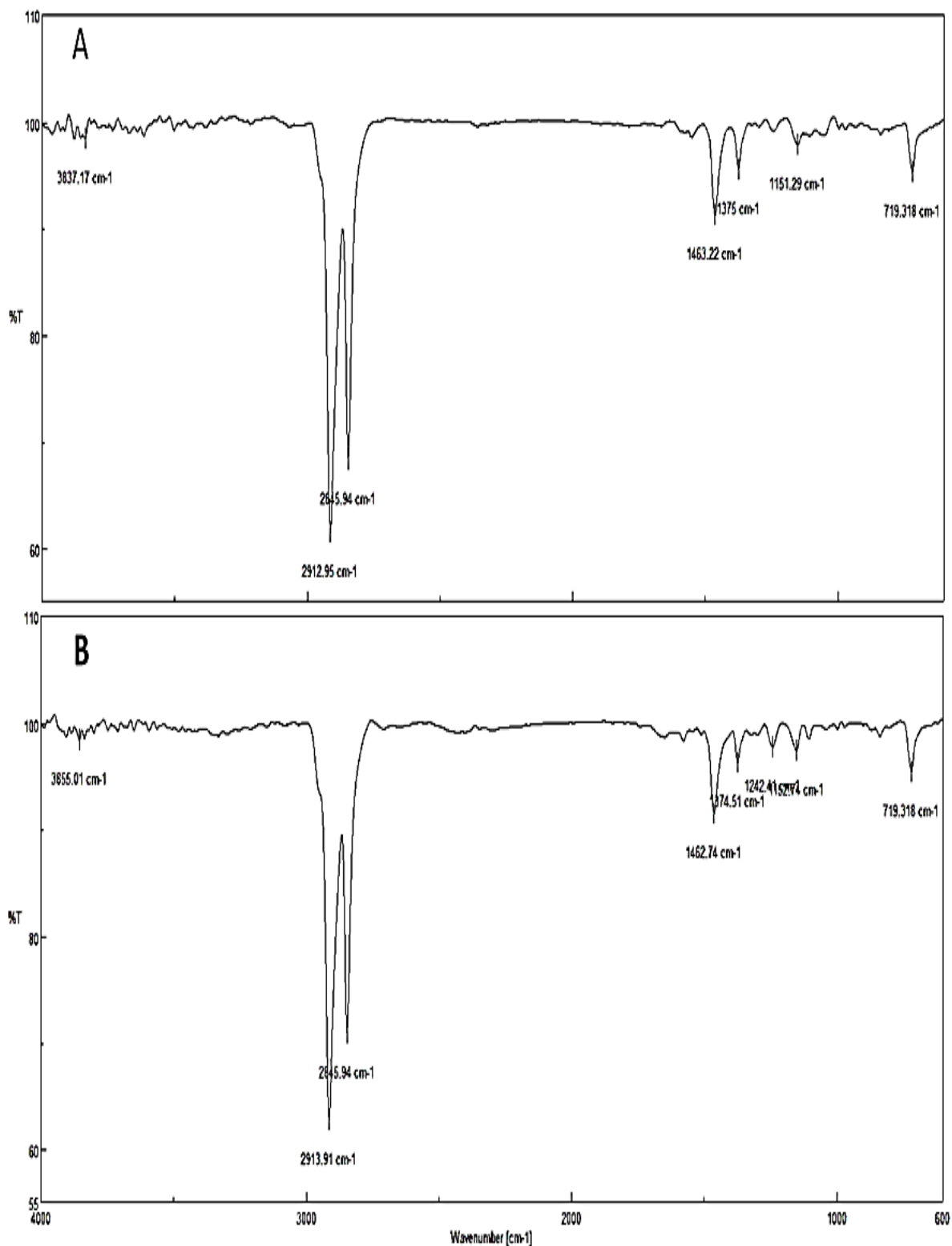


Figure 13: FTIR spectra of the investigated PES membranes (A) PES-10 before the process, (B) PES-10 after the process, (C) PES-30 before the process, and (D) PES-30 after the process

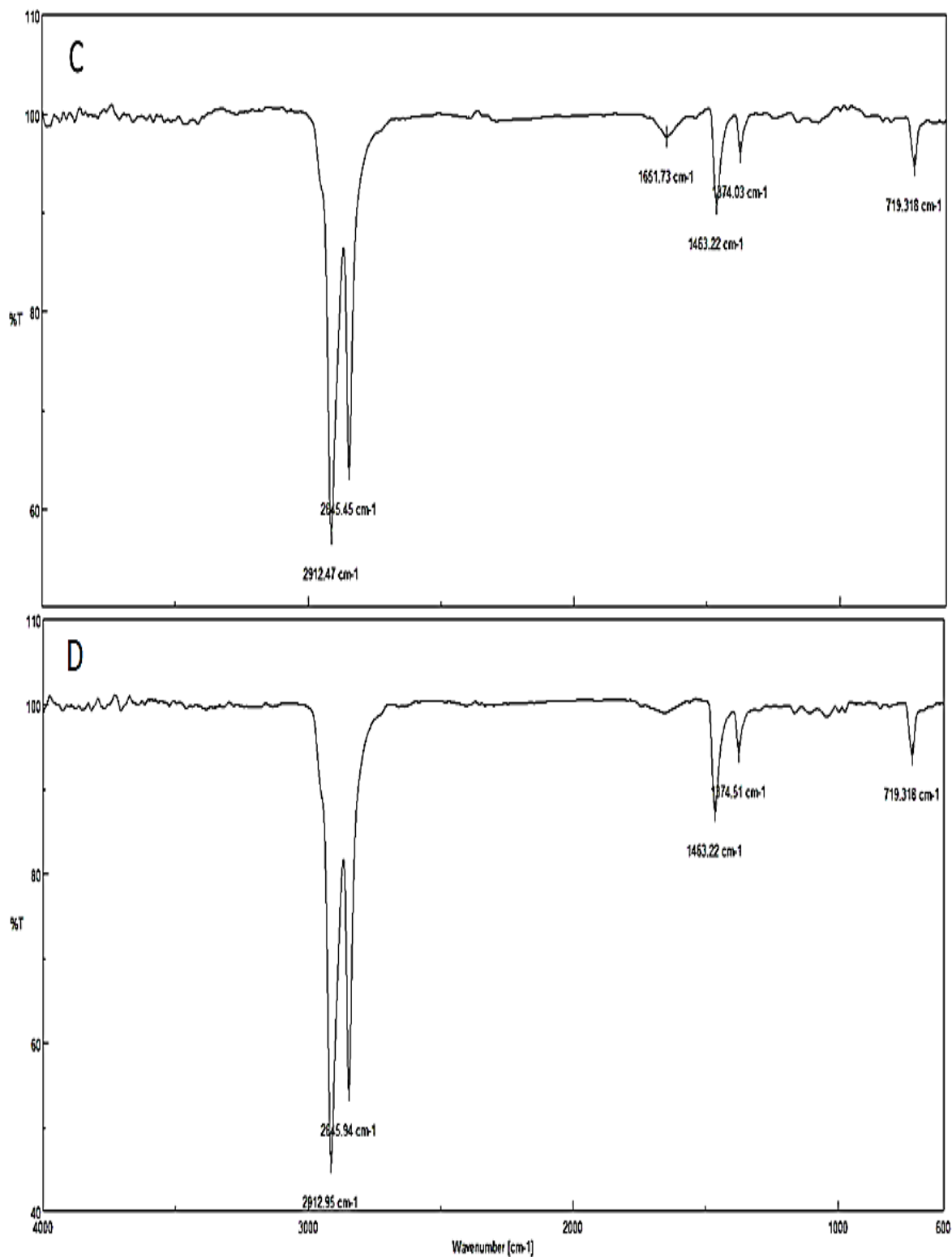


Figure 13: FTIR spectra of the investigated PES membranes (A) PES-10 before the process, (B) PES-10 after the process, (C) PES-30 before the process, and (D) PES-30 after the process (Continued)

The aforementioned findings were further confirmed using XRD analysis, which was carried out to investigate changes in the crystalline structure of the membrane. As shown in Figure 14, there were no clear changes in the XRD spectra for either PES-10 or PES-30 membranes before and after enzymatic substrate hydrolysis, proving that they were not affected by the reaction process.

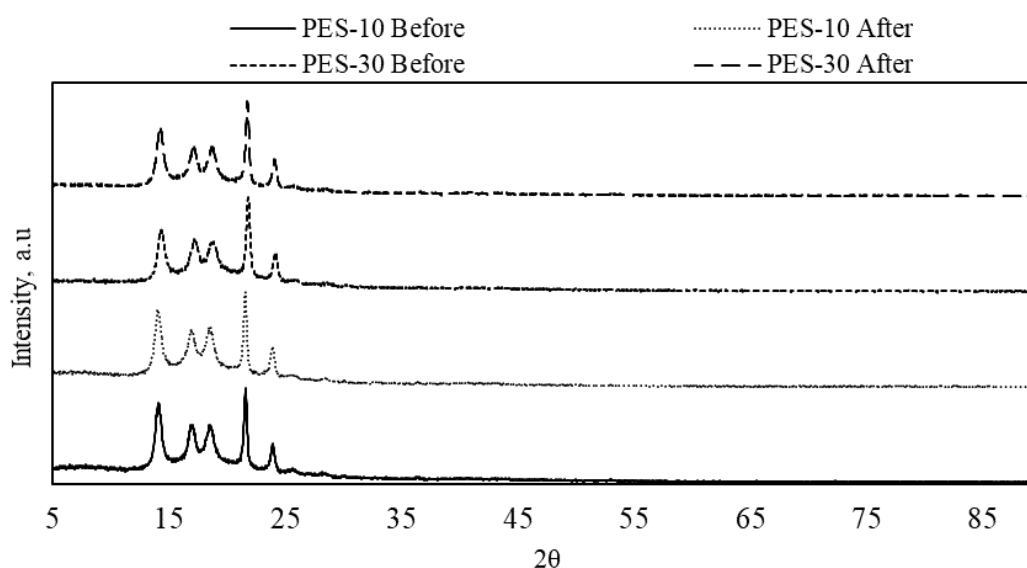


Figure 14: XRD of the investigated PES membrane, PES-10 and PES-30, before and after the process

5.1.3 Enzymatic Hydrolysis with Product Separation

To prove the concept of enhanced enzymatic hydrolysis with simultaneous product separation, the experiment was run at 48°C using the PES-10 membrane, 6.67 g/L of filter paper as pieces, 0.48 g/L of *T. reesei* cellulase, and a water flowrate of 0.4 mL/min ($\tau = 31.3$ h). The results were compared with a reaction conducted under the same conditions but without product separation. As shown in Figure 15, a total glucose yield of 45% was achieved within 8 h in the MBR with product separation, whereas the yield did not exceed 7% in the reactor without product separation. The lines shown on the figure are the connection between the points, added to highlight the trend. It should be noted that the error bars were too small to be observable at the various data

points of the curve, which indicates a good reproducibility of the data. The results clearly prove the concept and highlight the crucial effect of product or glucose inhibition on the enzymatic activity.

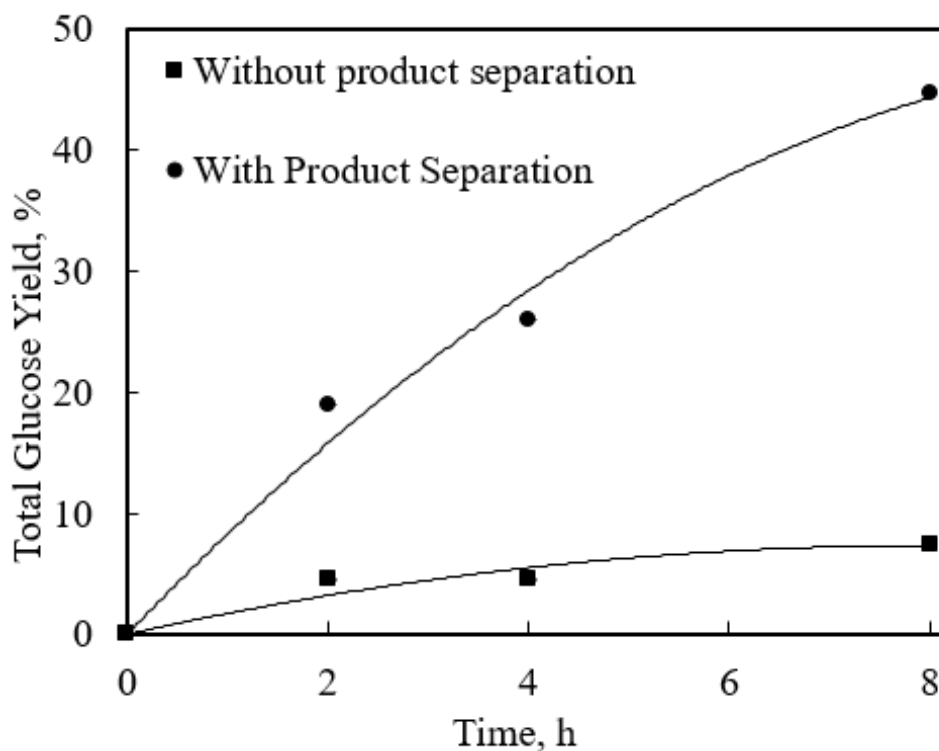


Figure 15: Comparison in glucose production yield in MBR with and without glucose separation under the same conditions using substrate and cellulase concentrations of 6.67 g/L and 0.48 g/L, at pH 4.8 and 48°C and water flow of 0.4 mL/min ($\tau = 31.3$ h)

To confirm that the dominant factor for product separation was convection flow and to further confirm that the effect of MWCO and internal fouling were negligible, the simultaneous hydrolysis–product separation experiment was repeated using PES-30 membrane, under the same reaction conditions of 48°C, a water flowrate of 0.4 mL/min ($\tau = 31.3$ h), and initial substrate and cellulase concentrations of 6.67 g/L and 0.48 g/L, respectively. As explained in Section 5.1.2, internal fouling is expected to be more significant as the MWCO increases and become closer to the size of the cellulase. Therefore, should this effect be significant, the behaviour of membranes of different MWCOs would have been different, with PES-30 displaying a lower permeability.

However, as shown in Figure 16, similar results were obtained using both membranes in the total yield and the accumulated yield measured in the reaction cell, which supports the assumption that the convection flow was the dominant permeation mechanism, the effect of MWCOs was confirmed to be insignificant, and further supports the previous finding that internal fouling was not significant.

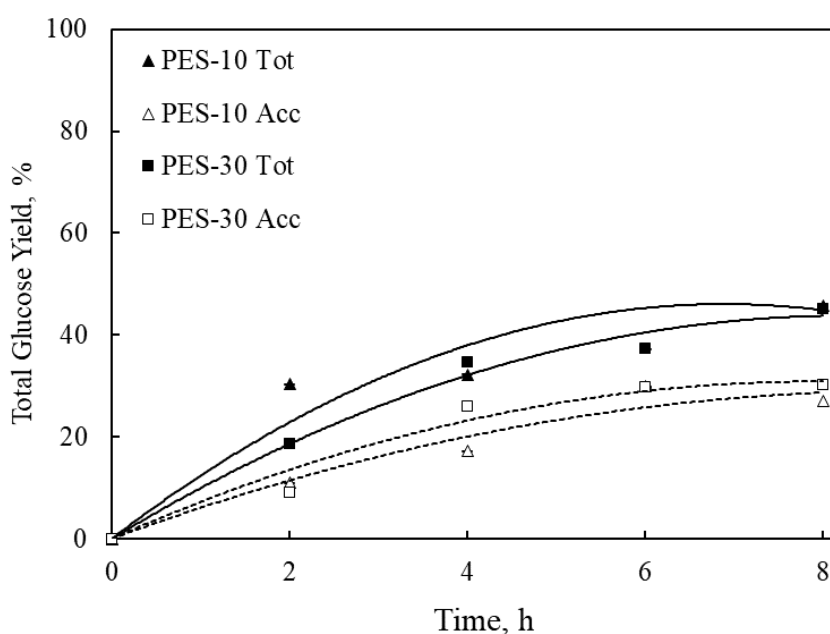


Figure 16: Total glucose yields, and glucose produced in reaction cell operated using PES membranes of different molecular weight cutoffs with initial substrate and cellulase concentrations of 6.67 g/L and 0.48 g/L, respectively, and a water flowrate of 0.4 mL/min ($\tau = 31.3$ h), at 48°C and a pH of 4.8. Acc, accumulated glucose in the reaction cell; FR, water flow flowrate; Tot, total glucose yield; C_0 , substrate concentration.

5.1.4 Effects of the Substrate Concentration and Water Flowrate on Standard Cellulose Hydrolysis

The effects of different water flowrates and substrate concentrations as a function of time on product yield after 6 h were measured using the PES-10 membrane at the levels listed in Table 4. As explained in Section 4.2.2, the product yield is determined by dividing the total amount of produced product by the amount of initial substrate added to the reaction cell. Figure 17 shows the effects of two different water flowrates on the total glucose yield and the glucose yield in the

reaction cell using the PES-10 membrane at an initial substrate concentration of 13.3 g/L. The curves clearly show that the total production increased with an increase in the water flowrate. This was mainly due to an increase in product removal, which had a positive effect in reducing enzyme inhibition by the product and pushed the reaction forward. To confirm these results, the results obtained using the DNS method were compared with the glucose oxidase measurement method. The latter method specifically measures glucose only, by binding glucose oxidase enzyme specifically to glucose molecules to form gluconic acid that can be measured at 540 nm with a UV spectrophotometer [190]. The two methods were used to measure the amounts of sugars produced after 8 h from two hydrolysis experiment using initial substrate, standard cellulose, concentrations of 6.67 and 13.3 g/L at 0.48 g/L cellulase, 48°C and pH of 4.8. In both cases, the difference between the two readings was less than 2%, which confirms the accuracy of the measurement using the DNS reagent and that the cellobiose content was negligible compared to glucose.

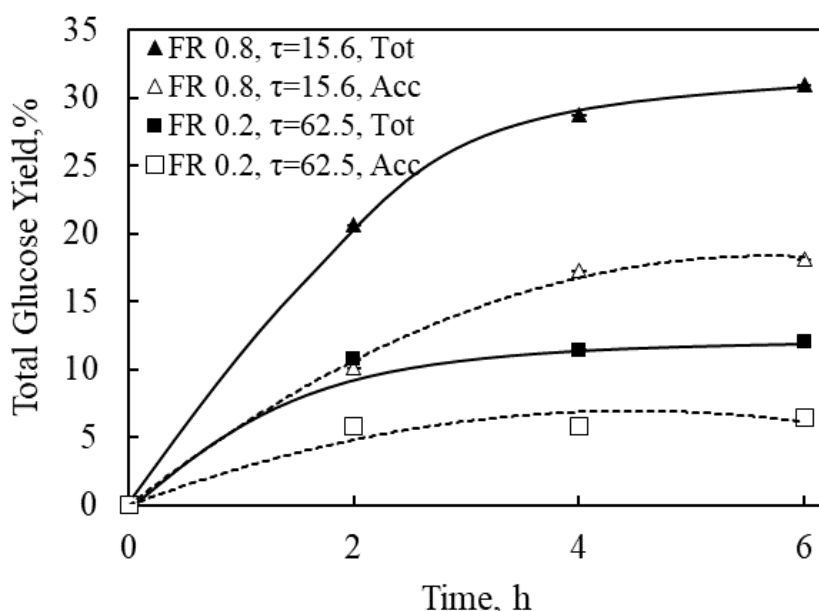


Figure 17: Total glucose yield and glucose produced in reaction cell operated using a PES-10 membrane with constant substrate and cellulase concentrations of 13.33 g/L and 0.48 g/L, respectively, and different water flowrates, at 48°C and a pH of 4.8 Acc, accumulated glucose in the reaction cell; FR, water flowrate (mL/min); τ , residence time (h); Tot, total glucose yield; C_0 , substrate concentration.

Figure 18 shows the effects of two different initial substrate concentrations (2.7 and 13.3 g/L) on the total glucose yield and the glucose yield in the bottom portion of the MBR cell using PES-10 at a water flowrate of 0.8 mL/min ($\tau = 15.6$ h). The results showed that increasing the substrate concentration positively affected glucose production in the reaction cell. This is the general behaviour of chemical reactions, where an increase in the reacting molecules to form the products will push the reaction forward. The slight drop in the curve observed toward the end of the observation period for the 2.7 g/L substrate concentration was due to the dilution effect. At the beginning of the reaction, the product was produced at a rate faster than the dilution effect generated by the introduced water flowrate, allowing the accumulation of the product and hence an increase in its concentration. After some time, the rate of product formation decreased, and the dilution effect became more prominent, resulting in the observed drop in the product concentration in the reaction chamber. The yield in the reaction chamber drops if the dilution effect, caused by the water flow, was higher than the production rate. This was obviously not the case with the total glucose yields, which continued to increase as shown in Figure 18. However, the effect of increasing the substrate concentration had an opposite effect on the total glucose yield. This should not be mistakenly attributed to the substrate concentration; it is because the yield did not increase linearly with the increase in substrate concentration. The total glucose concentration after 6 h reached 2.9 and 3.6 g/L using initial substrate concentrations of 2.7 and 13.3 g/L, respectively. Hence, to calculate the glucose yield, the amount of the produced glucose is divided by the initial amount of substrate, which resulted in the observed yield decrease. In the inverted dead-end MBR, the maximum substrate concentration that could be tested was 13.3 g/L and above this concentration a vigorous agitation was required, which imposes a shear stress on the enzymes that could result in enzyme denaturation. Hence, increasing the substrate concentration was avoided to prevent enzyme damage. However, for industrial applications, the substrate concentration has

to be increased to enhance the yield. To overcome this technical issue, semi-batch addition of substrate can be adapted to increase the yield and make the operation industrially feasible.

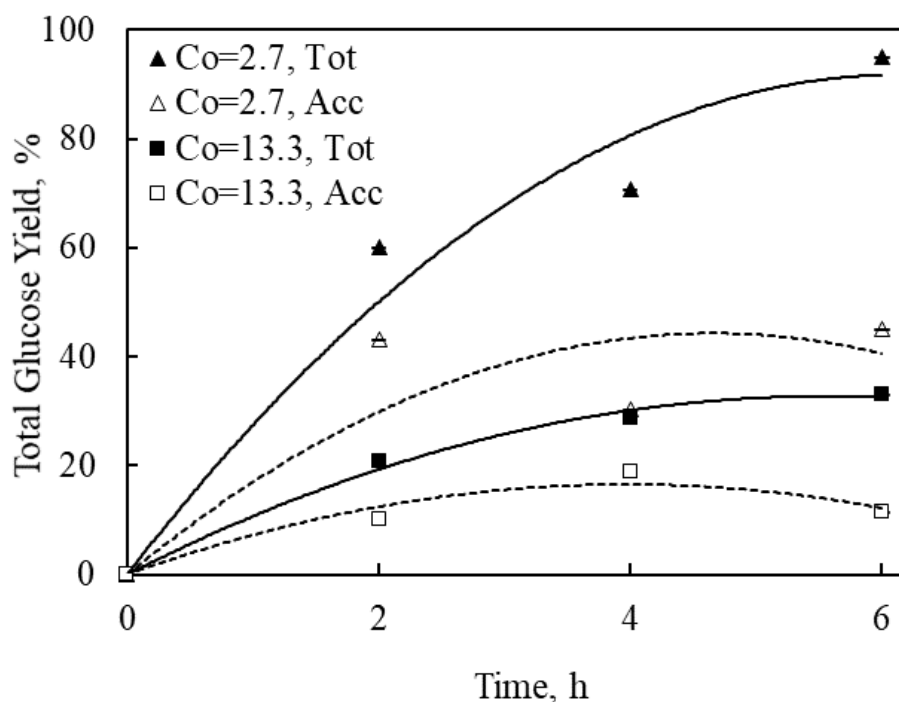


Figure 18: Total glucose yields and glucose produced in reaction cell operated using a PES-10 membrane with different substrate concentrations, a cellulase concentration of 0.48 g/L, and a water flowrate of 0.8 mL/min ($\tau=15.6$ h). At 48°C and a pH of 4.8 Acc, accumulated glucose in the reaction cell; FR, water flow flowrate; Tot, total glucose yield; Co, substrate concentration.

5.1.5 Evaluation of the Kinetic Model Parameters

The Polymath software was used to determine the numerical values of the parameters in Equation (15). The equation was solved using estimated kinetic parameters, which were changed to minimize the error between the experimental results and the model predictions. The determined parameters are presented in Table 7, and comparisons between the experimental data and the model predictions are presented in Figure 19. The figure shows the total glucose yields at different initial substrate concentrations and water flowrates as (A) 13.3 g/L, 0.2 mL/min ($\tau=62.5$ h), and

0.8 mL/min ($\tau = 15.6$ h), and (B) 6.67 g/L and 0.4 mL/min ($\tau = 31.3$ h), respectively, using the PES-10 membrane with 0.48 g/L cellulase at 48°C and pH of 4.8. The results showed that the developed kinetic model with the determined parameters could largely predict the experimental data.

Table 7: Estimations of the kinetic model parameters

Kinetic parameter	Value	Unit
k_s	3.5×10^{-2}	$\text{m}^3/\text{g.h}$
k_{-s}	0.33	1/h
k_p	0.33	1/h
k_{EP}	0.5	1/h
k_{EP2}	9.0×10^{-3}	$\text{m}^3/\text{g.h}$

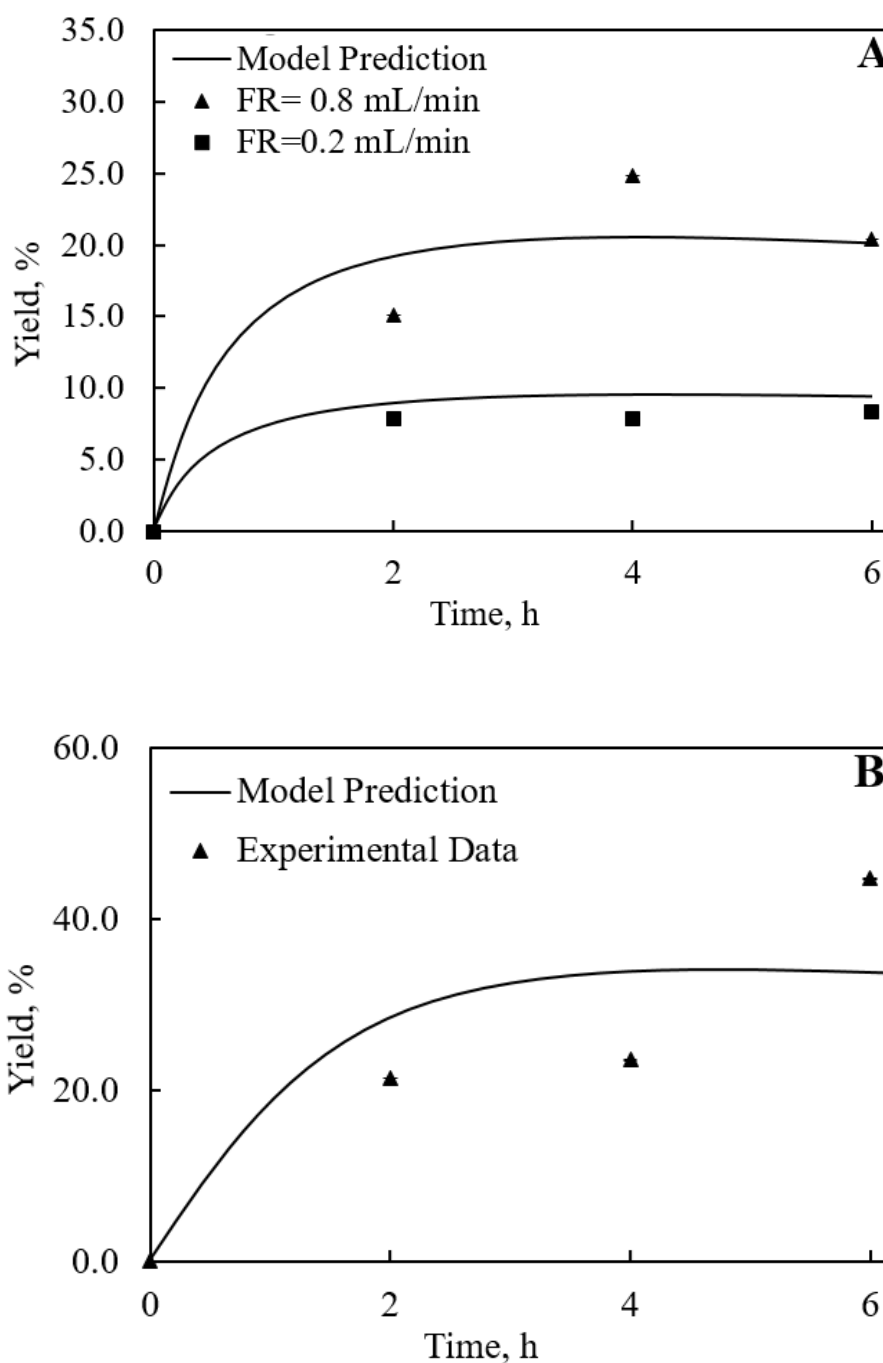


Figure 19: Comparison between the experimentally determined total glucose yield and the kinetic model-predicted yield for enzymatic hydrolysis at 48°C and a pH of 4.8 using the polyethersulfone (PES)-10 membrane, a cellulase concentration of 0.48 g/L, and initial substrate concentrations and water flowrates of (A) 13.3 g/L, 0.2 mL/min ($\tau = 62.5$ h), and 0.8 mL/min ($\tau = 15.6$ h), and (B) 6.67 g/L and 0.4 mL/min ($\tau = 31.3$ h), respectively. Co, substrate concentration; FR, water flowrate

As shown in Table 8, a comparison of the yields after 6 h resulted in an R^2 value of 0.96, which was close to that found using the statistical model. To the best of our knowledge, this is the first study to present a kinetic model developed from mechanistic reaction steps that can be used to describe the behavior of the complex enzymatic hydrolysis of cellulose in a MBR with simultaneous product separation.

Table 8: Total glucose yield after 6 h at different substrate concentrations (X_1) and water flowrates (X_2)

Substrate concentration (g/L)	Water flowrate (mL/min)	Residence time (h)	Experimental yield (%)	Yield by statistical model (%)	R^2	Model yield (%)	R^2
X_1	X_2						
2.67	0.2	62.5	64.45±0.03	64.46		-	
13.33	0.2	62.5	8.33±0.008	8.39		15.08	
2.67	0.8	15.6	86.63±0.017	86.65	0.97	-	0.96
13.33	0.8	15.6	20.40±0.016	20.47		17.98	
6.67	0.4	31.3	44.75±0.038	32.61		37.49	

5.1.6 Statistical Analysis

Response surface regression analysis was performed using the Minitab 19 software with the statistical significance established at a P -value of <0.05 . Table 9 shows the results of the analysis of variance obtained after examining the effects of two independent variables, *i.e.*, substrate concentration (X_1) and water flowrate (X_2), on the total glucose yield after 6 h of hydrolysis. The linear effects of both the substrate concentration and water flowrate were found to be significant, with P -values of 0.000 and 0.035, respectively. The P -values indicated that although both factors were significant, the substrate concentration effect was more significant. The quadratic term of the substrate concentration (X_1^2) was also significant ($P = 0.007$), whereas that of the water flowrate (X_2^2) was not estimated and removed from the model because of the sample size by the software. This indicates that, unlike the water flowrate effect, the substrate concentration effect would have a parabolic shape. It was also found that both X_1 and X_1X_2

negatively contributed to the yield of glucose production, which agrees with the previous observation discussed in Section 5.1.4.

Table 9: Response surface regression analyses of product yield versus substrate concentration (X1) and water flowrate (X2): (A) coded coefficients; (B) analysis of variance.

A. Term	Coef	SE Coef	T-Value	P-Value	VIF
Constant	26.89	2.91	9.22	0.000	
X1	-30.59	3.14	-9.73	0.000	1.04
X2	8.56	3.14	2.72	0.035	1.07
X1*X1	18.07	4.44	4.07	0.007	1.11
X1*X2	-2.53	3.14	-0.80	0.452	1.00
B. Source	DF	Adj SS	Adj MS	F-Value	P-Value
Model	4	4451.00	1112.75	28.13	0.000
Linear	2	4035.73	2017.87	51.02	0.000
X1	1	3742.55	3742.55	94.62	0.000
X2	1	293.18	293.18	7.41	0.035
Square	1	655.42	655.42	16.57	0.007
X1*X1	1	655.42	655.42	16.57	0.007
2-Way Interaction	1	25.57	25.57	0.65	0.452
X1*X2	1	25.57	25.57	0.65	0.452
Error	6	237.32	39.55		
Total	10				

A second-order interactive regression model, Equation (38), was developed to relate the product yield (%) and the two independent parameters, X_1 and X_2 . This model was referred to as “statistical model” in the manuscript. The equation was used to draw a three-dimensional (3D) plot of the combined effects of substrate concentration and water flowrate on the total glucose yield (Figure 20).

$$\text{Yield (\%)} = 92.9 - 0.15.12 X_1 + 41.2 X_2 + 0.636 X_1^2 - 1.58 X_1 X_2 \quad (38)$$

The process was optimized using Response Optimizer in Minitab, which showed that the lowest substrate concentration (2.67 g/L) and the highest water flowrate (0.8 mL/min), which corresponds to the lowest residence time of 15.6 h, would result in the maximum yield of 86.65%

(Table 8). The experimental results agreed closely with the model prediction and obtained an actual yield of $86.63 \pm 0.017\%$. These results agreed with the 3D surface graph (Figure 20), which also showed the positive effect of the water flowrate and the negative effect of the substrate concentration on the yield. This figure also showed that the substrate concentration effect was more significant than the water flowrate effect, which agreed with the *P*-values discussed above.

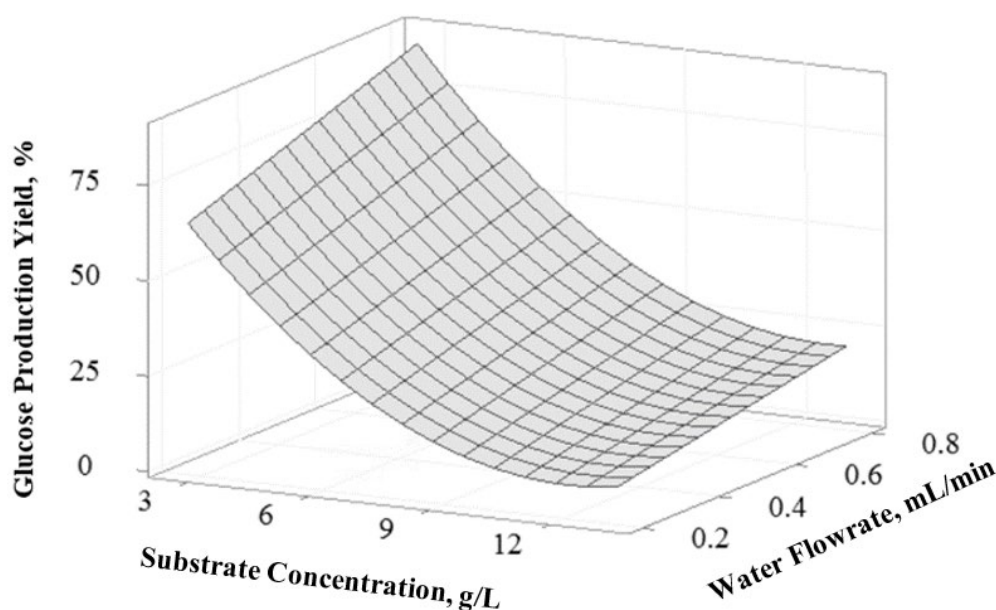


Figure 19: Three-dimensional plot of total glucose yields as a function of the substrate concentration and water flowrate after 6 h of enzymatic hydrolysis at 48°C and a pH of 4.8 using the polyethersulfone PES-10 membrane for product separation.

5.2 Radial-flow Tubular MBR Analysis

5.2.1 Biomass Characterization and the Effect of Pretreatment on Substrate

The fresh date seeds (DSs), after removing the extractives, were characterized. Cellulose, hemicellulose, and lignin contents were determined to be $47 \pm 0.7\%$, $28 \pm 0.4\%$, and $25 \pm 0.6\%$, respectively. This analysis falls within the typical ranges of the constituents of most lignocellulosic materials [191]. To confirm the lignin content and to investigate the efficiency of NaOH pretreatment, acid-insoluble lignin (Klason lignin) and acid-soluble lignin were quantified.

Klason lignin and soluble lignin in the fresh untreated DSs were determined to be $24.01\% \pm 2.47$ and $0.16\% \pm 5.59 \times 10^{-5}$, respectively. The determined total lignin content of 24.17% was in agreement with that found by the constituents' analysis. Klason lignin and acid-soluble lignin in the NaOH treated samples were found to be $16.6\% \pm 2.6$ and $3.95 \times 10^{-4}\% \pm 1.8 \times 10^{-4}$, respectively. Hence, over 30% of total lignin was removed by the NaOH pretreatment. The method has been reported as an efficient method for lignin removal and biomass swelling to enhance the enzymatic hydrolysis of lignocellulosic material, while preventing the solvation of hemicellulose [192]. The biomass type, alkaline concentrations, temperatures, and pretreatment time all affect the percentage removal of lignin. By using alkaline treatment at 4% NaOH for 1 h at room temperature 15.68% of the lignin content was removed from DSs [193]. Operating at a higher temperature of 80°C, a higher lignin removal of 70% was achieved using 2% NaOH on herbaceous lignocellulose, such as wheat straw, corn straw, and sugar bagasse. However, the increase in temperature was less effective with hardwood and softwood biomass, achieving 39.6% and 16%, respectively [194].

The effects of the HCl+NaOH pretreatment and NaOH pretreatment on crystallinity of the DSs were examined with XRD, as shown in Figure 21. The analysis showed slight increase in the intensities after both pretreatments, which indicate an increase in the crystallinity. The peaks at 16° and 23° reflect the crystalline cellulose type I, while cellulose type II is presented at 20° . The intensity of those peaks increased in both HCl+NaOH pretreated DSs and NaOH pretreated DSs biomass, which indicates a higher crystallinity degree in the structure of the treated fibers due to the partial removal of lignin [195]. A similar increase in the intensity of peaks that represent crystalline cellulose, was also observed with DSs from *Phoenix dactylifera L.* after lignin and hemicellulose removal [29]. It was also noticed that the increase in peak intensity with HCl+NaOH pretreatment (*i.e.*, removing partially both lignin and hemicellulose) was higher than that with partial removal of lignin only. This suggests that the acid used in the HCl+NaOH

pretreatment may not have hydrolyzed hemicellulose only but also the amorphous parts of cellulose structure, resulting in increased crystallinity [196]. As a result, the peaks at 25° and 26° , which reflect cellulose crystallinity and crystalline carbon, respectively, appeared only in the HCl+NaOH pretreated sample.

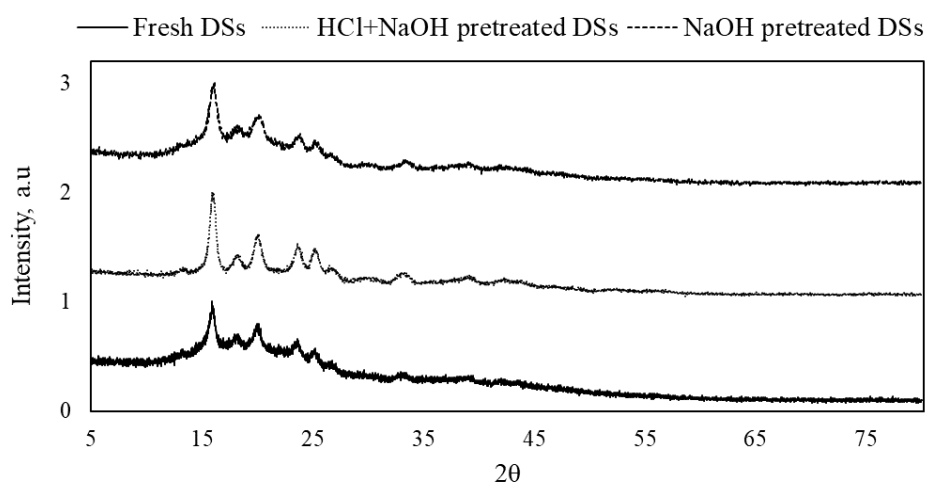


Figure 20: X-ray diffraction spectra of fresh, HCl+NaOH pretreated, and NaOH pretreated DSs

FTIR analysis was carried out to investigate the effect of HCl+NaOH pretreatment and NaOH pretreatment on the composition and functional groups in DSs. Figure 22 shows the FTIR spectrums of fresh DSs, HCl+NaOH pretreated DSs, and NaOH pretreated DSs. The peaks between $4000\text{-}2995\text{ cm}^{-1}$ are assigned to hydrogen bonded OH stretching vibration [40]. Peaks at 2905 and 2855 cm^{-1} are assigned to asymmetric and symmetric C-H stretching in methyl and methylene groups, respectively, and the peak at 2870 cm^{-1} represents the aliphatic CH stretching [197], which all three main constituents, cellulose, hemicellulose, and lignin contribute in. The peak at 1654 cm^{-1} reflects the C=C or C=N vibration in the aromatic region, which is influenced by the lignin [40]. The band at 993 cm^{-1} represents the C-O-C glycosidic bond vibration, and C-

C stretching is assigned to the peak at 791 cm^{-1} , which are related to cellulose component [198]. After NaOH pretreatment, where lignin is partially removed, a similar spectrum to that of the fresh DSs was observed, but with the appearance of two peaks at 1743 and 864 cm^{-1} . The former is assigned to the C=O bond that can be due to either acetyl or ester group found in hemicellulose, while the latter represents the C-H rocking vibration of cellulose [28, 199, 200]. The appearance of those two peaks is a sign of structural distribution and that the partial removal of lignin allowed the exposure of both cellulose and hemicellulose. By comparing the spectrum of the HCl+NaOH pretreated DSs, it was observed that peaks at 1371 and 1338 cm^{-1} appeared, which are assigned to CH stretching of cellulose, which indicates the biomass structural deformation after hemicellulose and lignin partial removal. The appearance of the band at 1238 cm^{-1} can represent either C-O-H deformation or C-O phenolic stretching that might reflect remaining of lignin found in the biomass. The appearance of a band at 864 cm^{-1} represents, as mentioned earlier, the C-H rocking vibration of cellulose [28].

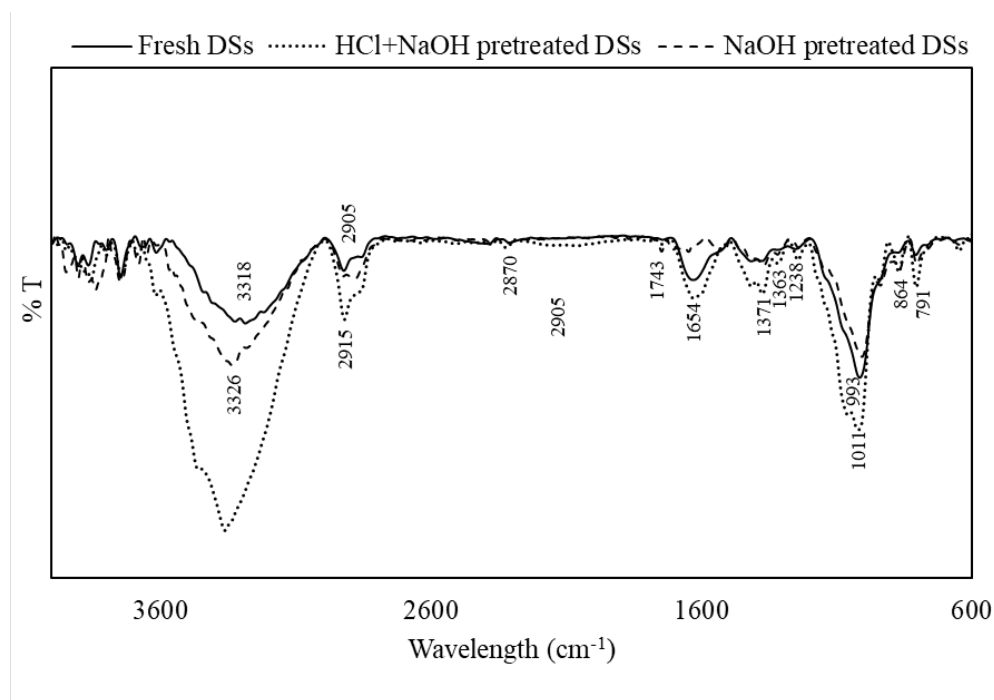


Figure 21: Fourier-transform infrared spectra of fresh, HCl+NaOH pretreated, and NaOH pretreated DSs

SEM was used to analyze the morphological changes as a result of HCl+NaOH pretreatment and NaOH pretreatment, as shown in Figure 23. The fresh DSs biomass, shown in Figure 23A, was characterized by a smooth and solid surface. The effect of HCl+NaOH pretreatment is shown in Figure 23B. It can be seen that the structure has been disrupted, due to the action of NaOH, leaving holes that can be observed on the surface of the molecules, while elongated, structural cracks indicate the severe action of acid treatment, attributed to the partial hydrolysis of the amorphous part of the biomass. Image of the NaOH pretreated DSs biomass is shown in Figure 23C. It can be seen that the structure contained holes that indicate the disruption of the matrix due to lignin partial removal. However, unlike with the HCl+NaOH treated samples, with NaOH pretreatment the samples maintained a similar overall structure without cracks [40].

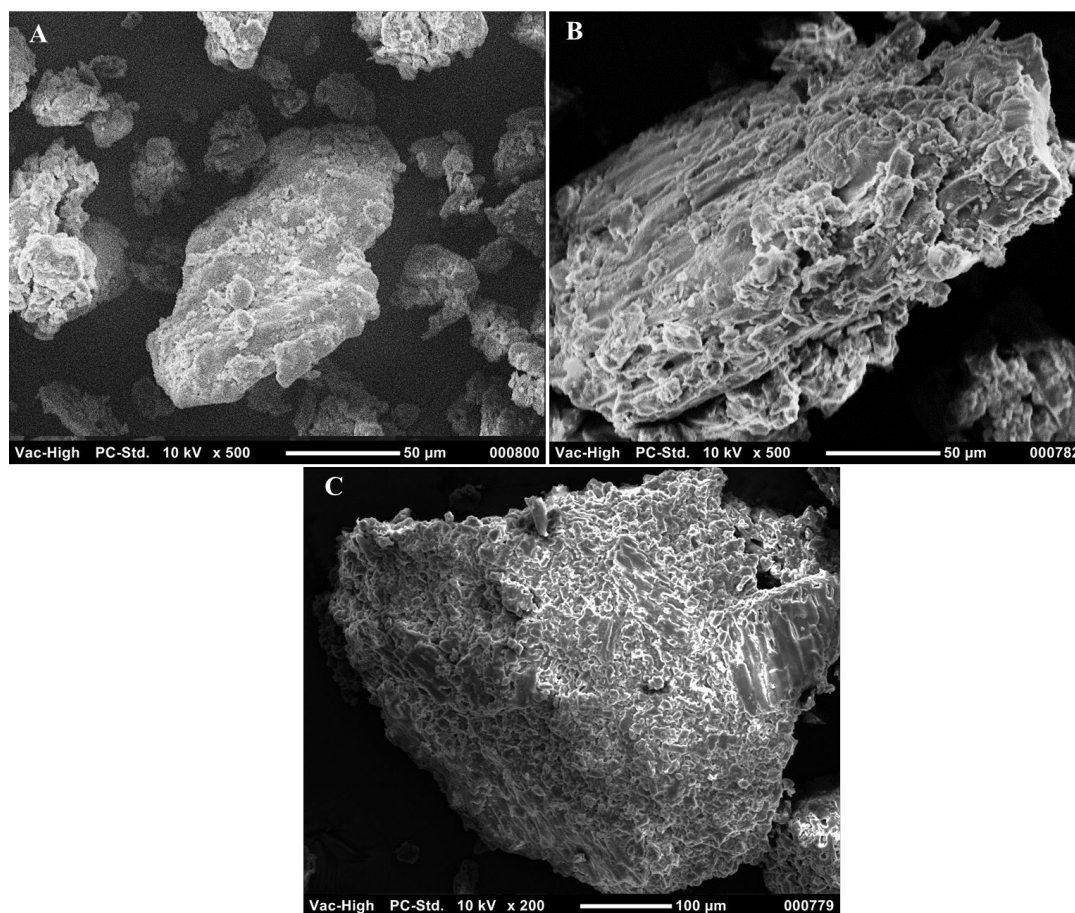


Figure 22: Scanning electron microscopy images of (A) fresh, (B) HCl+NaOH pretreated, and (C) NaOH pretreated DSs

5.2.2 Enzymatic Hydrolysis with Product Separation

HCl+NaOH pretreatment was used to remove partially both hemicellulose and lignin, to disrupt the lignocellulose structure and enhance the enzyme accessibility to cellulose. A preliminary test was done to evaluate the need for the hemicellulose removing step. The total reducing sugars yield from enzymatic hydrolysis of HCl+NaOH pretreated DSs was found to be close to that obtained using NaOH pretreated DSs. With the HCl+NaOH pretreatment, the total reducing sugars yield after 8 h of hydrolysis was 3.2%. Under the same conditions, the yield obtained from the NaOH pretreated DSs was 3.5%. Similar results were also observed when comparing the hydrolysis yield of corn stalk biomass acid-alkaline pretreated for lignin and hemicellulose removal and alkaline pretreated for lignin removal only. After 96 h of hydrolysis,

the cellulose conversion in the acid-alkaline pretreated samples was 70.3%, whereas it reached 100% in alkaline pretreated samples. Delignification only of loblolly pine biomass was also shown to increase the cellulose hydrolysis conversion after 72 h by 88% as compared to untreated samples, where cellulose conversion was only 16% [201]. The lower conversion of the acid-alkaline pretreated samples is attributed to the use of acid, which in addition to removing hemicellulose dissolves some of the amorphous portion of cellulose. This increases the percentage of the crystalline cellulose in the HCl+NaOH pretreated sample observed in the XRD analysis, which results in a drop in the conversion yield [40]. Therefore, all subsequent experiments using the MBR were carried out using NaOH pretreated DSs samples with partial removal of lignin only.

The enzymatic hydrolysis of standard cellulose with simultaneous product removal in inverted dead-end MBR was evaluated and modeled, as previously shown in Section 5.1.5. The results clearly showed the significant enhancement in reaction rate and production yield with the continuous in situ removal of the products. In this study, the developed inverted dead-end MBR was tested on the lignocellulosic biomass, DSs, which is more complex and more difficult to degrade than the standard cellulose. Initially, the glucose production yield by enzymatic hydrolysis of fresh DSs was compared to the NaOH pretreated DSs without product separation. With the NaOH pretreated DSs, the yield after 8 h of reaction reached 3.5%, compared to less than 2.1% with fresh DSs. This further confirms the significance of lignin partial removal in enhancing the cellulase accessibility to cellulose that enhanced the hydrolysis. In addition, the production yield from the NaOH pretreated DSs in a batch reactor without product removal was compared to that with product removal in the inverted dead-end flat sheet filtration MBR, at the same reaction conditions. As shown in Figure 24, without product separation, the production yield reached a plateau at 3.5% after 4 h and no increase was observed after that. This was mainly due to the product inhibition effect, which was also observed with the standard cellulose, as explained

in Section 5.1.3. With continuous product separation, however, the yield significantly increased to 10.8%. This further proves the significance effect of product removal on enhancing the reaction rate and yield. The production yield of standard cellulose in the same MBR with product removal was 34% under the same conditions. The lower yield observed using DSs is attributed to the limited accessibility of cellulase, as compared to the standard cellulose case, which composed of pure hydrolysable amorphous cellulose. The results also show the significance of the pretreatment method on the effectiveness of the hydrolysis process, which is a key challenge with using any lignocellulosic biomass [22].

These findings agree with previously reported enhancement in cellulose hydrolysis by the use of MBR. In general, by simultaneous product separation, in a dead-end MBR system, an increase in conversion by up to 40% can be achieved as compared to case without product separation in the conventional batch reactor [159]. Enhanced enzymatic hydrolysis conversion of α -cellulose to 53%, after 48 h, was achieved using dead-end MBR with flat-sheet polysulfone membrane, 10 kDa, compared to 35% in batch reaction [112]. In addition, the use of CSTR with dead-end filtration module with a 2 kDa polyethersulfone membrane, for the enzymatic hydrolysis of cotton cellulose achieved 19% conversion, with semi-continuous product removal after 72 h, compared to only 5% in a batch system [202]. In a stirred tank reactor with crossflow membrane module, pretreated rice straw with dilute sulfuric acid for 30 min at 100°C achieved 81% cellulose conversion after 72h, which was reasoned by the effect of both pretreatment and product removal [203].

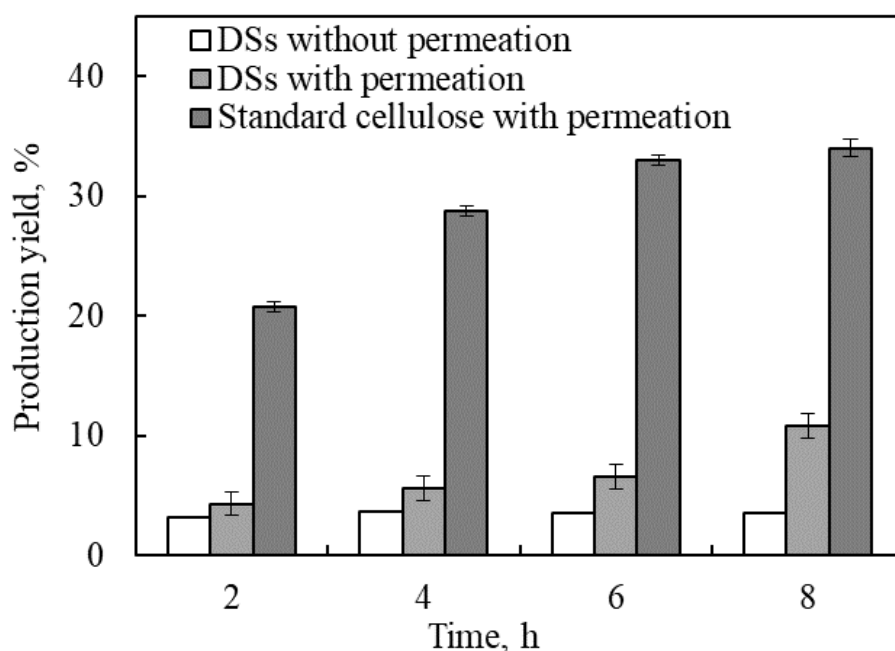


Figure 23: Production yield from NaOH pretreated DSs with and without permeation, and standard cellulose with permeation in the inverted dead-end MBR using substrate and enzyme concentrations of 13.3 g/L and 0.48 g/L, respectively, at pH 4.8, 48°C, and water flowrate of 0.8 mL/min ($\tau = 15.6$ h)

The most important finding of this work is testing the novel tubular MBR with radial flow MBR. The new design provides a larger diffusional surface area, which increases the product diffusion and in turn results in a further enhancement of the reaction rate and production yield. This idea was previously suggested [141], for a simulated case. In this work, however, the reactor was physically built and challenged by a real test. The reducing sugars production yield from the enzymatic hydrolysis of the NaOH pretreated DSs is shown in Figure 25, compared to that achieved using the inverted dead-end MBR, under the same conditions. The superiority of the new design was evident with a yield reaching up to 29% within 8 h. The enhancement in the yield in the radial MBR is attributed to the increase in the diffusion area. The tubular membrane surrounding the reaction area throughout the reactor allowed for more product separation and pushed the reaction to the forward direction, compared to the limited membrane area allowing

diffusion in the flat-sheet MBR. In addition, at the substrate concentration used, no mixing problems were encountered, which suggests that the reactor can handle higher concentrations, which is a major challenge facing the inverted dead-end MBR design.

In comparison with a 30 kDa flat-sheet membrane (NADIR 30) in a dead-end module, the enzymatic hydrolysis of Solka Floc cellulose with a flowrate of 80 mL/min in a tubular reactor using porous stainless steel, 0.1 μm , showed 53% conversion compared to 48% conversion in flat-sheet after 25h [138]. The difference in the conversion yield was partially attributed to the limitation in product removal due to the smaller membrane surface area in the flat-sheet membrane. In addition, the hydrolysis of pretreated Mavicell, using thermal pretreatment at 120°C for 20 min, in the same tubular reactor achieved 70% conversion after 10h [138]. The effect of product removal in these studies agree with the results presented in this work and reflect the contributions of both pretreatment effect on substrate disruption and increasing product removal by increasing membrane surface area in the tubular design. In addition, the viscous slurry that may result by high solid loading and mass transfer limitations are eliminated in the tubular reactor allowing to further enhance the yield. However, substrate inhibition can be evident at certain high concentrations which was reported before [141, 204]. This can be solved with the intermittent substrate feeding to sustain a high yield production. The positive results from this work are promising, and the work will continue to model and optimize the process.

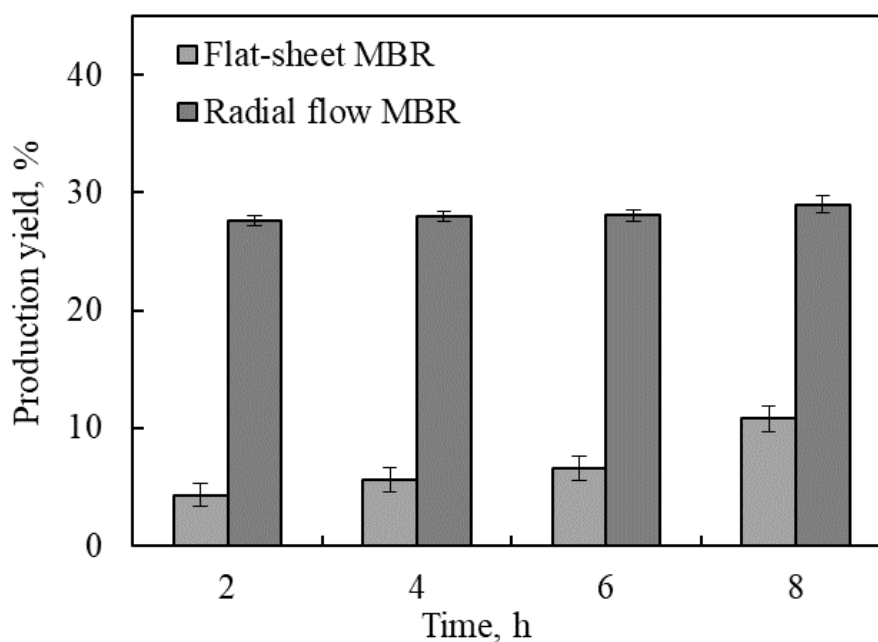


Figure 24: Reducing sugars production yield from NaOH pretreated DSs using inverted dead-end MBR and radial flow MBR, using substrate and enzyme concentrations of 13.3 g/L and 0.48 g/L, respectively at pH 4.8, 48°C, and water flowrate of 0.8 mL/min ($\tau = 15.6$ h)

5.2.3 Effects of the Substrate Concentration and Water Flowrate on DSs Hydrolysis

The effects of different water flow rates and substrate concentrations on biomass conversion as function of time were investigated by measuring the total reducing sugars produced using PES-10 membrane at the levels listed in Table 5. Figure 26A shows the results at the lowest initial substrate concentration of 14.3g/L. It was found that at this substrate concentration, increasing the water flow rate initially had low significant effect on the biomass conversion, especially at the initial times. However, as the water flow rate increased to 1.2 mL/min ($\tau = 10.4$ h), the effect becomes more evident, and the amount produced total reducing sugars increased significantly. This indicates that the effect of increasing the water flow rate becomes more evident as the amount of produced total reducing sugars increases, and its inhibition becomes more significant. At the medium concentration of 21.4 g/L, shown in Figure 26B, a similar trend was observed where increasing flow rate had initially showed low significance on total produced reducing sugars, and the effect became more pronounced at 1.2 mL/min ($\tau = 10.4$ h), especially

at the time of reaction progressed. The effect of increasing the initial substrate concentration from 14.3 to 21.4 g/L was more evident at lower flow rates of 0.4 and 0.8 ml/min, with a residence of time 31.3 and 15.6 h, respectively. At the highest tested concentration of 39.6 g/L, shown in Figure 26C, the effect of increasing water flow rate was more evident at the medium and the highest flow rates used, 0.8 and 1.2 mL/min, with a residence of time 15.6 and 10.4 h, respectively, which can be attributed to the enhanced removal of product that was required with higher initial substrate concentration. Generally, as the positive effect of increasing water flow rate on reducing the product inhibition and pushing the reaction forward by enhancing the product removal becomes more evident as the amount of produced total reducing sugars increase, it becomes more significant at longer reaction times and at the higher initial substrate concentrations of 21.4 and 39.6 g/L, shown in Figures 26B and 26C, respectively.

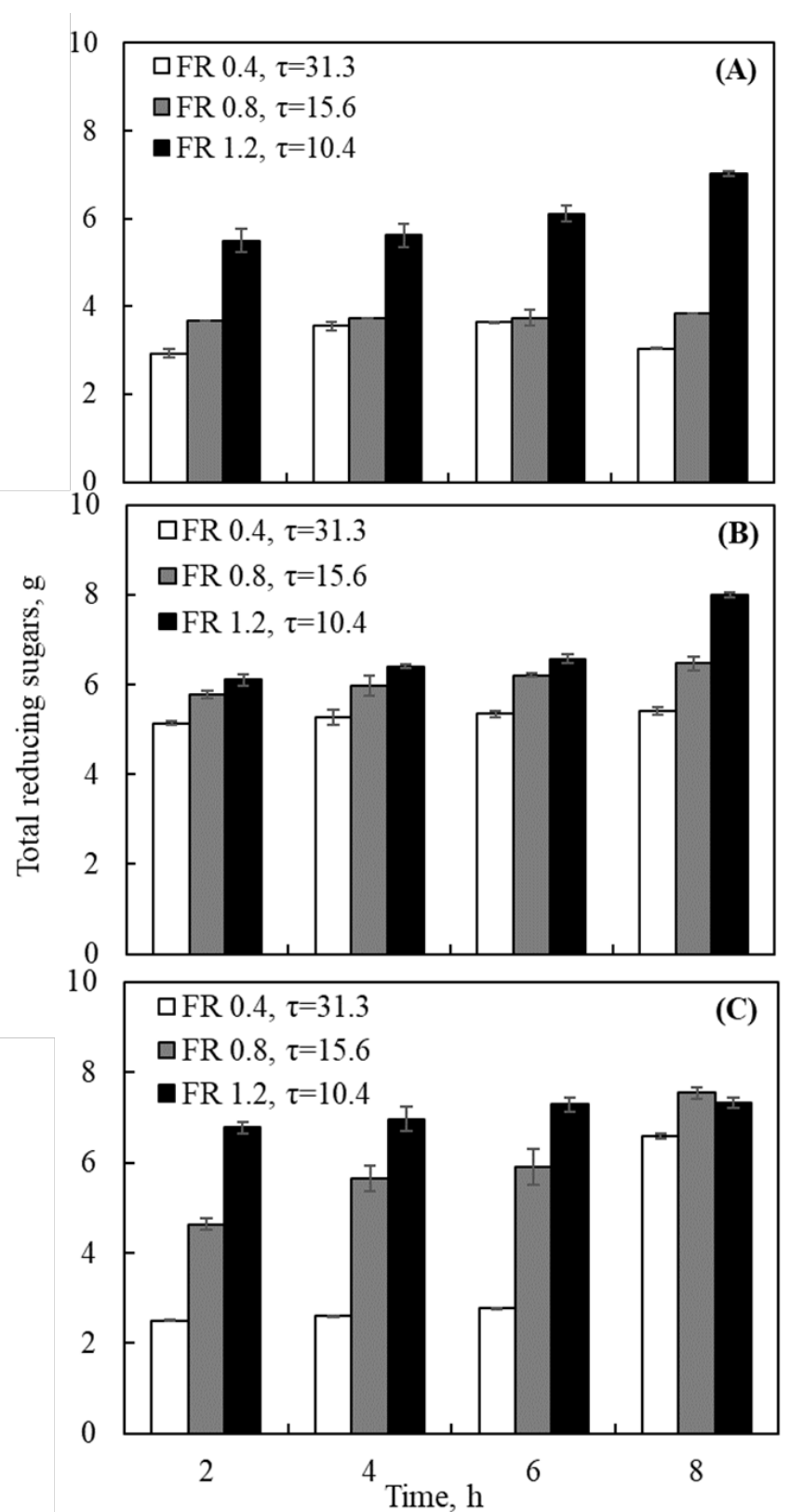


Figure 25: Total reducing sugars produced using different water flowrates of 0.4, 0.8, and 1.2 mL/min ($\tau = 31.3, 15.6,$ and 10.4 h, respectively), and substrate concentrations of (A) 14.3 g/L, (B) 21.4 g/L, and (C) 39.6 g/L, operated at pH 4.8, 48°C, enzymes concentration of 0.48 g/L and PES-10

The effects of substrate concentration and water flow rate on the total reducing sugars production and total reducing sugars yield after 8 h of reaction time are presented in Figure 27. As explained earlier, both factors have a positive effect on the biomass conversion. However, as shown in Figure 27A, the effects of both factors, were only pronounced at low values and tended to fade as the factors increase. It can also be seen that the effect of water flow rate was less significant than that of the substrate concentration. This is because as the water flow rate increases, the concentration of total reducing sugars in the reaction zone reduces to levels at which the product inhibition effect becomes insignificant. Hence, further increase in water flow rate would have an insignificant effect on the reaction rate. Increasing the substrate concentration, on the other hand, results in increasing their availability for binding to the active sites for enzyme productive binding. However, at the highest water flow rate of 1.2 mL/min ($\tau = 10.4$ h) a slight substrate inhibition effect was encountered. Substrate inhibition effect, in which an increase in substrate concentration result in a decrease in the reaction rate, was observed in previous studies [205–208]. Substrate inhibition could be attributed to the decrease in enzyme adsorption with increasing substrate concentration [209], this was shown in cellulase adsorption on Avicell cellulose, in which the adsorption dropped by 30% with increasing the substrate loading from 1% to 5% (w/v) [209]. Enzyme adsorption, however, may not be the only reason for the substrate inhibition. For example, a drop in the in the hydrolysis rate of Solka floc cellulose was shown to drop as the concentration of the substrate exceeded 75 g/L, despite showing an increase in enzyme adsorption with the increase in initial substrate concentration [210]. The substrate inhibition was therefore attributed to other effects, such as the formation of clustered cellulose network upon wetting, which traps water inside the cellulose pores, leaving less water volume for cellulose suspension. This results in a thicker suspension that limits the cellulase diffusion into the cellulose pores [210]. The complex cellulosic structure of the lignocellulosic biomass may play a more significant role in substrate inhibition. As mentioned earlier, the cellulose consists of hydrolysable

and non-hydrolyzable parts. Initially, the readily available first layer of hydrolyzable cellulose is hydrolyzed, resulting in an increment in the hydrolysis rate. However, with the progress of the reaction, the percentage of the non-hydrolyzable parts increases, resulting in more non-productive binding with the enzyme and an inevitable decrease in reaction rate. This effect was not only observed as reaction time increases, but also as the substrate concentration increases, which limits the amount of substrate concentration to be used.

MBRs were suggested to overcome the product inhibition effect, while allowing for the repeated use of the enzyme in a soluble form. These major problems, which are encountered in conventional reactor systems, were successfully overcome and the performance superiority of MBRs over batch reactors with no product separation was clearly shown. For example, the hydrolysis of the NaOH pretreated DSs with product separation in the inverted dead-end MBR resulted in 10.8% production yield after 8 h compared to only 3.5% at the same conditions but with no product separation, as shown in this work. These favorable effects were shown to be further improved in the radial flow MBR, used in this work, due to the larger diffusion specific interfacial area as compared to the inverted dead-end MBR. Indeed, by using the radial flow MBR, the enzymatic hydrolysis of pretreated DSs significantly increased to 29% within 8 h, under the same conditions. The effects of water flow rate and substrate concentration on the total reducing sugars yield after 8 h in the radial flow MBR are shown in Figure 27B. Both factors have a positive effect on the yield with the maximum achieved at flow rate and substrate concentration of 1.2 mL/min ($\tau = 10.4$ h) and 14.3 g/L, respectively. Substrate inhibition can be observed in the yield at 39.6 g/L decreased at the flow rate of 1.2 mL/min. The good performance of the radial flow MBR was confirmed in this work, in which a yield of 53% was achieved within 8 h. The drop in the observed yield with increasing substrate concentration, shown in Figure 27B, should not be mistaken by the substrate inhibition, discussed earlier. This drop, however, was mainly because the total reducing sugars production did not increase linearly with the increase in substrate

concentration, and hence, dividing the amount produced by the initial amount of substrate used resulted in the observed decrease in the yield. A similar decline in production yield was observed when Avicell cellulose was hydrolyzed using *T. reesei* cellulase in a batch reactor. The sugar yield after 72 h showed a 33% drop when the substrate concentration was increased from 1 to 5% (w/v) [209]. Generally, investigation of high solid loading in MBR has been scarce in the literature. In dead-end MBRs, the maximum substrate concentration did not exceed 25 g/L, which was essential to minimize membrane fouling [112, 129, 136, 137]. A similar maximum concentration of 25 g/L was also used with thermally pretreated Mavicell cellulose enzymatically hydrolyzed in a tubular MBR design [138]. To address the membrane fouling effect, while allowing for higher solid loading, a modified configuration of the dead-end MBR was tested, in which the substrate was confined inside a nylon bag that allows the diffusion of both enzymes and product. This allowed loading higher concentrations of microcrystalline cellulose substrate pretreated with NaOH [135]. Although higher concentrations of 100 and 200 g/L were used, trapping the substrate inside the bag limited the mixing and, thus, enzyme-substrate binding, which resulted in low biomass conversion yield of only 4.50% and 3.25% at the two concentrations, respectively [135]. As shown in Figure 27B, the radial flow MBR, used in this work, did not only show a superior performance to other MBRs in terms of reducing sugars production, but also in its effectiveness in handling solid loading of complex lignocellulosic biomass, which was three times higher than the maximum limit that could be handled using the previous inverted dead-end MBR design. Furthermore, this was achieved without mixing problems that might limit enzyme-substrate binding. By using a more efficient pretreatment method that reduces the cellulose crystallinity, the drop in production yield at high substrate concentration, could be improved and the full potential of the tubular MBR could then be reached.

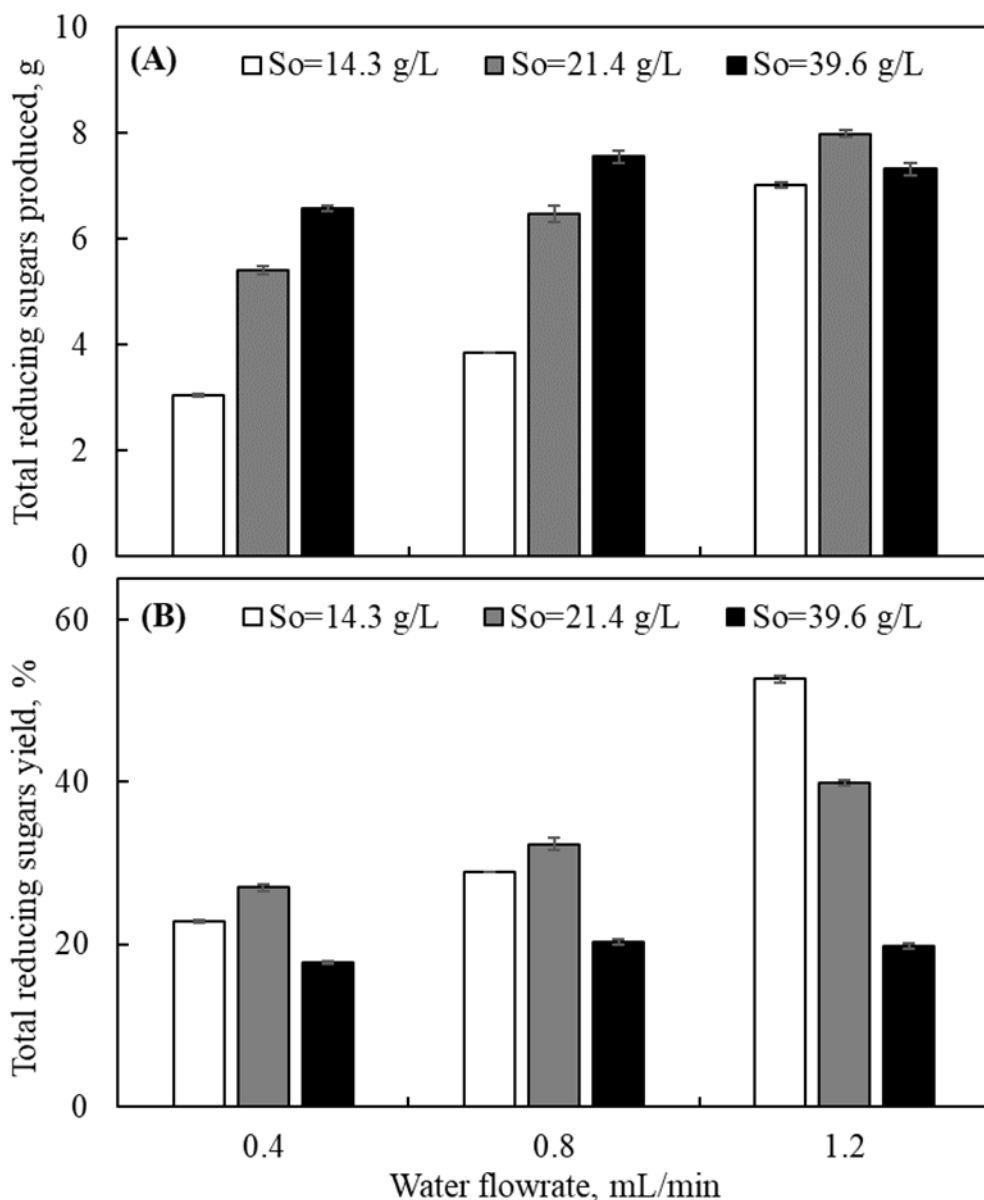


Figure 26: Total reducing sugars production after 8 h using different water flowrates of 0.4, 0.8, and 1.2 mL/min ($\tau = 31.3$, 15.6, and 10.4 h, respectively), and substrate concentrations of 14.3 g/L, 21.4 g/L, and 39.6 g/L, (A) total reducing sugars produced, g, and (B) total reducing sugars yield, %. At pH 4.8, 48°C, enzymes concentration of 0.48 g/L and PES-10

5.2.4 Kinetic Model

Polymath software was used to determine the numerical values of the parameters in Equations (29) – (34). The equations were solved using estimated kinetic parameters, which were changed to minimize the error between the experimental results and the model predictions for all tested conditions. Assuming a value of non-hydrolyzable fraction coefficient to be 0.6, the

determined parameters are presented in Table 10. Comparisons between the experimental data and the model predictions are presented in Figure 28. The figure shows the total reducing sugars produced at different initial substrate concentration at the center flow rate of 0.8 mL/min ($\tau = 15.6$ h). The figure shows that the model predicted the experimental data at the same order, especially at the low substrate concentrations. The model tended to overestimate the results at the highest substrate concentration, which suggests that other hydrodynamics factors at the higher substrate concentrations could have interfered with the reaction. This was attributed to the dynamic changes in the substrate quality during the reaction, especially at the higher substrate concentrations, which resulted in higher initial total reducing sugars production and a faster exposure of the non-hydrolyzable substrate to the enzymes. This leads to faster non-productive binding and a decline in the total reducing sugars production [171]. A better presentation of the changes in substrate structure with time could overcome this drawback and improve the model predictions. A similar overestimation of experimental results was also observed at high substrate concentrations using a kinetic model developed to estimate enzymatic hydrolysis of α -cellulose in a batch reactor at 40°C and pH of 4.7. The model developed using α -cellulose hydrolysis also underestimated the results at low substrate concentrations [171].

Table 10: Kinetic model parameters estimation

Kinetic parameter	Value	Unit
k_{c1}	0.1	$\text{m}^3/\text{g}\cdot\text{h}$
k_{c2}	0.33	1/h
k_p	9.5	1/h
k_{ep1}	100	1/h
k_{ep2}	3×10^{-3}	$\text{m}^3/\text{g}\cdot\text{h}$
k_{x1}	0.05	$\text{m}^3/\text{g}\cdot\text{h}$
k_{x2}	10	1/h
α	4.7×10^{-6}	1/h
φ	0.6	-

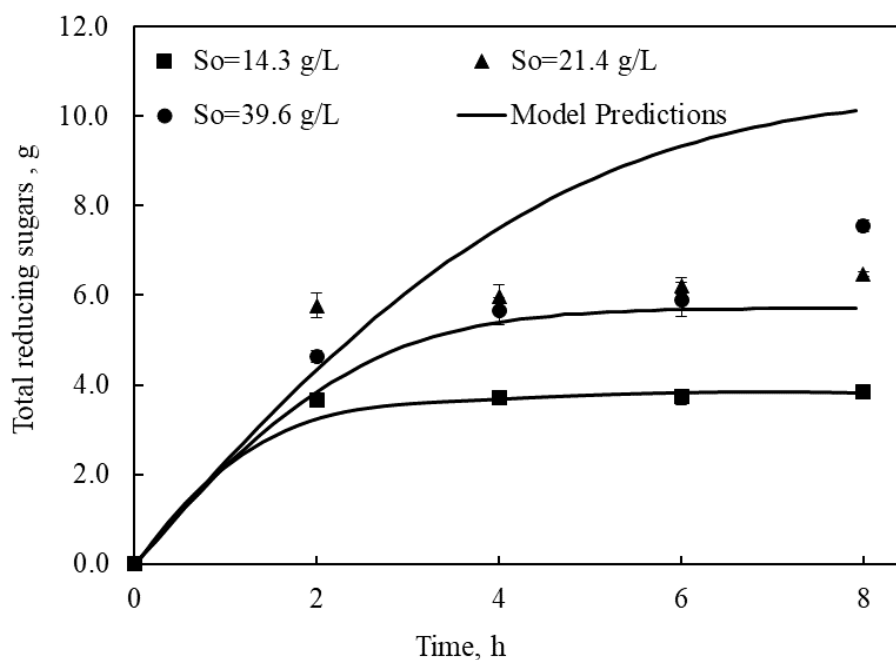


Figure 27: Comparison between the experimentally determined total reducing sugars produced and the kinetics model predictions at pH 4.8, 48°C, enzymes concentration of 0.48 g/L, PES-10, and the center water flowrate of 0.8 mL/min ($\tau = 15.6$ h) (*i.e.*, X_2 factor level of zero) different initial substrate concentrations

5.2.5 Sensitivity Analysis

Sensitivity analysis was carried out to examine the significant of the kinetic parameters on the total reducing sugars produced, thus, knowing the determining parameter affecting the overall kinetics. Figures 29A and 29B show the sensitivity analysis of the estimated parameters of direct effect on the total reducing sugars produced, namely k_{c1} , k_{x2} , k_p , and k_{ep1} and those of inverse effect, namely, k_{x1} , and φ . The parameters k_{c2} , and k_{ep2} also showed inverse effects, but they were insignificant, and hence not shown in Figure 29B, which can be removed from the model for further simplification. Figure 29A shows that all direct effect parameters had an effect in the range of $\pm 3.8\%$ from the original estimated value, with a stronger effect in the negative side. The most significant parameter was the substrate crystallinity factor, φ , which resulted in over $\pm 20\%$ change in the total reducing sugars produced compared to the original estimated value, which was also higher in the negative effect. This reflects the importance of the substrate quality and the importance of pretreatment method that contributes to better substrate quality on estimating the kinetic parameters and enhances overall hydrolysis rate.

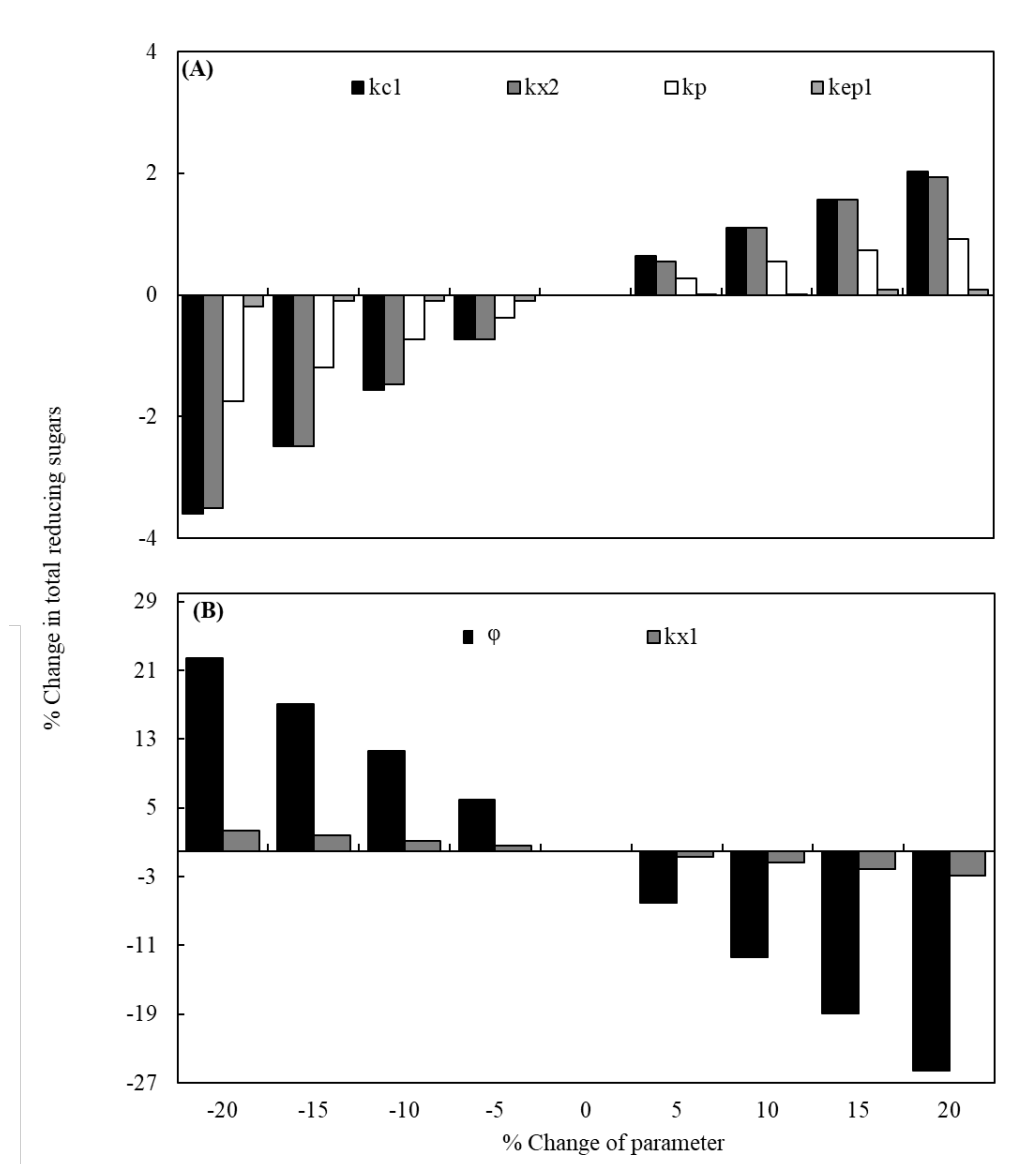


Figure 28: Sensitivity analysis of estimated parameters on the total reducing sugars produced

5.2.6 Statistical Analysis

Response surface regression analysis was performed using the Minitab 19 software with a statistical significance established at a p -value of <0.05 . Table 11 shows the results of the analysis of variance obtained after examining the effects of the two independent variables, substrate concentration (X_1) and water flow rate (X_2), on the total reducing sugars produced after 8 h of hydrolysis. As shown in the table, the linear effects of both substrate concentration and water flow rate were found to be significant, with p -values of 0.015 and 0.014, respectively. Although both

factors were significant, the substrate concentration effect was slightly more significant. None of the quadratic terms, substrate concentration (X_1^2) and water flow rate (X_2^2), however, were found to be significant. These results are in agreement with those reported in Section 5.1.6. In addition, the quadratic term (X_1^2) and X_1X_2 negatively contributed to the total reducing sugars production, which agreed with the previous observation where increasing the substrate concentration to the highest concentration resulted in substrate inhibition phenomena which negatively affected the yield at the end of the reaction time.

Table 11: Response Surface Regression: product produced versus substrate concentration and water flowrate:(A) Coded Coefficients (B) Analysis of Variance

A. Term	Coef	SE Coef	T-Value	P-Value	VIF
Constant	6.917	0.508	13.61	0.001	
X1	1.696	0.339	5.00	0.015	2.78
X2	1.287	0.250	5.14	0.014	1.01
X1*X1	-1.130	0.390	-2.89	0.063	2.78
X2*X2	0.269	0.431	0.62	0.576	1.00
X1*X2	-0.654	0.249	-2.63	0.078	1.01
B. Source	DF	Adj SS	Adj MS	F-Value	P-Value
Model	5	22.1627	4.4325	11.93	0.034
Linear	2	19.1166	9.5583	25.72	0.013
X1	1	9.2997	9.2997	25.02	0.015
X2	1	9.8169	9.8169	26.42	0.014
Square	2	3.2581	1.6290	4.38	0.129
X1*X1	1	3.1130	3.1130	8.38	0.063
X2*X2	1	0.1451	0.1451	0.39	0.576
2-Way Interaction	1	2.5711	2.5711	6.92	0.078
X1*X2	1	2.5711	2.5711	6.92	0.078
Error	3	1.1149	0.3716		
Total	8				

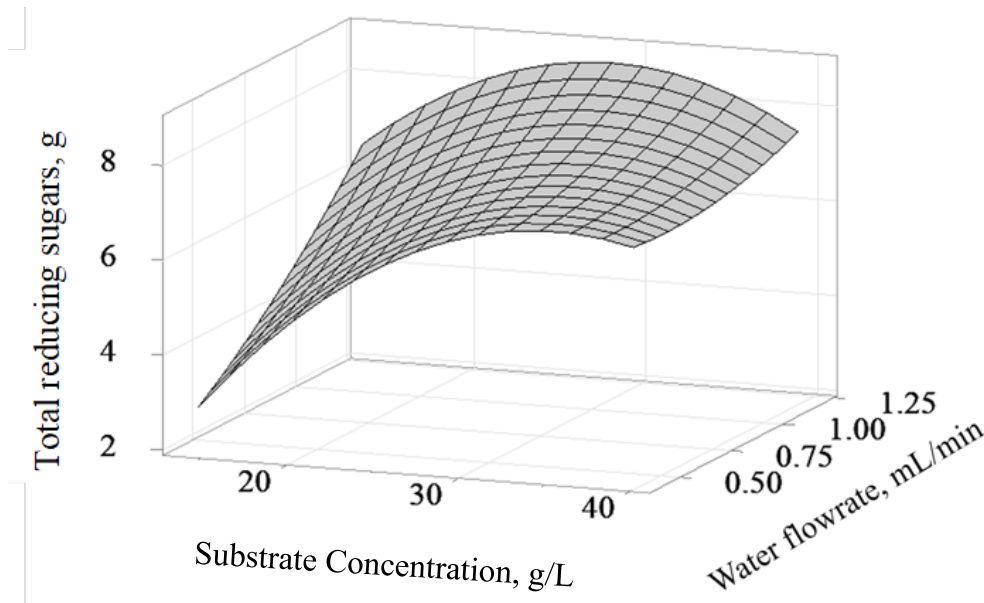


Figure 29: 3-D plot of total reducing sugars produced using PES-10 after 8 h. Operated at pH 4.8 and 48°C as a function of substrate concentration and water flowrate

A second-order interactive regression model, Equation (39), was developed to relate the total reducing sugars produced (P) and the two independent parameters, X_1 and X_2 . The equation was used to draw a three-dimensional (3D) plot of the combined effects of substrate concentration and water flow rate on the total reducing sugars produced (Figure 30).

$$P = -7.06 + 0.759 X_1 + 4.2 X_2 - 0.00996 X_1^2 + 1.68 X_2^2 - 0.1536 X_1 X_2 \quad (39)$$

As shown in Table 12, the total reducing sugars produced predicted by the statistical model after 8 h resulted in an R^2 value of 0.95. The positive effect of both the water flow rate and the substrate concentration on the biomass conversion and the slightly negative effect at the highest concentration, which were observed in the experimental results (Figure 26) were also observed in the 3D surface graph shown in Figure 33. The more significant effect of the substrate concentration over the water flow rate effect, as suggested by the p -values, can also be observed in the 3D surface graph.

The process was optimized using Response Optimizer in Minitab, which showed that the highest water flow rate of 1.2 mL/min ($\tau = 10.4$ h) and a substrate concentration of 28.9 g/L would result in the maximum total reducing sugars amount of 8.7 g. The experimental result obtained at 1.2 mL/min ($\tau = 10.4$ h) and 18.7 g/L, which was 7.99 ± 0.06 closely agreed with the model prediction.

Table 12: Total reducing sugars produced after 8 h at different substrate concentrations (X1) and water flowrates (X2)

Substrate concentration (g/L)	Water flowrate (mL/min)	Residence time (h)	Experimental product produced (g)	Product produced by statistical model (g)	R ²
X1	X2				
14.3	0.4	31.3	3.04±0.01	2.83	
14.3	0.8	15.6	3.85±0.01	4.43	
14.3	1.2	10.4	7.01±0.05	6.58	
21.4	0.4	31.3	5.41±0.08	5.26	
21.4	0.8	15.6	6.47±0.03	6.43	0.95
21.4	1.2	10.4	7.99±0.06	8.14	
39.6	0.4	31.3	6.58±0.05	6.89	
39.6	0.8	15.6	7.55±0.12	6.95	
39.6	1.2	10.4	7.32±0.11	7.54	

5.3 Glucose Permeation

5.3.1 Parametric Study

The amount of permeated glucose to the upper cell with time through PES-10 membrane at different initial glucose concentrations and water flowrates is shown in Figure 31. The lines shown on the figure are the connection between the points, added to highlight the trend. Similar

trends to those shown in Figure 31 were found for other tested conditions but presenting them in the figure would overcrowd it. Increasing the glucose concentration and water flowrates resulted in increasing the glucose permeation rate. At a water flowrate of 0.2 mL/min ($\tau = 62.5$ h) and glucose concentration of 27 g/L, 11% of the glucose permeated through the membrane within 3 h. By increasing the flowrate to 0.8 mL/min ($\tau = 15.6$ h) and glucose concentration to 53 g/L, the glucose permeation increased to 51%.

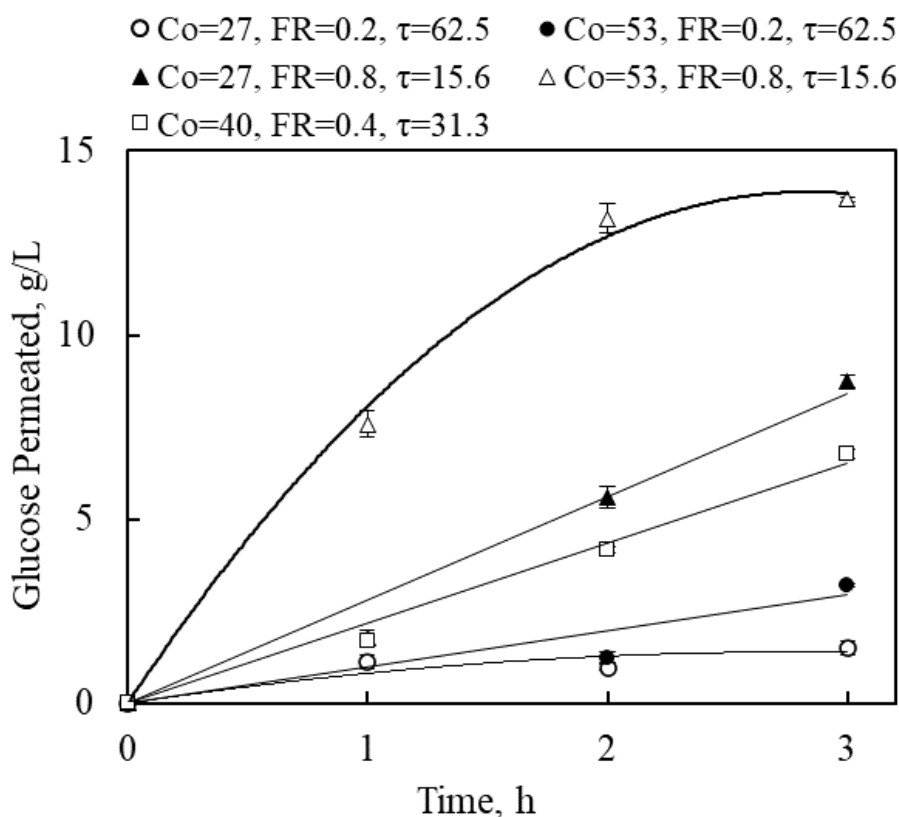


Figure 30: Effects of initial glucose concentrations, C_o (g/L), and water flowrates, FR (mL/min), corresponding to residence time, τ (h), on permeated glucose through PES-10 membrane.

The permeation rates were determined from the slopes of the permeation amount curves, similar to the ones shown in Figure 32. The effects of an increasing initial glucose concentration at a constant water flowrate of 0.4 mL/min ($\tau = 31.3$ h) and increasing water flowrate at a constant initial concentration of 40 g/L, on glucose permeation rate through PES-30 membrane are shown

in Figures 32A and 32B, respectively. The results clearly show the positive effect of both factors on the permeation rate. The significance of both effects, however, was found to diminish as they increase. Based on the central composite design (CCD), PES-30 was the central point, thus, there were more data points using it, to show the effect of each parameter on the permeation rate. However, permeation rates for all runs are presented in Table 14.

The increase in glucose permeation rate with the increase in initial concentration, at constant water flowrate, was only due to the increase in the molecular diffusion, as a result of increasing the diffusion driving force. The increase of glucose permeation with the increase in water flowrate, at constant initial concentration, however, was due to the increase in convective flow. As the flowrate increased from 0.1 to 1.6 mL/min, which corresponds to a decrease in the residence time from 125 to 7.8 h, respectively, at constant initial glucose concentration of 40 g/L, the permeation rate increased from 0.4 to 4.59 g/h. By increasing the initial concentration from 13.3 to 66.67 g/L, at a water flowrate of 0.4 mL/min ($\tau = 31.3$ h), the permeation rate increased from 1.23 to 3.59 g/h.

The effect of increasing the MWCO of the membrane on the glucose permeation rate at a constant glucose concentration and a water flowrate of 40 g/L and 0.4 mL/min ($\tau = 31.3$ h), respectively, is shown in Figure 32C. It can be seen that increasing the membrane MWCO resulted in a slight increase in the permeation rate. This can be attributed to the significant difference in the molecular weight of glucose in comparison to the pore sizes of PES-10, 30 and 50 kDa membranes. The relatively larger pore size allows glucose to pass easily in all MWCO.

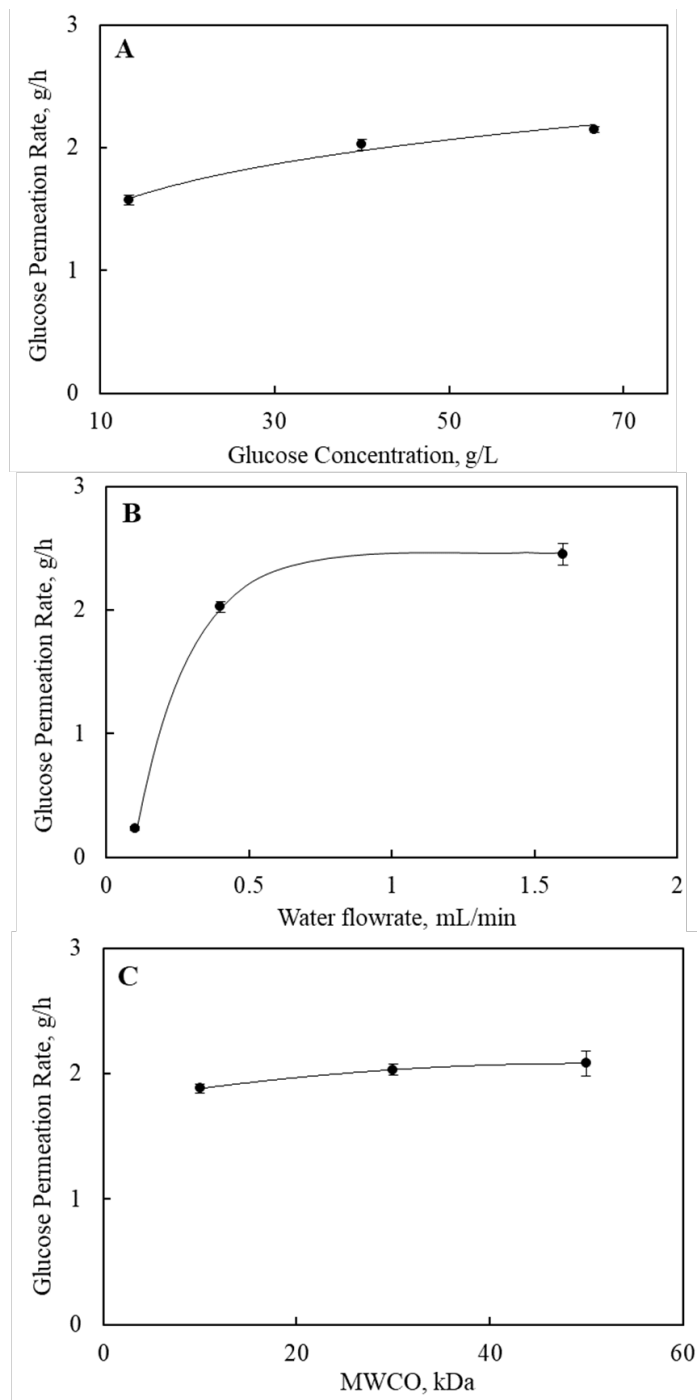


Figure 31: Glucose permeation rate using PES-30 at (A) 0.4 mL/min ($\tau = 31.3$ h) water flowrate and different initial glucose concentrations, (B) glucose concentration of 40 g/L and different water flowrates and (C) glucose concentration of 40 g/L, 0.4 mL/min ($\tau = 31.3$ h) water flowrate and different MWCOs

5.3.2 Statistical Analysis

Response surface regression analysis was performed using Minitab 19 software with statistical significance established at a P -value of <0.05 . Table 13 shows the results of the analysis of variance obtained after examining the effects of three independent variables, *i.e.*, glucose concentration (X_1) water flowrate (X_2), and MWCOs (X_3) on glucose permeation rate. The analysis shows that the linear effects of both glucose concentration and water flowrate are significant, with P -values of 0.000 for both, with more contribution by water flowrate effect. However, the effect of the MWCO was found insignificant. These results are in agreement with those discussed in Section 5.3.1. The quadratic term of the water flow (X_2^2) was found significant ($P = 0.001$), whereas those of the glucose concentration (X_1^2) and MWCOs were insignificant. However, both quadratic term of water flowrate (X_2^2) and the interaction between MWCO and water flowrate showed a negative contribution on the permeation rate.

Table 13: Response surface regression analysis of glucose permeation rate versus glucose concentration (X_1), water flowrates (X_2), and MWCOs (X_3): (A) Coded Coefficients (B) Analysis of Variance

A. Term	Coef	SE Coef	T-Value	P-Value	VIF
Constant	3.599	0.186	19.40	0.000	
X1	1.577	0.256	6.17	0.000	4.61
X2	2.107	0.137	15.42	0.000	1.23
X3	0.055	0.120	0.46	0.660	2.63
X1*X1	0.456	0.231	1.98	0.088	1.33
X2*X2	-1.109	0.208	-5.35	0.001	1.43
X3*X3	0.186	0.148	1.25	0.251	1.42
X1*X2	0.564	0.421	1.34	0.223	4.61
X1*X3	0.318	0.173	1.83	0.110	1.00
X2*X3	-0.297	0.204	-1.45	0.190	2.60

B. Source	DF	Adj SS	Adj MS	F-Value	P-Value
Model	9	31.9831	3.5537	59.18	0.000
Linear	3	16.7736	5.5912	93.11	0.000
X1	1	2.2842	2.2842	38.04	0.000
X2	1	14.2804	14.2804	237.82	0.000
X3	1	0.0127	0.0127	0.21	0.660
Square	3	3.2597	1.0866	18.10	0.001
X1*X1	1	0.2349	0.2349	3.91	0.088
X2*X2	1	1.7160	1.7160	28.58	0.001
X3*X3	1	0.0940	0.0940	1.57	0.251
2-Way Interaction	3	0.4362	0.1454	2.42	0.151
X1*X2	1	0.1075	0.1075	1.79	0.223
X1*X3	1	0.2016	0.2016	3.36	0.110
X2*X3	1	0.1268	0.1268	2.11	0.190
Error	7	0.4203	0.0600		
Total	16				

Coef, coefficient; SE Coef, standard error of the coefficient; VIF, variance inflation factor; DF, degrees of freedom; Adj SS, adjusted sum of the squares; Adj MS, adjusted mean square

A second-order interactive regression model, Equation (40), was developed to relate the permeation rate (n_g) and the three independent parameters, X_1 , X_2 , and X_3 . The equation was used to draw a three-dimensional (3D) plot of the combined effects of glucose concentration and water flowrate at a fixed MWCO of 10 kDa on the permeation rate (Figure 33).

$$n_g = -0.049 - 0.034 X_1 + 93.8 X_2 - 0.0321 X_3 + 0.000641 X_1^2 - 548 X_2^2 + 0.000464 X_3^2 + 0.47 X_1 X_2 + 0.000595 X_1 X_3 - 0.329 X_2 X_3 \quad (40)$$

Table 14: Glucose permeation rate after 3 h at different glucose concentrations (X_1), water flowrates (X_2), and MWCOs (X_3)

Glucose concentration (g/L)	Water flowrate (mL/min)	Residence time (h)	MWCO (kDa)	Glucose permeation rate (g/h)	Statistical model (g/h)	R^2
X_1	X_2		X_3			
26.67	0.2	62.5	10	0.74	0.54183	
53.33	0.2	62.5	10	1.11	1.311697	
26.67	0.8	15.6	10	2.85	3.06771	
53.33	0.8	15.6	10	4.52	4.288777	
26.67	0.2	62.5	50	1.88	1.887792	
53.33	0.2	62.5	50	0.63	0.848177	
26.67	0.8	15.6	50	2.5	2.25271	
53.33	0.8	15.6	50	3.09	2.900297	
40	0.4	31.3	10	4.53	4.75603	0.99
40	0.4	31.3	50	2.3	2.353552	
40	0.8	15.6	50	3.78	3.714208	
40	0.1	125	30	0.4	0.381852	
40	0.4	31.3	30	2.03	1.935072	
40	1.6	7.8	30	4.59	4.596912	
13.33	0.4	31.3	30	1.23	1.153253	
26.67	0.4	31.3	30	1.29	1.430228	
66.67	0.4	31.3	30	3.59	3.628763	

As shown in Table 14, the glucose permeation rate predicted by the statistical model after 3 h resulted in an R^2 value of 0.99. The process was optimized using Response Optimizer in Minitab, and the optimum conditions were found to be the highest glucose concentration of 66.67 g/L, highest MWCO of 50 kDa and water flow of 1.6 mL/min ($\tau = 7.8$ h). Under these optimum conditions, the maximum permeation rate of 4.5 g/h could be achieved, which was very close to that experimentally determined at conditions of glucose concentration of 53.3 g/L and water

flowrate of 0.8 mL/min ($\tau = 15.6$ h), using both PES-10 and PES-50, and using PES-30 at conditions of glucose concentration of 40 g/L and water flowrate of 1.6 mL/min ($\tau = 7.8$ h). Figure 33 clearly shows the slight positive effect of glucose concentration compared to the significant effect of water flowrate on the permeation rate, which agrees with the experimental findings presented in Section 5.3.1 that persists throughout the tested range.

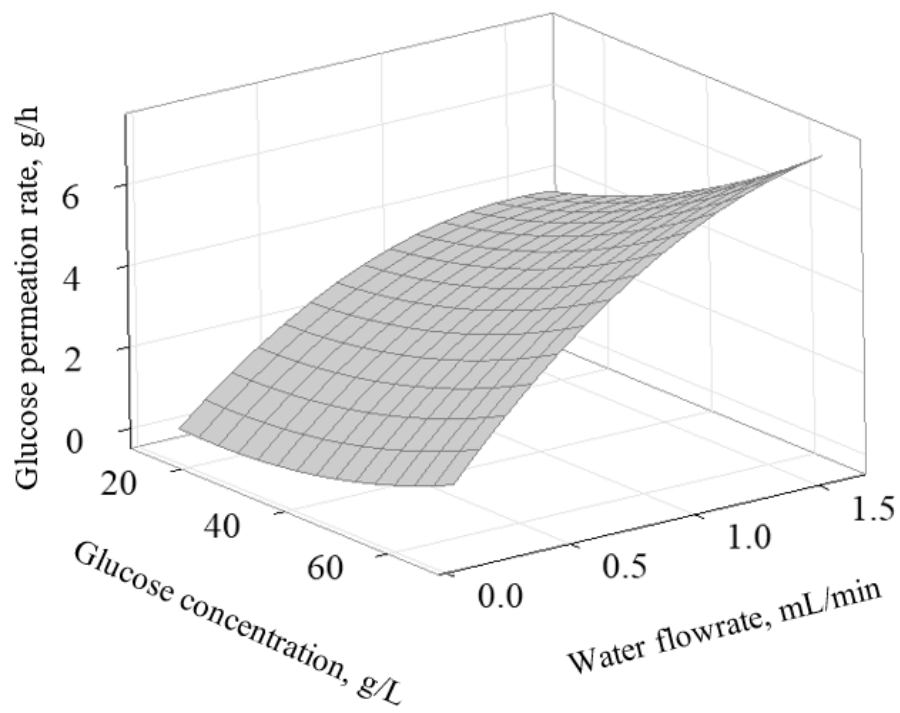


Figure 32: Combined effects of initial glucose concentration and water flowrate on glucose permeation rate through PES-10 membrane

Chapter 6: Conclusion and Future Perspectives

6.1 Conclusion

Enzymatic hydrolysis of cellulose is a complicated process. Understanding and modelling the reaction are key factors for enhancing the process and improving the feasibility. The two main obstacles facing the enzymatic hydrolysis of cellulose, namely enzymes recycling and product inhibition, are addressed in this work. To solve these obstacles, a novel inverted dead-end ultrafiltration MBR was designed, tested, and modelled to enhance the product yield. In addition, the applicability of high solids loading was further tested in a newly designed radial flow tubular MBR system with a lignocellulosic biomass, DSs, which is a major concern in large-scale production.

To simultaneously address the problems of product inhibition and confining soluble enzyme inside the reactor system, an MBR was designed using PES-10 membrane in an inverted dead-end filtration concept. The PES membrane was shown to completely reject cellulase and only allow the permeation of glucose. By using the MBR for enzymatic hydrolysis of standard cellulose by *T. reesei* cellulase, the efficient continuous separation of the products enhanced the total yield after 8 h from 7% (without product separation) to 45%. This was mainly due to the elimination of product inhibition effect and the pushing of the reaction in the forward by the continuous product removal. In addition, the novel design eliminated membrane fouling occurrence, which was a major concern with other MBR configurations. This was proven by SEM, FTIR, and XRD analyses, which showed absence of internal or surface fouling. Statistical analysis of the effect of initial substrate concentration and water flowrate on the production yield showed that both effects were significant. A kinetic model was developed from the mechanistic reaction steps and was successfully fitted to the experimental data to determine the kinetics parameters.

The applicability of an inverted dead-end MBR was further evaluated using a real lignocellulosic waste biomass, namely date seeds (DSs). Using fresh, untreated DSs, enzymatic hydrolysis yield did not exceed 2.1% after 8 h. However, by removing 30% of lignin from the DSs, the hydrolysis yield enhanced to 3.5% under the same conditions. This shows the significance of biomass pretreatment on the enzymatic hydrolysis yield. The effect of partial removal of lignin on opening of the lignocellulose structure and exposing the cellulose was confirmed using SEM, FTIR, and XRD analyses.

The effect of continuous products separation was also tested in a novel radial flow MBR, which offered a much larger specific interfacial area and allowed for higher solids loading that those were not provided by the inverted dead-end MBR. The membrane surface in the inverted dead-end MBR was 44 cm². However, the specific surface area of the radial flow MBR was 578 cm², and the specific area per volume of reaction was 0.62 cm²/cm³, compared to only 0.06 cm²/cm³ in the inverted dead-end MBR, which resulted in a further enhanced separation. In addition, high solids loading above 13.3 g/L, which was a barrier to overcome in the inverted dead-end MBR, was shown to be applicable in the radial flow MBR, which is promising for scaling up the process. The results of this work represent a significant addition to MBR research for enhancing the enzymatic hydrolysis of lignocellulose for bioethanol production.

6.2 Future Perspectives

The global annual bioethanol production is estimated to reach up to 140 billion liters in 2022, with a compound annual growth rate (CAGR) of 7.6%. These figures are still low compared to other industrial applications, which is mainly due to the challenges faced in large scale bioethanol production [212]. Therefore, an important aspect is the use of MBR for simultaneous enzymatic hydrolysis, which could have a positive effect on simplifying the process.

To improve the performance of lignocellulosic-to-ethanol production process and bring it closer to commercialization, it is essential to enhance the cellulose hydrolysis rate and yield, while operating at high substrate loading to increase the concentration of the produced sugars [213]. To achieve this, an effective substrate pretreatment method, which result in improving the substrate-cellulase productive binding, should be adopted [214]. By using the NaOH pretreatment, 30% of lignin was removed. However, higher concentrations of the alkaline, coupled with other pretreatment methods, could be investigated to increase the removal of lignin. Nevertheless, care should be taken to avoid the production of by-product inhibitors to the enzyme. In addition, a high pH after the alkaline pretreatment would require an additional neutralization step to avoid enzyme deactivation.

Enhancing enzymatic hydrolysis and the subsequent fermentation step both require high solids loading, which proved to be a major problem in most conventional stirred reactors. This was addressed in the radial-flow MBR using PES membrane, which showed promising results for enhanced enzymatic hydrolysis while allowing for high solids loading. To improve this further and to be industrially applicable, a membrane with a high mechanical strength that can withstand high separation fluxes would be needed. Ceramic membranes have shown promising results in this regard, and can be tested as an alternative to the PES membranes. The use of ceramic membranes in MBRs for enhanced enzymatic hydrolysis of cellulose has never been addressed in literature, and for large scale production, more investigations would be needed.

References

1. W. Erskine, A.T. Moustafa, A.E. Osman, Z. Lashine, A. Nejatian, T. Badawi, and S.M. Ragy: "Date palm in the GCC countries of the Arabian Peninsula." Presented at the Proc. Regional Workshop on Date Palm Development in the Arabian Peninsula, Abu Dhabi, UAE 2004.
2. I. Hanif: "Impact of fossil fuels energy consumption, energy policies, and urban sprawl on carbon emissions in East Asia and the Pacific: A panel investigation." *Energy Strategy Reviews*. vol. 21, pp. 16–24, 2018.
3. S.A. Solarin, U. Al-Mulali, G.G.G. Gan, and M. Shahbaz: "The impact of biomass energy consumption on pollution: evidence from 80 developed and developing countries." *Environ Sci Pollut Res*. vol. 25, no. 23, pp. 22641–22657, 2018.
4. A. García-Olivares, J. Solé, and O. Osychenko: "Transportation in a 100% renewable energy system." *Energy Conversion and Management*. vol. 158, pp. 266–285, 2018.
5. J. Mączyńska, M. Krzywonos, A. Kupczyk, K. Tucki, M. Sikora, H. Pińkowska, A. Bączyk, and I. Wielewska: "Production and use of biofuels for transport in Poland and Brazil – The case of bioethanol." *Fuel*. vol. 241, pp. 989–996, 2019.
6. Danish and Z. Wang: "Does biomass energy consumption help to control environmental pollution? Evidence from BRICS countries." *Science of The Total Environment*. vol. 670, pp. 1075–1083, 2019.
7. R. Sindhu, P. Binod, A. Pandey, S. Ankaram, Y. Duan, and M.K. Awasthi: "Chapter 5 - Biofuel Production From Biomass: Toward Sustainable Development." In: Kumar, S., Kumar, R., and Pandey, A. (eds.) *Current Developments in Biotechnology and Bioengineering*. pp. 79–92. Elsevier 2019.
8. H.C. Ong, W.-H. Chen, Y. Singh, Y.Y. Gan, C.-Y. Chen, and P.L. Show: "A state-of-the-art review on thermochemical conversion of biomass for biofuel production: A TG-FTIR approach." *Energy Conversion and Management*. vol. 209, pp. 112634–112655, 2020.
9. Y. Hadar: "Sources for Lignocellulosic Raw Materials for the Production of Ethanol." In: Faraco, V. (ed.) *Lignocellulose Conversion: Enzymatic and Microbial Tools for Bioethanol Production*. Springer, Berlin, Heidelberg. pp. 21–38, 2013.
10. H. Yang, X. Zhang, H. Luo, B. Liu, T.M. Shiga, X. Li, J.I. Kim, P. Rubinelli, J.C. Overton, V. Subramanyam, B.R. Cooper, H. Mo, M.M. Abu-Omar, C. Chapple, B.S. Donohoe, L. Makowski, N.S. Mosier, M.C. McCann, N.C. Carpita, and R. Meilan: "Overcoming cellulose recalcitrance in woody biomass for the lignin-first biorefinery." *Biotechnology for Biofuels*. vol. 12, no. 1, pp. 171–189, 2019.

11. N. Sathitsuksanoh, A. George, and Y.-H.P. Zhang: “New lignocellulose pretreatments using cellulose solvents: a review.” *Journal of Chemical Technology & Biotechnology*. vol. 88, no. 2, pp. 169–180, 2013.
12. S.N. Naik, V.V. Goud, P.K. Rout, and A.K. Dalai: “Production of first and second generation biofuels: A comprehensive review.” *Renewable and Sustainable Energy Reviews*. vol. 14, no. 2, pp. 578–597, 2010.
13. J.-L. Wertz and O. Bédué: “Lignocellulosic Biorefineries.” *EPFL Press*, 2013. Accessed from <https://doi.org/10.1201/b15443>. Accessed on 7 Jan 2022.
14. H. Chen, J. Liu, X. Chang, D. Chen, Y. Xue, P. Liu, H. Lin, and S. Han: “A review on the pretreatment of lignocellulose for high-value chemicals.” *Fuel Processing Technology*. vol. 160, pp. 196–206, 2017.
15. S.I. Mussatto and J.A. Teixeira: “Lignocellulose as raw material in fermentation processes.” pp. 11–32, 2010.
16. R. Chang, A.S. Gross, and J.-W. Chu: “Degree of Polymerization of Glucan Chains Shapes the Structure Fluctuations and Melting Thermodynamics of a Cellulose Microfibril.” *J. Phys. Chem. B*. vol. 116, no. 28, pp. 8074–8083, 2012.
17. M.J. Taherzadeh and K. Karimi: “ACID-BASED HYDROLYSIS PROCESSES FOR ETHANOL FROM LIGNOCELLULOSIC MATERIALS: A REVIEW.” *BioResources*. vol. 2, no. 3, pp. 472-499–499, 2007.
18. S. Schläfle, T. Tervahartiala, T. Senn, and R. Kölling-Paternoga: “Quantitative and visual analysis of enzymatic lignocellulose degradation.” *Biocatalysis and Agricultural Biotechnology*. vol. 11, pp. 42–49, 2017.
19. J. Yu, N. Paterson, J. Blamey, and M. Millan: “Cellulose, xylan and lignin interactions during pyrolysis of lignocellulosic biomass.” *Fuel*. vol. 191, pp. 140–149, 2017.
20. D.L. Gall, J. Ralph, T.J. Donohue, and D.R. Noguera: “Biochemical transformation of lignin for deriving valued commodities from lignocellulose.” *Current Opinion in Biotechnology*. vol. 45, pp. 120–126, 2017.
21. B.O. Abo, M. Gao, Y. Wang, C. Wu, H. Ma, and Q. Wang: “Lignocellulosic biomass for bioethanol: an overview on pretreatment, hydrolysis and fermentation processes.” *Reviews on Environmental Health*. vol. 34, no. 1, pp. 57–68, 2019.
22. N. Gupta and H. Kushwaha: “Date Palm as a Source of Bioethanol Producing Microorganisms.” In: Jain, S.M., Al-Khayri, J.M., and Johnson, D.V. (eds.) *Date Palm Biotechnology*. Springer Netherlands, Dordrecht. pp. 711–727, 2011.

23. E. Elnajjar, S. Al-Zuhair, S. Hasan, S. Almardeai, S.A.B. Al Omari, and A. Hilal-Alnaqbi: "Morphology characterization and chemical composition of United Arab Emirates date seeds and their potential for energy production." *Energy*. vol. 213, pp. 118810–118819, 2020.
24. F. Bouaziz, A.B. Abdeddayem, M. Koubaa, F.J. Barba, K.B. Jeddou, I. Kacem, R.E. Ghorbel, and S.E. Chaabouni: "Bioethanol Production from Date Seed Cellulosic Fraction Using *Saccharomyces cerevisiae*." *Separations*. vol. 7, no. 4, pp. 67–79, 2020.
25. A. Taghizadeh-Alisaraei, A. Motevali, and B. Ghobadian: "Ethanol production from date wastes: Adapted technologies, challenges, and global potential." *Renewable Energy*. vol. 143, pp. 1094–1110, 2019.
26. M.J.A. Afiq, R.A. Rahman, Y.B.C. Man, H.A. AL-Kahtani, and T.S.T. Mansor: "Date seed and date seed oil." *International Food Research Journal*. vol. 20, no. 5, pp. 2035–2043, 2013.
27. S. Ghnimi, S. Umer, A. Karim, and A. Kamal-Eldin: "Date fruit (*Phoenix dactylifera* L.): An underutilized food seeking industrial valorization." *NFS Journal*. vol. 6, pp. 1–10, 2017.
28. A. Nabili, A. Fattoum, R. Passas, and E. Elaloui: "Extraction and characterization of cellulose from date palm seeds (*Phoenix dactylifera* L.)." *Cellul. Chem. Technol.* vol. 50, pp. 1015–1023, 2016.
29. N.Y. Abu-Thabit, A.A. Judeh, A.S. Hakeem, A. Ul-Hamid, Y. Umar, and A. Ahmad: "Isolation and characterization of microcrystalline cellulose from date seeds (*Phoenix dactylifera* L.)." *International Journal of Biological Macromolecules*. vol. 155, pp. 730–739, 2020.
30. O. Ishurd, Y. Ali, W. Wei, F. Bashir, A. Ali, A. Ashour, and Y. Pan: "An alkali-soluble heteroxylyan from seeds of *Phoenix dactylifera* L." *Carbohydrate Research*. vol. 338, no. 15, pp. 1609–1612, 2003.
31. N. George, A.A.M. Andersson, R. Andersson, and A. Kamal-Eldin: "Lignin is the main determinant of total dietary fiber differences between date fruit (*Phoenix dactylifera* L.) varieties." *NFS Journal*. vol. 21, pp. 16–21, 2020.
32. V.B. Agbor, N. Cicek, R. Sparling, A. Berlin, and D.B. Levin: "Biomass pretreatment: Fundamentals toward application." *Biotechnology Advances*. vol. 29, no. 6, pp. 675–685, 2011.
33. L. da Costa Sousa, S.P. Chundawat, V. Balan, and B.E. Dale: "'Cradle-to-grave' assessment of existing lignocellulose pretreatment technologies." *Current opinion in biotechnology*. vol. 20, no. 3, pp. 339–347, 2009.
34. A. Gaikwad: "Effect of Particle Size on the Kinetics of Enzymatic Hydrolysis of Microcrystalline Cotton Cellulose: a Modeling and Simulation Study." *Appl Biochem Biotechnol*. vol. 187, no. 3, pp. 800–816, 2019.

35. D. Kim: "Physico-chemical conversion of lignocellulose: Inhibitor effects and detoxification strategies: A mini review." *Molecules*. vol. 23, no. 2, pp. 309–320, 2018.
36. S. Sun, S. Sun, X. Cao, and R. Sun: "The role of pretreatment in improving the enzymatic hydrolysis of lignocellulosic materials." *Bioresource Technology*. vol. 199, pp. 49–58, 2016.
37. T.A. Lloyd and C.E. Wyman: "Combined sugar yields for dilute sulfuric acid pretreatment of corn stover followed by enzymatic hydrolysis of the remaining solids." *Bioresource Technology*. vol. 96, no. 18, pp. 1967–1977, 2005.
38. R.P. Chandra, R. Bura, W.E. Mabee, A. Berlin, X. Pan, and J.N. Saddler: "Substrate Pretreatment: The Key to Effective Enzymatic Hydrolysis of Lignocellulosics?" In: Olsson, L. (ed.) *Biofuels*. Springer, Berlin, Heidelberg. pp. 67–93, 2007.
39. T.-C. Hsu, G.-L. Guo, W.-H. Chen, and W.-S. Hwang: "Effect of dilute acid pretreatment of rice straw on structural properties and enzymatic hydrolysis." *Bioresource Technology*. vol. 101, no. 13, pp. 4907–4913, 2010.
40. Y. Song, J. Zhang, X. Zhang, and T. Tan: "The correlation between cellulose allomorphs (I and II) and conversion after removal of hemicellulose and lignin of lignocellulose." *Bioresource Technology*. vol. 193, pp. 164–170, 2015.
41. J.S. Kim, Y.Y. Lee, and T.H. Kim: "A review on alkaline pretreatment technology for bioconversion of lignocellulosic biomass." *Bioresource Technology*. vol. 199, pp. 42–48, 2016.
42. H. Wu, X. Dai, S.-L. Zhou, Y.-Y. Gan, Z.-Y. Xiong, Y.-H. Qin, J. Ma, L. Yang, Z.-K. Wu, T.-L. Wang, W.-G. Wang, and C.-W. Wang: "Ultrasound-assisted alkaline pretreatment for enhancing the enzymatic hydrolysis of rice straw by using the heat energy dissipated from ultrasonication." *Bioresource Technology*. vol. 241, pp. 70–74, 2017.
43. Z. Ling, S. Chen, X. Zhang, and F. Xu: "Exploring crystalline-structural variations of cellulose during alkaline pretreatment for enhanced enzymatic hydrolysis." *Bioresource Technology*. vol. 224, pp. 611–617, 2017.
44. K. Raj and C. Krishnan: "High sugar yields from sugarcane (*Saccharum officinarum*) bagasse using low-temperature aqueous ammonia pretreatment and laccase-mediator assisted enzymatic hydrolysis." *Industrial Crops and Products*. vol. 111, pp. 673–683, 2018.
45. W. Den, V.K. Sharma, M. Lee, G. Nadadur, and R.S. Varma: "Lignocellulosic Biomass Transformations via Greener Oxidative Pretreatment Processes: Access to Energy and Value-Added Chemicals." *Front Chem*. vol. 6, 2018. Accessed from <https://doi.org/10.3389/fchem.2018.00141>. Accessed on 12 Nov 2021.
46. S. An, W. Li, Q. Liu, Y. Xia, T. Zhang, F. Huang, Q. Lin, and L. Chen: "Combined dilute hydrochloric acid and alkaline wet oxidation pretreatment to improve sugar recovery of corn stover." *Bioresource Technology*. vol. 271, pp. 283–288, 2019.

47. A. Johansson, O. Aaltonen, and P. Ylisen: "Organosolv pulping—methods and pulp properties." *Biomass*. vol. 13, no. 1, pp. 45–65, 1987.
48. F. Sun and H. Chen: "Organosolv pretreatment by crude glycerol from oleochemicals industry for enzymatic hydrolysis of wheat straw." *Bioresource Technology*. vol. 99, no. 13, pp. 5474–5479, 2008.
49. S.J. Kim, B.H. Um, D.J. Im, J.H. Lee, and K.K. Oh: "Combined Ball Milling and Ethanol Organosolv Pretreatment to Improve the Enzymatic Digestibility of Three Types of Herbaceous Biomass." *Energies*. vol. 11, no. 9, pp. 2457–2467, 2018.
50. C. Tang, J. Shan, Y. Chen, L. Zhong, T. Shen, C. Zhu, and H. Ying: "Organic amine catalytic organosolv pretreatment of corn stover for enzymatic saccharification and high-quality lignin." *Bioresource Technology*. vol. 232, pp. 222–228, 2017.
51. I. Salapa, C. Katsimpouras, E. Topakas, and D. Sidiras: "Organosolv pretreatment of wheat straw for efficient ethanol production using various solvents." *Biomass and Bioenergy*. vol. 100, pp. 10–16, 2017.
52. Z. Zhu, N. Sathitsuksanoh, T. Vinzant, D.J. Schell, J.D. McMillan, and Y.-H.P. Zhang: "Comparative study of corn stover pretreated by dilute acid and cellulose solvent-based lignocellulose fractionation: Enzymatic hydrolysis, supramolecular structure, and substrate accessibility." *Biotechnology and Bioengineering*. vol. 103, no. 4, pp. 715–724, 2009.
53. J.A. Rollin, Z. Zhu, N. Sathitsuksanoh, and Y.-H.P. Zhang: "Increasing cellulose accessibility is more important than removing lignin: A comparison of cellulose solvent-based lignocellulose fractionation and soaking in aqueous ammonia." *Biotechnology and Bioengineering*. vol. 108, no. 1, pp. 22–30, 2011.
54. Y. Cao, R. Zhang, T. Cheng, J. Guo, M. Xian, and H. Liu: "Imidazolium-based ionic liquids for cellulose pretreatment: recent progresses and future perspectives." *Appl Microbiol Biotechnol*. vol. 101, no. 2, pp. 521–532, 2017.
55. R. M. Wahlström and A. Suurnäkki: "Enzymatic hydrolysis of lignocellulosic polysaccharides in the presence of ionic liquids." *Green Chemistry*. vol. 17, no. 2, pp. 694–714, 2015.
56. J. Grewal, R. Ahmad, and S.K. Khare: "Development of cellulase-nanoconjugates with enhanced ionic liquid and thermal stability for in situ lignocellulose saccharification." *Bioresource Technology*. vol. 242, pp. 236–243, 2017.
57. E. Husson, T. Auxenfans, M. Herbaut, M. Baralle, V. Lambertyn, H. Rakotoarivonina, C. Rémond, and C. Sarazin: "Sequential and simultaneous strategies for biorefining of wheat straw using room temperature ionic liquids, xylanases and cellulases." *Bioresource Technology*. vol. 251, pp. 280–287, 2018.

58. T.R. Sarker, F. Pattnaik, S. Nanda, A.K. Dalai, V. Meda, and S. Naik: "Hydrothermal pretreatment technologies for lignocellulosic biomass: A review of steam explosion and subcritical water hydrolysis." *Chemosphere*. vol. 284, pp. 131372–131388, 2021.
59. R. Kataria, A. Mol, E. Schulten, A. Happel, and S.I. Mussatto: "Bench scale steam explosion pretreatment of acid impregnated elephant grass biomass and its impacts on biomass composition, structure and hydrolysis." *Industrial Crops and Products*. vol. 106, pp. 48–58, 2017.
60. J.M. Oliva, M.J. Negro, P. Manzanares, I. Ballesteros, M.Á. Chamorro, F. Sáez, M. Ballesteros, and A.D. Moreno: "A Sequential Steam Explosion and Reactive Extrusion Pretreatment for Lignocellulosic Biomass Conversion within a Fermentation-Based Biorefinery Perspective." *Fermentation*. vol. 3, no. 2, pp. 1–15, 2017.
61. A.L. Scholl, D. Menegol, A.P. Pitarelo, R.C. Fontana, A. Zandoná Filho, L.P. Ramos, A.J.P. Dillon, and M. Camassola: "Ethanol production from sugars obtained during enzymatic hydrolysis of elephant grass (*Pennisetum purpureum*, Schum.) pretreated by steam explosion." *Bioresource technology*. vol. 192, pp. 228–237, 2015.
62. H. Stanley, C. Ezeife, and C. Onwukwe: "Bioethanol Production from Elephant Grass (*Pennisetum purpureum*)." *Nigerian Journal of Biotechnology*. vol. 32, no. 1, pp. 1–6, 2017.
63. S. Montipó, I. Ballesteros, R.C. Fontana, S. Liu, A.F. Martins, M. Ballesteros, and M. Camassola: "Integrated production of second generation ethanol and lactic acid from steam-exploded elephant grass." *Bioresource technology*. vol. 249, pp. 1017–1024, 2018.
64. R. Zheng, H. Zhang, J. Zhao, M. Lei, and H. Huang: "Direct and simultaneous determination of representative byproducts in a lignocellulosic hydrolysate of corn stover via gas chromatography–mass spectrometry with a Deans switch." *Journal of Chromatography A*. vol. 1218, no. 31, pp. 5319–5327, 2011.
65. J. Du, Y. Li, H. Zhang, H. Zheng, and H. Huang: "Factors to decrease the cellulose conversion of enzymatic hydrolysis of lignocellulose at high solid concentrations." *Cellulose*. vol. 21, no. 4, pp. 2409–2417, 2014.
66. H.K. Sharma, C. Xu, and W. Qin: "Biological Pretreatment of Lignocellulosic Biomass for Biofuels and Bioproducts: An Overview." *Waste Biomass Valor*. vol. 10, pp. 235–251, 2017.
67. P.D. Maibam and S.K. Maiti: "A Strategy for Simultaneous Xylose Utilization and Enhancement of Cellulase Enzyme Production by *Trichoderma reesei* Cultivated on Liquid Hydrolysate Followed by Induction with Feeding of Solid Sugarcane Bagasse." *Waste and Biomass Valorization*. pp. 1–10, 2019.
68. S.B. Ummalyma, R.D. Supriya, R. Sindhu, P. Binod, R.B. Nair, A. Pandey, and E. Gnansounou: "Chapter 7 - Biological pretreatment of lignocellulosic biomass—Current trends and future perspectives." In: Basile, A. and Dalena, F. (eds.) *Second and Third Generation of Feedstocks*. Elsevier. pp. 197–212. 2019.

69. A. da S. Machado and A. Ferraz: "Biological pretreatment of sugarcane bagasse with basidiomycetes producing varied patterns of biodegradation." *Bioresource Technology*. vol. 225, pp. 17–22, 2017.
70. A.K. Kumar and S. Sharma: "Recent updates on different methods of pretreatment of lignocellulosic feedstocks: a review." *Bioresources and Bioprocessing*. vol. 4, no. 1, pp. 1–7, 2017.
71. Y. Wu, S. Ge, C. Xia, C. Mei, K.-H. Kim, L. Cai, L.M. Smith, J. Lee, and S.Q. Shi: "Application of intermittent ball milling to enzymatic hydrolysis for efficient conversion of lignocellulosic biomass into glucose." *Renewable and Sustainable Energy Reviews*. vol. 136, pp. 110442–110452, 2021.
72. X. Fei, W. Jia, J. Wang, T. Chen, and Y. Ling: "Study on enzymatic hydrolysis efficiency and physicochemical properties of cellulose and lignocellulose after pretreatment with electron beam irradiation." *International Journal of Biological Macromolecules*. vol. 145, pp. 733–739, 2020.
73. H. Gu, R. An, and J. Bao: "Pretreatment refining leads to constant particle size distribution of lignocellulose biomass in enzymatic hydrolysis." *Chemical Engineering Journal*. vol. 352, pp. 198–205, 2018.
74. N. Manmai, Y. Unpaprom, V.K. Ponnusamy, and R. Ramaraj: "Bioethanol production from the comparison between optimization of sorghum stalk and sugarcane leaf for sugar production by chemical pretreatment and enzymatic degradation." *Fuel*. vol. 278, pp. 118262–118276, 2020.
75. G. Sołowski, I. Konkol, and A. Cenian: "Production of hydrogen and methane from lignocellulose waste by fermentation. A review of chemical pretreatment for enhancing the efficiency of the digestion process." *Journal of Cleaner Production*. vol. 267, pp. 121721–121742, 2020.
76. H. Jørgensen, J.B. Kristensen, and C. Felby: "Enzymatic conversion of lignocellulose into fermentable sugars: challenges and opportunities." *Biofuels, Bioproducts and Biorefining*. vol. 1, no. 2, pp. 119–134, 2007.
77. N. Srivastava, M. Srivastava, P. Mishra, V.K. Gupta, G. Molina, S. Rodriguez-Couto, A. Manikanta, and P. Ramteke: "Applications of fungal cellulases in biofuel production: advances and limitations." *Renewable and Sustainable Energy Reviews*. vol. 82, pp. 2379–2386, 2018.
78. R. Tiwari, L. Nain, N.E. Labrou, and P. Shukla: "Bioprospecting of functional cellulases from metagenome for second generation biofuel production: a review." *Critical reviews in microbiology*. vol. 44, no. 2, pp. 244–257, 2018.

79. L. Rosgaard, S. Pedersen, J.R. Cherry, P. Harris, and A.S. Meyer: "Efficiency of new fungal cellulase systems in boosting enzymatic degradation of barley straw lignocellulose." *Biotechnology progress*. vol. 22, no. 2, pp. 493–498, 2006.
80. C.A. Barcelos, V.A. Rocha, C. Groposo, A.M. de Castro, and N. Pereira Jr: "Enzymes and accessory proteins involved in the hydrolysis of lignocellulosic biomass for bioethanol production." *Mycology: current and future developments*. vol. 1, pp. 23–56, 2016.
81. T. Jeoh, M. J. Cardona, N. Karuna, A. R. Mudinoor, and J. Nill, "Mechanistic kinetic models of enzymatic cellulose hydrolysis—A review," *Biotechnology and Bioengineering*, vol. 114, no. 7, pp. 1369–1385, 2017.
82. S. Al-Zuhair: "The effect of crystallinity of cellulose on the rate of reducing sugars production by heterogeneous enzymatic hydrolysis." *Bioresource Technology*. vol. 99, no. 10, pp. 4078–4085, 2008.
83. Z. Petrášek, M. Eibinger, and B. Nidetzky: "Modeling the activity burst in the initial phase of cellulose hydrolysis by the processive cellobiohydrolase Cel7A." *Biotechnology and Bioengineering*. vol. 116, no. 3, pp. 515–525, 2019.
84. E. Praestgaard, J. Elmerdahl, L. Murphy, S. Nymand, K.C. McFarland, K. Borch, and P. Westh: "A kinetic model for the burst phase of processive cellulases." *The FEBS Journal*. vol. 278, no. 9, pp. 1547–1560, 2011.
85. P. Bansal, M. Hall, M.J. Realff, J.H. Lee, and A.S. Bommarius: "Modeling cellulase kinetics on lignocellulosic substrates." *Biotechnology Advances*. vol. 27, no. 6, pp. 833–848, 2009.
86. A.C. Warden, B.A. Little, and V.S. Haritos: "A cellular automaton model of crystalline cellulose hydrolysis by cellulases." *Biotechnology for Biofuels*. vol. 4, no. 1, pp. 39–53, 2011.
87. B. Yang, D.M. Willies, and C.E. Wyman: "Changes in the enzymatic hydrolysis rate of Avicel cellulose with conversion." *Biotechnology and Bioengineering*. vol. 94, no. 6, pp. 1122–1128, 2006.
88. A.A. Huang: "Kinetic studies on insoluble cellulose–cellulase system." *Biotechnology and Bioengineering*. vol. 17, no. 10, pp. 1421–1433, 1975.
89. N. Peitersen and E.W. Ross: "Mathematical model for enzymatic hydrolysis and fermentation of cellulose by *Trichoderma*." *Biotechnology and Bioengineering*. vol. 21, no. 6, pp. 997–1017, 1979.
90. Q. Gan, S. Allen, and G. Taylor: "Analysis of process integration and intensification of enzymatic cellulose hydrolysis in a membrane bioreactor." *Journal of Chemical Technology & Biotechnology: International Research in Process, Environmental & Clean Technology*. vol. 80, no. 6, pp. 688–698, 2005.

91. Q. Gan, S. Allen, and G. Taylor: “Kinetic dynamics in heterogeneous enzymatic hydrolysis of cellulose: an overview, an experimental study and mathematical modelling.” *Process Biochemistry*. vol. 38, no. 7, pp. 1003–1018, 2003.
92. J.M. van Zyl, E. van Rensburg, W.H. van Zyl, T.M. Harms, and L.R. Lynd: “A Kinetic Model for Simultaneous Saccharification and Fermentation of Avicel With *Saccharomyces cerevisiae*.” *Biotechnology and Bioengineering*. vol. 108, no. 4, pp. 924–933, 2011.
93. Y.-H.P. Zhang and L.R. Lynd: “A functionally based model for hydrolysis of cellulose by fungal cellulase.” *Biotechnology and Bioengineering*. vol. 94, no. 5, pp. 888–898, 2006.
94. J. Valentine, J. Clifton-Brown, A. Hastings, P. Robson, G. Allison, and P. Smith: “Food vs. fuel: the use of land for lignocellulosic ‘next generation’ energy crops that minimize competition with primary food production.” *GCB Bioenergy*. vol. 4, no. 1, pp. 1–19, 2012.
95. E. Vasile and Ş.D. Bran: “Lignocellulose Bio Resources and Renewable Energy.” *Internal Auditing & Risk Management*. vol. 12, pp. 1–8, 2017.
96. X. Zhao, F. Qi, and D. Liu: “Hierarchy Nano- and Ultrastructure of Lignocellulose and Its Impact on the Bioconversion of Cellulose.” In: Rai, M. and da Silva, S.S. (eds.) *Nanotechnology for Bioenergy and Biofuel Production*. Springer International Publishing, Cham. pp. 117–151, 2017.
97. M. Londo, J. van Stralen, A. Uslu, H. Mozaffarian, and C. Kraan: “Lignocellulosic biomass for chemicals and energy: an integrated assessment of future EU market sizes, feedstock availability impacts, synergy and competition effects, and path dependencies.” *Biofuels, Bioproducts and Biorefining*. vol. 12, no. 6, pp. 1065–1081, 2018.
98. I.N. Ahmed, X.-L. Yang, A.A. Dubale, R.-F. Li, Y.-M. Ma, L.-M. Wang, G.-H. Hou, R.-F. Guan, and M.-H. Xie: “Hydrolysis of cellulose using cellulase physically immobilized on highly stable zirconium based metal-organic frameworks.” *Bioresource Technology*. vol. 270, pp. 377–382, 2018.
99. B. Qi, J. Luo, and Y. Wan: “Immobilization of cellulase on a core-shell structured metal-organic framework composites: Better inhibitors tolerance and easier recycling.” *Bioresource Technology*. vol. 268, pp. 577–582, 2018.
100. J. Sánchez-Ramírez, J.L. Martínez-Hernández, P. Segura-Ceniceros, G. López, H. Saade, M.A. Medina-Morales, R. Ramos-González, C.N. Aguilar, and A. Ilyina: “Cellulases immobilization on chitosan-coated magnetic nanoparticles: application for *Agave Atrovirens* lignocellulosic biomass hydrolysis.” *Bioprocess Biosyst Eng*. vol. 40, no. 1, pp. 9–22, 2017.
101. L. Tan, Z. Tan, H. Feng, and J. Qiu: “Cellulose as a template to fabricate a cellulase-immobilized composite with high bioactivity and reusability.” *New J. Chem*. vol. 42, no. 3, pp. 1665–1672, 2018.

102. K. Saha, P. Verma, J. Sikder, S. Chakraborty, and S. Curcio: "Synthesis of chitosan-cellulase nanohybrid and immobilization on alginate beads for hydrolysis of ionic liquid pretreated sugarcane bagasse." *Renewable Energy*. vol. 133, pp. 66–76, 2019.
103. T. Nguyenhuynh, R. Nithyanandam, C.H. Chong, and D. Krishnaiah: "A Review on Using Membrane Reactors in Enzymatic Hydrolysis of Cellulose." vol. 12, no. 4, pp. 1129 – 1152, 2017.
104. M. Anuganti, H. Fu, S. Ekatan, C.V. Kumar, and Y. Lin: "Kinetic Study on Enzymatic Hydrolysis of Cellulose in an Open, Inhibition-Free System." *Langmuir*. vol. 37, no. 17, pp. 5180–5192, 2021.
105. F. Ahamed, H.-S. Song, C.W. Ooi, and Y.K. Ho: "Modelling heterogeneity in cellulose properties predicts the slowdown phenomenon during enzymatic hydrolysis." *Chemical Engineering Science*. vol. 206, pp. 118–133, 2019.
106. H. Sitaraman, N. Danes, J.J. Lischeske, J.J. Stickel, and M.A. Sprague: "Coupled CFD and chemical-kinetics simulations of cellulosic-biomass enzymatic hydrolysis: Mathematical-model development and validation." *Chemical Engineering Science*. vol. 206, pp. 348–360, 2019.
107. S.K. Dutta and S. Chakraborty: "Mixing effects on the kinetics and the dynamics of two-phase enzymatic hydrolysis of hemicellulose for biofuel production." *Bioresource Technology*. vol. 259, pp. 276–285, 2018.
108. D. Haldar, K. Gayen, and D. Sen: "Enumeration of monosugars' inhibition characteristics on the kinetics of enzymatic hydrolysis of cellulose." *Process Biochemistry*. vol. 72, pp. 130–136, 2018.
109. D. Voet and J.G. Voet: "Biochemistry, Wiley, 2011: Biochemistry." *Bukupedia* , 2011.
110. D.B. Northrop: "On the meaning of K_m and V/K in enzyme kinetics." *Journal of Chemical Education*. vol. 75, no. 9, pp. 1153, 1998. Accessed from <https://doi.org/10.1021/ed075p1153>. Accessed on 26 May 2021.
111. J. Shi et al., "Dynamic changes of substrate reactivity and enzyme adsorption on partially hydrolyzed cellulose," *Biotechnology and bioengineering*, vol. 114, no. 3, pp. 503–515, 2017
112. Q. Gan, S. Allen, and G. Taylor: "Design and operation of an integrated membrane reactor for enzymatic cellulose hydrolysis." *Biochemical engineering journal*. vol. 12, no. 3, pp. 223–229, 2002.
113. Y. Wang, D. Chen, G. Wang, C. Zhao, Y. Ma, and W. Yang: "Immobilization of cellulase on styrene/maleic anhydride copolymer nanoparticles with improved stability against pH changes." *Chemical Engineering Journal*. vol. 336, pp. 152–159, 2018.

114. S. Gaikwad, A.P. Ingle, S.S. da Silva, and M. Rai: "Immobilized Nanoparticles-Mediated Enzymatic Hydrolysis of Cellulose for Clean Sugar Production: A Novel Approach." *Current Nanoscience*. vol. 15, no. 3, pp. 296–303, 2019.
115. R. Guo, X. Zheng, Y. Wang, Y. Yang, Y. Ma, D. Zou, and Y. Liu: "Optimization of Cellulase Immobilization with Sodium Alginate-Polyethylene for Enhancement of Enzymatic Hydrolysis of Microcrystalline Cellulose Using Response Surface Methodology." *Appl Biochem Biotechnol*. vol. 193, no. 7, pp. 2043–2060, 2021.
116. M.P. Desai and K.D. Pawar: "Immobilization of cellulase on iron tolerant *Pseudomonas stutzeri* biosynthesized photocatalytically active magnetic nanoparticles for increased thermal stability." *Materials Science and Engineering: C*. vol. 106, pp. 110169–110190, 2020.
117. I.N. Ahmed, R. Chang, and W.-B. Tsai: "Poly(acrylic acid) nanogel as a substrate for cellulase immobilization for hydrolysis of cellulose." *Colloids and Surfaces B: Biointerfaces*. vol. 152, pp. 339–343, 2017.
118. Q. Zhang, J. Kang, B. Yang, L. Zhao, Z. Hou, and B. Tang: "Immobilized cellulase on Fe₃O₄ nanoparticles as a magnetically recoverable biocatalyst for the decomposition of corncob." *Chinese Journal of Catalysis*. vol. 37, no. 3, pp. 389–397, 2016.
119. W. Zhang, J. Qiu, H. Feng, L. Zang, and E. Sakai: "Increase in stability of cellulase immobilized on functionalized magnetic nanospheres." *Journal of Magnetism and Magnetic Materials*. vol. 375, pp. 117–123, 2015.
120. M.R. Ladole, J.S. Mevada, and A.B. Pandit: "Ultrasonic hyperactivation of cellulase immobilized on magnetic nanoparticles." *Bioresource Technology*. vol. 239, pp. 117–126, 2017.
121. K. Khoshnevisan, A.-K. Bordbar, D. Zare, D. Davoodi, M. Noruzi, M. Barkhi, and M. Tabatabaei: "Immobilization of cellulase enzyme on superparamagnetic nanoparticles and determination of its activity and stability." *Chemical Engineering Journal*. vol. 171, no. 2, pp. 669–673, 2011.
122. H. Liao, D. Chen, L. Yuan, M. Zheng, Y. Zhu, and X. Liu: "Immobilized cellulase by polyvinyl alcohol/Fe₂O₃ magnetic nanoparticle to degrade microcrystalline cellulose." *Carbohydrate Polymers*. vol. 82, no. 3, pp. 600–604, 2010.
123. Q. Zhang, Z. Lu, C. Su, Z. Feng, H. Wang, J. Yu, and W. Su: "High yielding, one-step mechano-enzymatic hydrolysis of cellulose to cellulose nanocrystals without bulk solvent." *Bioresource Technology*. vol. 331, pp. 125015–125026, 2021.

124. B. He, P. Chang, X. Zhu, and S. Zhang: "Anemone-inspired enzymatic film for cellulose heterogeneous catalysis." *Carbohydrate Polymers*. vol. 260, pp. 117795–117801, 2021.
125. K.N. Rajnish, M.S. Samuel, A. John J, S. Datta, N. Chandrasekar, R. Balaji, S. Jose, and E. Selvarajan: "Immobilization of cellulase enzymes on nano and micro-materials for breakdown of cellulose for biofuel production-a narrative review." *International Journal of Biological Macromolecules*. vol. 182, pp. 1793–1802, 2021.
126. S. Bhagia, C.E. Wyman, and R. Kumar: "Impacts of cellulase deactivation at the moving air–liquid interface on cellulose conversions at low enzyme loadings." *Biotechnology for Biofuels*. vol. 12, no. 1, pp. 96–112, 2019.
127. F. Fenila and Y. Shastri: "Optimization of cellulose hydrolysis in a non-ideally mixed reactors." *Computers & Chemical Engineering*. vol. 128, pp. 340–351, 2019.
128. H. Shokrkar, S. Ebrahimi, and M. Zamani: "A review of bioreactor technology used for enzymatic hydrolysis of cellulosic materials." *Cellulose*. vol. 25, no. 11, pp. 6279–6304, 2018.
129. R. Acosta-Fernández, T. Poerio, D. Nabarlatz, L. Giorno, and R. Mazzei: "Enzymatic Hydrolysis of Xylan from Coffee Parchment in Membrane Bioreactors." *Ind. Eng. Chem. Res.* vol. 59, no. 16, pp. 7346–7354, 2020.
130. M.S. Pino, R.M. Rodríguez-Jasso, M. Michelin, A.C. Flores-Gallegos, R. Morales-Rodríguez, J.A. Teixeira, and H.A. Ruiz: "Bioreactor design for enzymatic hydrolysis of biomass under the biorefinery concept." *Chemical Engineering Journal*. vol. 347, pp. 119–136, 2018.
131. N. Mameri, F. Hamdache, N. Abdi, D. Belhocine, H. Grib, H. Lounici, and D. Piron: "Enzymatic saccharification of olive mill solid residue in a membrane reactor." *Journal of Membrane Science*. vol. 178, no. 1–2, pp. 121–130, 2000.
132. J.S. Knutsen and R.H. Davis: "Cellulase Retention and Sugar Removal by Membrane Ultrafiltration During Lignocellulosic Biomass Hydrolysis." In: Finkelstein, M., McMillan, J.D., Davison, B.H., and Evans, B. (eds.) *Proceedings of the Twenty-Fifth Symposium on Biotechnology for Fuels and Chemicals Held May 4–7, 2003, in Breckenridge, CO*. pp. 585–599. *Humana Press*, Totowa, NJ (2004).
133. C. Abels, K. Thimm, H. Wulfhorst, A.C. Spiess, and M. Wessling: "Membrane-based recovery of glucose from enzymatic hydrolysis of ionic liquid pretreated cellulose." *Bioresource technology*. vol. 149, pp. 58–64, 2013.
134. R. Mazzei, A. Yihdego Gebreyohannes, E. Papaioannou, S.P. Nunes, I.F.J. Vankelecom, and L. Giorno: "Enzyme catalysis coupled with artificial membranes towards process intensification in biorefinery- a review." *Bioresource Technology*. vol. 335, pp. 125248–125251, 2021.

135. T. Nguyenhuynh, R. Nithyanandam, C.H. Chong, and D. Krishnaiah: "Configuration modification of a submerged membrane reactor for enzymatic hydrolysis of cellulose." *Biocatalysis and Agricultural Biotechnology*. vol. 12, pp. 50–58, 2017.
136. M. Zhang, R. Su, Q. Li, W. Qi, and Z. He: "Enzymatic saccharification of pretreated corn stover in a fed-batch membrane bioreactor." *Bioenerg. Res.* vol. 4, no. 2, pp. 134–140, 2011.
137. P. Andrić, A.S. Meyer, P.A. Jensen, and K. Dam-Johansen: "Effect and modeling of glucose inhibition and in situ glucose removal during enzymatic hydrolysis of pretreated wheat straw." *Applied biochemistry and biotechnology*. vol. 160, no. 1, pp. 280–298, 2010.
138. K. Bélafi-Bakó, A. Koutinas, N. Nemestóthy, L. Gubicza, and C. Webb: "Continuous enzymatic cellulose hydrolysis in a tubular membrane bioreactor." *Enzyme and Microbial Technology*. vol. 38, no. 1–2, pp. 155–161, 2006.
139. Z. Su, J. Luo, X. Li, and M. Pinelo: "Enzyme membrane reactors for production of oligosaccharides: A review on the interdependence between enzyme reaction and membrane separation." *Separation and Purification Technology*. vol. 243, pp. 116840–116857, 2020.
140. M.M. Zain, A.W. Mohammad, and N.H.H. Hairom: "Flux and permeation behaviour of ultrafiltration in sugaring out cellulose hydrolysate solution: A membrane screening." *Journal of Physical Science*. vol. 28, pp. 25–39, 2017.
141. S. Al-Zuhair, M. Al-Hosany, Y. Zooba, A. Al-Hammadi, and S. Al-Kaabi: "Development of a membrane bioreactor for enzymatic hydrolysis of cellulose." *Renewable Energy*. vol. 56, pp. 85–89, 2013.
142. W.W. Na'aman, S.M. Saufi, M.A. Seman, H.W. Yussof, and A. Mohammad: "Fabrication of Asymmetric Nanofiltration Flatsheet Membrane for the Separation of Acetic Acid from Xylose and Glucose." *Chemical Engineering Transactions*. vol. 56, pp. 1201–1206, 2017.
143. B. Qi, J. Luo, G. Chen, X. Chen, and Y. Wan: "Application of ultrafiltration and nanofiltration for recycling cellulase and concentrating glucose from enzymatic hydrolyzate of steam exploded wheat straw." *Bioresource Technology*. vol. 104, pp. 466–472, 2012.
144. K. Saha, U.M. R, J. Sikder, S. Chakraborty, S.S. da Silva, and J.C. dos Santos: "Membranes as a tool to support biorefineries: Applications in enzymatic hydrolysis, fermentation and dehydration for bioethanol production." *Renewable and Sustainable Energy Reviews*. vol. 74, pp. 873–890, 2017.
145. F. Ran, J. Li, Y. Lu, L. Wang, S. Nie, H. Song, L. Zhao, S. Sun, and C. Zhao: "A simple method to prepare modified polyethersulfone membrane with improved hydrophilic surface by one-pot: The effect of hydrophobic segment length and molecular weight of copolymers." *Materials Science and Engineering: C*. vol. 37, pp. 68–75, 2014.

146. A. Rahimpour, S.S. Madaeni, and Y. Mansourpanah: "Fabrication of polyethersulfone (PES) membranes with nano-porous surface using potassium perchlorate (KClO₄) as an additive in the casting solution." *Desalination*. vol. 258, no. 1–3, pp. 79–86, 2010.
147. N.H.T. Thy and R. Nithyanandam: "Fractionation of hydrolyzed microcrystalline cellulose by ultrafiltration membrane." *Journal of Engineering Science and Technology*. vol. 11, no. 1, pp. 136–148, 2016.
148. P. Lozano, B. Bernal, A.G. Jara, and M.-P. Belleville: "Enzymatic membrane reactor for full saccharification of ionic liquid-pretreated microcrystalline cellulose." *Bioresource Technology*. vol. 151, pp. 159–165, 2014.
149. K. Amit, M. Nakachew, B. Yilikal, and Y. Mukesh: "A review of factors affecting enzymatic hydrolysis of pretreated lignocellulosic biomass." *Res J Chem Environ*. vol. 22, no. 7, pp. 62–67, 2018.
150. J. Liu, J. Lu, and Z. Cui: "Enzymatic hydrolysis of cellulose in a membrane bioreactor: assessment of operating conditions." *Bioprocess Biosyst Eng*. vol. 34, no. 5, pp. 525–532, 2011.
151. P. Alvira, E. Tomás-Pejó, M. Ballesteros, and M.J. Negro: "Pretreatment technologies for an efficient bioethanol production process based on enzymatic hydrolysis: A review." *Bioresource Technology*. vol. 101, no. 13, pp. 4851–4861, 2010.
152. B. Yang and C.E. Wyman: "Pretreatment: the key to unlocking low-cost cellulosic ethanol." *Biofuels, Bioproducts and Biorefining: Innovation for a sustainable economy*. vol. 2, no. 1, pp. 26–40, 2008.
153. D. Koullas, P. Christakopoulos, D. Kekos, B.J. Macris, and E.G. Koukios: "Correlating the effect of pretreatment on the enzymatic hydrolysis of straw." *Biotechnology and bioengineering*. vol. 39, no. 1, pp. 113–116, 1992.
154. A.E.K. Afedzi, K. Rattanaporn, and P. Parakulsuksatid: "Impeller selection for mixing high-solids lignocellulosic biomass in stirred tank bioreactor for ethanol production." *Bioresource Technology Reports*. vol. 17, pp. 100935–100948, 2022.
155. A. Mahboubi, C. Uwineza, W. Doyen, H. De Wever, and M.J. Taherzadeh: "Intensification of lignocellulosic bioethanol production process using continuous double-staged immersed membrane bioreactors." *Bioresource Technology*. vol. 296, pp. 122314–122325, 2020.
156. H.-J. Huang, B.V. Ramarao, and S. Ramaswamy: "Separation and purification technologies in biorefineries." *John Wiley & Sons*, 2013. Accessed from <https://doi.org/10.1002/9781118493441>. Accessed on 17 Feb 2021.
157. P. Le-Clech, B. Jefferson, and S.J. Judd: "A comparison of submerged and sidestream tubular membrane bioreactor configurations." *Desalination*. vol. 173, no. 2, pp. 113–122, 2005.

158. Y. Zheng, W. Zhang, B. Tang, J. Ding, and Z. Zhang: "Membrane fouling mechanism of biofilm-membrane bioreactor (BF-MBR): Pore blocking model and membrane cleaning." *Bioresource technology*. vol. 250, pp. 398–405, 2018.
159. P. Andrić, A.S. Meyer, P.A. Jensen, and K. Dam-Johansen: "Reactor design for minimizing product inhibition during enzymatic lignocellulose hydrolysis: I. Significance and mechanism of cellobiose and glucose inhibition on cellulolytic enzymes." *Biotechnology Advances*. vol. 28, no. 3, pp. 308–324, 2010.
160. Chen, J. Mo, X. Du, Z. Zhang, and W. Zhang, "Biomimetic dynamic membrane for aquatic dye removal." *Water Research*. vol. 151, pp. 243–251, 2019.
161. Z. Xu, Q. Wang, Z. Jiang, X. Yang, and Y. Ji: "Enzymatic hydrolysis of pretreated soybean straw." *Biomass and Bioenergy*. vol. 31, no. 2, pp. 162–167, 2007.
162. P.R.N. Childs: "Chapter 6 - Rotating Cylinders, Annuli, and Spheres." In: Childs, P.R.N. (ed.) *Rotating Flow*. Butterworth-Heinemann, Oxford. pp. 177–247. 2011.
163. S. Al-Zuhair, Y.L. Fan, K.S. Chui, and S. Rizwan: "Kinetics of *Aspergillus niger* Cellulase Inhibition by Reducing Sugar Produced by the Hydrolysis of Carboxymethylcellulose." *International Journal of Chemical Reactor Engineering*. vol. 5, no. 1, 2007. Accessed from doi: 10.2202/1542-6580.1385. Accessed on 7 Jun 2021.
164. S. Al-Zuhair: "The effect of crystallinity of cellulose on the rate of reducing sugars production by heterogeneous enzymatic hydrolysis." *Bioresource technology*. vol. 99, no. 10, pp. 4078–4085, 2008.
165. J. Liu, J. Lu, and Z. Cui: "Enzymatic hydrolysis of cellulose in a membrane bioreactor: assessment of operating conditions." *Bioprocess Biosyst Eng*. vol. 34, no. 5, pp. 525–532, 2011.
166. T. Juhász, A. Egyházi, and K. Réczey: " β -Glucosidase Production by *Trichoderma reesei*." In: Davison, B.H., Evans, B.R., Finkelstein, M., and McMillan, J.D. (eds.) *Twenty-Sixth Symposium on Biotechnology for Fuels and Chemicals*. Humana Press, Totowa, NJ. pp. 243–254. 2005.
167. R.R. Singhanian, A.K. Patel, R.K. Sukumaran, C. Larroche, and A. Pandey: "Role and significance of beta-glucosidases in the hydrolysis of cellulose for bioethanol production." *Bioresource Technology*. vol. 127, pp. 500–507, 2013.
168. N. Ortega, M. D. Busto, and M. Perez-Mateos: "Kinetics of cellulose saccharification by *Trichoderma reesei* cellulases." *International Biodeterioration & Biodegradation*. vol. 47, no. 1, pp. 7–14, 2001.

169. P. Tiwari, B.N. Misra, and N.S. Sangwan: “ β -Glucosidases from the Fungus *Trichoderma*: An Efficient Cellulase Machinery in Biotechnological Applications.” *BioMed Research International*. vol. 2013, pp. e203735, 2013. Accessed from doi: 10.1155/2013/203735. Accessed on 24 Aug 2020.
170. “Cellulase - Worthington Enzyme Manual,”. Accessed from <http://www.worthington-biochem.com/cel/default.html>. Accessed on 2 Dec 2020.
171. Q. Gan, S. Allen, and G. Taylor: “Kinetic dynamics in heterogeneous enzymatic hydrolysis of cellulose: an overview, an experimental study and mathematical modelling.” *Process Biochemistry*. vol. 38, no. 7, pp. 1003–1018, 2003.
172. L.A. Alcázar and J. Ancheyta: “Sensitivity analysis based methodology to estimate the best set of parameters for heterogeneous kinetic models.” *Chemical Engineering Journal*. vol. 128, no. 2, pp. 85–93, 2007.
173. M. Mohd Zaini Makhtar, H.A. Tajarudin, M.D.M. Samsudin, V.M. Vadivelu, N.F. Shoparwe, and N. ‘Izzah Zainuddin: “Membrane-less microbial fuel cell: Monte Carlo simulation and sensitivity analysis for COD removal in dewatered sludge.” *AIP Advances*. vol. 11, no. 6, pp. 65016–65025, 2021.
174. R.V. Nouroozi, M.V. Noroozi, and M. Ahmadizadeh: “Determination of protein concentration using Bradford microplate protein quantification assay.” *International Electronic Journal of Medicine*. vol. 4, no. 1, pp. 11–17, 2020.
175. N.J. Kruger: “The Bradford method for protein quantitation.” *The protein protocols handbook*. Springer. pp. 17–24, 2009.
176. C. Yang and X. Lü: “Chapter 5 - Composition of plant biomass and its impact on pretreatment.” In: Lü, X. (ed.) *Advances in 2nd Generation of Bioethanol Production*. Woodhead Publishing. pp. 71–85, 2021.
177. E. Galiwango and A.H. Al-Marzouqi: “Investigation of Nonisothermal Combustion Kinetics of Isolated Lignocellulosic Biomass: A Case Study of Cellulose from Date Palm Biomass Waste.” *IntechOpen*, 2020. Accessed from doi: 10.5772/intechopen.93549. Accessed on 19 March 2020.
178. D. Templeton and T. Ehrman: “Determination of acid-insoluble lignin in biomass: Chemical analysis and testing task laboratory analytical procedure (LAP-003).” *National Renewable Energy Laboratory, which is operated by the Midwest Research Institute for the Department Of Energy*. 1995. Accessed from <https://www.nrel.gov/docs/gen/fy13/42618.pdf>. Accessed on 17 April 2021.

179. J.S. Knutsen and R.H. Davis: "Cellulase Retention and Sugar Removal by Membrane Ultrafiltration During Lignocellulosic Biomass Hydrolysis." In: Finkelstein, M., McMillan, J.D., Davison, B.H., and Evans, B. (eds.) *Proceedings of the Twenty-Fifth Symposium on Biotechnology for Fuels and Chemicals Held May 4–7, 2003, in Breckenridge, CO.* pp. 585–599. *Humana Press*, Totowa, NJ, 2004.
180. M. Malmali, J. Stickel, and S.R. Wickramasinghe: "Investigation of a submerged membrane reactor for continuous biomass hydrolysis." *Food and Bioproducts Processing*. vol. 96, pp. 189–197, 2015.
181. N.M. Rad, S.M. Mousavi, M. Bahreini, and E. Saljoughi: "Use of membrane separation in enzymatic hydrolysis of waste paper." *Korean J. Chem. Eng.* vol. 34, no. 3, pp. 768–772, 2017.
182. L. Huang, S. Wang, H. Zhang, D. Li, Y. Zhang, L. Zhao, Q. Xin, H. Ye, and H. Li: "Enhanced hydrolysis of cellulose by catalytic polyethersulfone membranes with straight-through catalytic channels." *Bioresource Technology*. vol. 294, pp. 122119–12229, 2019.
183. J. Luo, S.T. Morthensen, A.S. Meyer, and M. Pinelo: "Filtration behavior of casein glycomacropeptide (CGMP) in an enzymatic membrane reactor: fouling control by membrane selection and threshold flux operation." *Journal of Membrane Science*. vol. 469, pp. 127–139, 2014.
184. M.A. Mohamed, J. Jaafar, A.F. Ismail, M.H.D. Othman, and M.A. Rahman: "Chapter 1 - Fourier Transform Infrared (FTIR) Spectroscopy." In: Hilal, N., Ismail, A.F., Matsuura, T., and Oatley-Radcliffe, D. (eds.) *Membrane Characterization*. pp. 3–29. *Elsevier*, 2017.
185. S. Belfer, R. Fainchtein, Y. Purinson, and O. Kedem: "Surface characterization by FTIR-ATR spectroscopy of polyethersulfone membranes-unmodified, modified and protein fouled." *Journal of Membrane Science*. vol. 172, no. 1, pp. 113–124, 2000.
186. P. Qu, H. Tang, Y. Gao, L. Zhang, and S. Wang: "Polyethersulfone composite membrane blended with cellulose fibrils." *BioResources*. vol. 5, no. 4, pp. 2323–2336, 2010.
187. M.D. Angione, T. Duff, A.P. Bell, S.N. Stamatina, C. Fay, D. Diamond, E.M. Scanlan, and P.E. Colavita: "Enhanced Antifouling Properties of Carbohydrate Coated Poly(ether sulfone) Membranes." *ACS Appl. Mater. Interfaces*. vol. 7, no. 31, pp. 17238–17246, 2015.
188. A. Pakdel Mojdehi, M. Pourafshari Chenar, M. Namvar-Mahboub, and M. Eftekhari: "Development of PES/polyaniline-modified TiO₂ adsorptive membrane for copper removal." *Colloids and Surfaces A: Physicochemical and Engineering Aspects*. vol. 583, pp. 123931–123941, 2019.
189. Z. Zhou, G. Huang, Y. Xiong, M. Zhou, S. Zhang, C.Y. Tang, and F. Meng: "Unveiling the Susceptibility of Functional Groups of Poly(ether sulfone)/Polyvinylpyrrolidone Membranes to NaOCl: A Two-Dimensional Correlation Spectroscopic Study." *Environ. Sci. Technol.* vol. 51, no. 24, pp. 14342–14351, 2017.

190. M. Katz and E. Reese: "Production of glucose by enzymatic hydrolysis of cellulose." *Applied Microbiology*. vol. 16, no. 2, pp. 419–428, 1968.
191. J. Saldarriaga, A. Pablos, R. Aguado, M. Amutio, and M. Olazar: "Characterization of lignocellulosic biofuels by TGA." *International Review of Chemical Engineering*. vol. 4, no. 6, pp. 585–588, 2012.
192. Y.C. Park and J.S. Kim: "Comparison of various alkaline pretreatment methods of lignocellulosic biomass." *Energy*. vol. 47, no. 1, pp. 31–35, 2012.
193. A. Aboragah, M. Embaby, M. Günal, and A. AbuGhazaleh: "Effect of alkaline and sonication pretreatments on the rumen degradability of date palm seeds." *Trop Anim Health Prod*. vol. 52, no. 2, pp. 771–776, 2020.
194. W. Wang, X. Wang, Y. Zhang, Q. Yu, X. Tan, X. Zhuang, and Z. Yuan: "Effect of sodium hydroxide pretreatment on physicochemical changes and enzymatic hydrolysis of herbaceous and woody lignocelluloses." *Industrial Crops and Products*. vol. 145, pp. 112145–112154, 2020.
195. S. Al-Zuhair, M. Abualreesh, K. Ahmed, and A. Abdul Razak: "Enzymatic delignification of biomass for enhanced fermentable sugars production." *Energy Technology*. vol. 3, no. 2, pp. 121–127, 2015.
196. C. Huang, W. Lin, C. Lai, X. Li, Y. Jin, and Q. Yong: "Coupling the post-extraction process to remove residual lignin and alter the recalcitrant structures for improving the enzymatic digestibility of acid-pretreated bamboo residues." *Bioresource Technology*. vol. 285, pp. 121355–121369, 2019.
197. Ö. Şahin and C. Saka: "Preparation and characterization of activated carbon from acorn shell by physical activation with H₂O–CO₂ in two-step pretreatment." *Bioresource Technology*. vol. 136, pp. 163–168, 2013.
198. R. Md Salim, J. Asik, and M.S. Sarjadi: "Chemical functional groups of extractives, cellulose and lignin extracted from native *Leucaena leucocephala* bark." *Wood Sci Technol*. vol. 55, no. 2, pp. 295–313, 2021.
199. H. Toribio Cuaya, L. Pedraza Segura, S. Macías Bravo, I. Gonzalez García, R.C. Vásquez Medrano, and E. Favela Torres: "Characterization of lignocellulosic biomass using five simple steps." *Biological and Physical Sciences*. vol. 4, no. 5, pp. 25–47, 2014.
200. Z. Belouadah, A. Ati, and M. Rokbi: "Characterization of new natural cellulosic fiber from *Lygeum spartum* L." *Carbohydrate Polymers*. vol. 134, pp. 429–437, 2015.
201. U.P. Agarwal, J. Zhu, and S.A. Ralph: "Enzymatic hydrolysis of biomass: effects of crystallinity, particle size, and lignin removal." Presented at the 6th international symposium on wood, fiber and pulping chemistry, 2011. Accessed from <https://www.researchgate.net/publication/252321816>. Accessed on 17 May 2021.

202. H.A. Gavlighi, A.S. Meyer, and J.D. Mikkelsen: “Enhanced enzymatic cellulose degradation by cellobiohydrolases via product removal.” *Biotechnol Lett.* vol. 35, no. 2, pp. 205–212, 2013.
203. O. Zahed, G.S. Jouzani, S. Abbasalizadeh, F. Khodaiyan, and M. Tabatabaei: “Continuous co-production of ethanol and xylitol from rice straw hydrolysate in a membrane bioreactor.” *Folia Microbiol.* vol. 61, no. 3, pp. 179–189, 2016.
204. K. Bélafi-Bakó, M. Eszterle, K. Kiss, N. Nemestóthy, and L. Gubicza: “Hydrolysis of pectin by *Aspergillus niger* polygalacturonase in a membrane bioreactor.” *Journal of Food Engineering.* vol. 78, no. 2, pp. 438–442, 2007.
205. A. Mohagheghi, M. Tucker, K. Grohmann, and C. Wyman: “High solids simultaneous saccharification and fermentation of pretreated wheat straw to ethanol.” *Appl Biochem Biotechnol.* vol. 33, no. 2, pp. 67–81, 1992.
206. C. Cara, M. Moya, I. Ballesteros, M.J. Negro, A. González, and E. Ruiz: “Influence of solid loading on enzymatic hydrolysis of steam exploded or liquid hot water pretreated olive tree biomass.” *Process Biochemistry.* vol. 42, no. 6, pp. 1003–1009, 2007.
207. E. Varga, H.B. Klinke, K. Réczey, and A.B. Thomsen: “High solid simultaneous saccharification and fermentation of wet oxidized corn stover to ethanol.” *Biotechnology and Bioengineering.* vol. 88, no. 5, pp. 567–574, 2004.
208. H. Ingesson, G. Zacchi, B. Yang, A.R. Esteghlalian, and J.N. Saddler: “The effect of shaking regime on the rate and extent of enzymatic hydrolysis of cellulose.” *Journal of Biotechnology.* vol. 88, no. 2, pp. 177–182, 2001.
209. W. Wang, L. Kang, H. Wei, R. Arora, and Y.Y. Lee: “Study on the Decreased Sugar Yield in Enzymatic Hydrolysis of Cellulosic Substrate at High Solid Loading.” *Appl Biochem Biotechnol.* vol. 164, no. 7, pp. 1139–1149, 2011.
210. Y.-H. Lee and L.T. Fan: “Kinetic studies of enzymatic hydrolysis of insoluble cellulose: Analysis of the initial rates.” *Biotechnology and Bioengineering.* vol. 24, no. 11, pp. 2383–2406, 1982.
211. I. Edeh: “Bioethanol Production: An Overview.” *IntechOpen* , 2020. Accessed from doi: 10.5772/intechopen.94895. Accessed on 10 June 2021.
212. Y.X. Wang, M.J. Dong, and W.C. Zhuang: “Enzymatic Saccharification of Cellulose Pretreated from Lignocellulosic Biomass: Status and Prospect.” *Advanced Materials Research.* vol. 446–449, pp. 2809–2814, 2012.
213. D. Wu, Z. Wei, T.A. Mohamed, G. Zheng, F. Qu, F. Wang, Y. Zhao, and C. Song: “Lignocellulose biomass bioconversion during composting: Mechanism of action of lignocellulase, pretreatment methods and future perspectives.” *Chemosphere.* vol. 286, pp. 131635–131645, 2022.

List of Publications

S. Al-Mardeai, E. Elnajjar, R. Hashaikeh, B. Kruczek, and S. Al-Zuhair: “Dynamic model of simultaneous enzymatic cellulose hydrolysis and product separation in a membrane bioreactor.” *Biochemical Engineering Journal*. vol. 174, pp. 108107, 2021.

S. Al-Mardeai, E. Elnajjar, R. Hashaikeh, B. Kruczek, B. Van der Bruggen, and S. Al-Zuhair: “Simultaneous Enzymatic Cellulose Hydrolysis and Product Separation in a Radial-Flow Membrane Bioreactor.” *Molecules*. vol. 27, no. 1, pp. 288, 2022.

Appendix

A sample calculation for the product yield is shown below for the case of using inverted dead-end MBR using PES-10 at 8 h of hydrolysis reaction, substrate and enzyme concentrations of 6.67 and 0.48 g/L, respectively, and a water flowrate of 0.4 mL/min:

Measured products concentration in the bottom chamber (accumulated) = 2.33 g/L

Measured products concentration in the upper chamber = 0.64 g/L

Measured products concentration in the collected overflow = 0.52 g/L

Volume of the bottom chamber = 0.75 L

Volume of the upper chamber = 0.65 L

Total volume of collected overflow after 8 h = 0.192 L (which is also equal to 0.4×10^{-3} L/min x 480 min):

$$\text{Total products amount} = 2.33 \left(\frac{\text{g}}{\text{L}}\right) \times 0.75(\text{L}) + 0.64 \left(\frac{\text{g}}{\text{L}}\right) \times 0.65(\text{L}) + 0.52 \left(\frac{\text{g}}{\text{L}}\right) \times 0.192(\text{L})$$

$$\text{Total product amount} = 2.26 \text{ g}$$

$$\text{Total amount of substrate used} = 6.67 \left(\frac{\text{g}}{\text{L}}\right) \times 0.75(\text{L}) = 5 \text{ g}$$

The total yield is calculated by dividing the total products amount by the amount of substrate initially added in the bottom chamber:

$$\text{Production yield} = \frac{2.26 \text{ g}}{5 \text{ g}} \times 100\% = 45.2\%$$

UAEUجامعة الإمارات العربية المتحدة
United Arab Emirates University**KU LEUVEN****UAE UNIVERSITY DOCTORATE DISSERTATION NO. 2022:3**

The potential of the enzymatic hydrolysis of lignocellulose is currently compromised by the cost of production in comparison to the yield. The main two challenges are related to the activity of the enzyme activity and to product inhibition. This study enhances the feasibility by developing a membrane bioreactor (MBR) technology. The different suggested MBR types in the literature allow for different ranges of enhancement, however, membrane fouling and high solid loadings are limiting their application. In this PhD dissertation, novel MBRs are designed to eliminate the product continuously and allow the handling of a high solids loading.

Saleha Al-Mardeai received her Dual PhD from the Department of Chemical Engineering, College of Engineering at UAE University, UAE, and the Doctor of Engineering Science (PhD): Chemical Engineering from the Arenberg Doctoral School, Faculty of Engineering Science, Department of Chemical Engineering at KU Leuven, Belgium. She received her MSc in Chemical Engineering from Masdar Institute (Khalifa University), UAE.

www.uaeu.ac.ae

Online publication of dissertation:
<https://scholarworks.uaeu.ac.ae/etds/>

UAEU عمادة المكتبات
Libraries Deanshipجامعة الإمارات العربية المتحدة
United Arab Emirates University

Digital Library Services Section - قسم الخدمات المكتبية الرقمية